

The pharmacokinetics and anti-inflammatory capacity of Bilirubin Sulfonate: A novel biliverdin metabolite

Author

Shiels, Ryan G

Published

2020-07-23

Thesis Type

Thesis (PhD Doctorate)

School

School of Medical Science

DOI

[10.25904/1912/3905](https://doi.org/10.25904/1912/3905)

Rights statement

The author owns the copyright in this thesis, unless stated otherwise.

Downloaded from

<http://hdl.handle.net/10072/396150>

Griffith Research Online

<https://research-repository.griffith.edu.au>



**The pharmacokinetics and anti-inflammatory capacity of Bilirubin
Sulfonate: A novel biliverdin metabolite**

Ryan Graeme Shiels

BHSc (Hons)

School of Medical Science

Griffith Health

Griffith University

**Submitted in fulfilment of the requirements of the degree of Doctor of
Philosophy**

February 2020

Acknowledgements

I would firstly like to sincerely thank my supervisors Associate Professor Andrew Bulmer PhD and Dr. Andrew Pearson PhD, without such stellar support, guidance, knowledge and experience; this thesis would not have been possible. Thank you both for your patience, encouragement and positive criticism throughout my tenure. Additional thanks to A/Prof Andrew Bulmer, for supplying the initial thesis topic as a continuation of his work in the field, and financially supporting the project and my own academic development.

To Mr Josif Vidimce, it has been an honour and a pleasure to toil alongside you. You are an excellent scientist, and I count you as one of my closest friends. Thank you for the mateship, rants, hilarity, and assistance, we were already good mates prior to this PhD, but our friendship, now forged in the fires of hell, will be one I value forever. We shared a roller-coaster of emotions, from feelings of failure, success in the face of overwhelming odds, to unmitigated range and unbridled sadness, and without you in my corner this PhD would have been insurmountable.

To Mr Evan Pennell, from getting to know you during our '17 trip to Japan, and as we explored the challenges of learning our respective analytical techniques, its been a pleasure. Your attention to detail, worth ethic and passion for excellence has earned my respect and helped me to improve my own abilities. It is an honour to count you as a good friend, and I thank you for the support and assistance as we stared down the barrel of many problems together.

To Mr Wenu Hewage, your assistance in this project has been invaluable. Teaching you has been an absolute pleasure, and I am so very proud of the scientist you have become. Thank you for being diligent, passionate and enthusiastic in all our projects, you will go very far in whatever field you choose.

To my girlfriend, Claire Ryan, thank you for your support from start to finish. You've been there for me through every highlight, disaster and have constantly encouraged me no matter the odds. You've fed me, loved me, looked after me and put up with me. I could not ask for a better person by my side in all this. Additional thanks to your mother Michelle Black, for stepping in for my own mother when I've needed it.

To my father, Graeme, you've always supported and encouraged my education, sometimes to your pleasure and sometimes against your better judgement. Its paid off and I couldn't thank you more.

Finally, to my darling mother Wendy who passed away suddenly and unexpectedly in December 2016. You've always been my biggest fan, unconditionally and selflessly supporting me through life when it was needed the most, regardless of your own situation. I stepped up and took care of my sister as I had silently promised to you the day after you passed, and thank you for all you taught me about toughness and self-belief. I miss you every day, and I wish you could see me graduate for a final time. This one's for you.

General Abstract

In mammals, tetrapyrroles formed following the catabolism of haem (i.e. bilirubin and biliverdin, bile pigments) protect against free radical mediated damage that is induced during inflammation and therefore represent potential therapeutic targets. Recently, novel metabolites of biliverdin were discovered in blood, urine and bile following intraduodenal biliverdin administration⁽¹⁾ indicating a new pathway for biliverdin metabolism had been discovered and required bacteria for biliverdin transformation. These data are important because oral biliverdin administration protects from inflammatory processes, however, based upon the discovery of this new metabolic pathway, biliverdin is unlikely to be responsible for protection. The main aims of this PhD thesis were to identify and characterise the principle novel biliverdin metabolite (bilirubin-10-sulfonate) formed within the gut before investigating the compound's pharmacokinetics and anti-inflammatory effects a clinically relevant animal model of sterile inflammation, thus providing pre-clinical evidence of bilirubin-10-sulfonate's therapeutic potential.

In the first study, novel biliverdin metabolites formed after intraduodenal biliverdin administration in rats and after biliverdin incubation in *C. youngae* bacterial cultures were analysed via liquid chromatography coupled to tandem mass spectrometry. Nuclear magnetic resonance (NMR) spectroscopy was also used in order to elucidate the principle metabolite's structure, and the compounds antioxidant potential was assessed using a ferric reducing capacity of plasma (FRAP) assay. Analysis revealed the principle metabolite had a m/z 663.215 with similar λ max and eluted at two different retention times. Tandem mass spectrometry and NMR confirmed the principle compound's identity as bilirubin-10-sulfonate (BRS) and FRAP analysis indicated bilirubin-10-sulfonate and biliverdin shared similar reductive capacity. This study confirmed the formation of a previously undocumented metabolite of biliverdin in

mammals and that this metabolite possessed antioxidant capacity, and therefore could protect against oxidative stressors *in vivo*.

Prior to testing the ability of bilirubin-10-sulfonate to inhibit oxidative/inflammatory processes *in vivo*, it was important to test its pharmacokinetics, so that an appropriate dose and route of administration could be formulated. Therefore, in the second study, the bile pigment biliverdin and its novel metabolite, bilirubin-10-sulfonate, were assessed in a single compartment model of pharmacokinetics in the rat. The two compounds were administered intravenously, intraperitoneally or intraduodenally to anaesthetised Wistar rats. The bile duct and jugular vein of animals were cannulated and the concentrations of bile pigments in blood and bile were measured over three hours using ultra high performance liquid chromatography coupled with mass spectrometry. When bilirubin-10-sulfonate was administered intravenously (n=6), it had a significantly ($p < 0.05$) longer elimination (146.0 ± 14.6 vs 61.3 ± 7.8 minutes) and distribution (38.3 ± 4.8 vs 6.3 ± 0.8 minutes) half-life compared to biliverdin (n=5) and had a significantly reduced volume of distribution (0.048 ± 0.005 vs 0.065 ± 0.003 L kg⁻¹). Furthermore, bilirubin-10-sulfonate was excreted intact in bile, whereas biliverdin was excreted after chemical reduction and conjugation. Consequently, intraperitoneal administration resulted in significantly greater blood concentrations of bilirubin-10-sulfonate (n=6) with similar bioavailabilities over 180 minutes. Intraduodenal bioavailability was very low for both compounds, however bilirubin-10-sulfonate (n=6) was absorbed then excreted to a greater extent compared to biliverdin (n=5). This study demonstrated that bilirubin-10-sulfonate and biliverdin are potently absorbed intraperitoneally, and that bilirubin-10-sulfonate has a superior pharmacokinetic profile when compared to biliverdin, due to reduced hepatic clearance, thereby providing guidance as to

an appropriate dose and route of administration for the final study where the *in vivo* anti-inflammatory capacity of both compounds were investigated.

In study three, the superior pharmacokinetic profile of bilirubin-10-sulfonate along with the promising intraperitoneal bioavailability of both bile pigments led to the investigation of their *in vivo* anti-inflammatory and antioxidant capacity in a model of monosodium urate induced sterile inflammation. Over 6 days, subcutaneous air pouches were created on the dorsal flanks of adult male Wistar rats. Rats were pre-treated with intraperitoneal bilirubin-10-sulfonate or biliverdin (27 mg kg⁻¹) one hour before the pouch was stimulated with monosodium urate (25 mg). Total and differential leukocyte counts were determined in pouch fluid aspirate over a 48 hour period with bile pigment quantification performed on pouch aspirate and serum via mass spectrometry as per study two. Pouch fluid inflammatory cytokine concentrations were also assessed after 6 hours via multiplex flow cytometry bead assay. In addition, markers of oxidant modification protein carbonyl and chloramine concentrations were assessed in pouch fluid after 24 hours using ELISA and spectrophotometry, respectively. Bilirubin-10-sulfonate and biliverdin significantly inhibited leukocyte infiltration into the pouch fluid from 6 to 48 hours. Both bilirubin-10-sulfonate and biliverdin significantly reduced pouch GM-CSF and MCP-1 concentrations at 6 hours whilst biliverdin additionally inhibited IL-6 and IL-18 concentrations at 6 hours. Despite these differences, no change in pouch chloramine or protein carbonyl concentrations occurred at 24 hours. Serum biliverdin concentrations rapidly diminished over 6 hours, however, BRS was readily detected in the serum until 48 hours, and in pouch fluid over 12 hours. This study is the first to elucidate the anti-inflammatory effects of bilirubin-10-sulfonate and biliverdin administration in an *in vivo* model of gouty inflammation. The reduced leukocyte infiltration

The pharmacokinetics and anti-inflammatory capacity of Bilirubin Sulfonate: A novel biliverdin metabolite and cytokine production in response to sterile inflammation after bile pigment administration further illustrate the importance of these natural products in physiology and their anti-inflammatory therapeutic potential.

This thesis documents the discovery, analysis, pharmacokinetics and *in vivo* anti-inflammatory capacity of bilirubin-10-sulfonate and concludes that bilirubin-10-sulfonate may be a viable treatment for inflammatory joint disease, thus laying the foundation for the development of future novel anti-inflammatory therapies.

Declaration of Originality

This work has not previously been submitted for a degree or diploma in any university. To the best of my knowledge and belief, the thesis contains no material previously published or written by another person except where due reference is made in the thesis itself.

X

Ryan G. Shiels, BHSc(Hon)

PhD Candidate

School of Medical Science

Griffith University, Gold Coast Campus

Table of Contents

ACKNOWLEDGEMENTS	II
GENERAL ABSTRACT	IV
TABLE OF CONTENTS	IX
LIST OF FIGURES	XI
LIST OF TABLES	XVII
LIST OF ABBREVIATIONS AND SYMBOLS	XVIII
AUTHORSHIP STATEMENT	XXIII
THESIS ORGANISATION	1
1. CHAPTER ONE: A GENERAL INTRODUCTION	1
2. CHAPTER TWO: A REVIEW OF THE LITERATURE	4
2.1 EVOLUTION OF HAEM	4
2.2 HAEM CATABOLISM	4
2.3 BILE PIGMENT METABOLISM AND EXCRETION	5
2.4 RECENT DISCOVERIES IN BILE PIGMENT METABOLISM	9
2.5 OXIDATIVE STRESS	10
2.6 INFLAMMATION	11
2.7 INITIATION OF INFLAMMATORY RESPONSE	11
2.8 IMMUNE CELLS	14
2.9 CYTOKINE SIGNALLING AND CHEMOTAXIS	18
2.10 NLRP3 INFLAMMASOME	19
2.11 INFLAMMATION IN GOUT	20
2.12 MONOSODIUM URATE MONOHYDRATE CRYSTAL-INDUCED INFLAMMATION IN VIVO: STERILE INFLAMMATION IN THE RAT 21	
2.13 BILE PIGMENTS AND LINEAR TETRAPYRROLES	24
2.14 BILE PIGMENTS AS ANTIOXIDANTS	25
2.15 GILBERT'S SYNDROME – UCB ELEVATION IN HUMANS	30
2.16 BILE PIGMENT ANTI-INFLAMMATORY EFFECTS	31

2.17	INTESTINAL BACTERIAL TETRAPYRROLE METABOLISM	34
2.18	ANALYSIS OF BILE PIGMENTS	35
2.19	CONCLUSION	37
3.	CHAPTER THREE: AIMS & HYPOTHESES.....	39
3.1	STUDY ONE (CHAPTER FOUR).....	39
3.2	STUDY TWO (CHAPTER FIVE).....	39
3.3	STUDY THREE (CHAPTER SIX).....	39
4.	CHAPTER FOUR: UNPRECEDENTED MICROBIAL CONVERSION OF BILIVERDIN INTO BILIRUBIN-10-SULFONATE.....	40
5.	CHAPTER FIVE: PHARMACOKINETICS OF BILIRUBIN-10-SULFONATE AND BILIVERDIN: THE POTENTIAL THERAPEUTIC ADMINISTRATION OF A NOVEL TETRAPYRROLE	61
6.	CHAPTER SIX: BILIVERDIN AND BILIRUBIN SULFONATE INHIBIT MONOSODIUM URATE INDUCED STERILE INFLAMMATION IN THE RAT	88
7.	CHAPTER SEVEN: THESIS SUMMARY AND CONCLUSION	120
7.1	INTRODUCTION	120
7.2	PROJECT SUMMARY	120
7.3	FUTURE DIRECTIONS	123
8.	REFERENCES.....	127

List of Figures

Figure 2.1: Catabolism of haem by haem oxygenase to biliverdin and unconjugated bilirubin. ⁽¹⁷⁾	6
Figure 2.2: Human metabolic pathways of haem and its metabolites BV/UCB. ⁽²⁴⁾ Haem liberated from cells via RBC catabolism (1) is metabolised to BV, where BVR converts it to UCB prior to binding with albumin. It is then transported to the liver (2), where hepatic uptake occurs (3). UCB is then conjugated (4) to bilirubin mono and di glucuronide (BMD/BDG) prior to biliary excretion, ending in excretion via faeces (5). Enterohepatic circulation also occurs (6) in the intestine as bacterial β -glucuronidase deconjugated BMG/BDG forming UCB which is then able to be reabsorbed by the intestine (back to (2)).	6
Figure 2.3: Structures and masses resulting from the sequential reduction/oxidation of UCB by the intestinal microflora. ⁽²⁸⁾	9
Figure 2.4: Damage associated molecular patterns (DAMPs) activate various immune cells, initiating pro-inflammatory signalling cascades observed in sterile inflammation. ⁽⁵³⁾	13
Figure 2.5: Mechanisms of neutrophils in the acute phase of inflammation. ⁽⁶¹⁾ Neutrophils are developed in bone marrow (top left), released into circulation where they patrol until they are stimulated by cytokines, and as a result undergo extravasation into the affected tissue (middle right). There they produce intra and extracellular ROS via MPO release, perform phagocytosis, NETosis, and participate in downstream signalling via further cytokine release.	15
Figure 2.6: Interactions between neutrophils (left hand side of figure) and macrophages (right hand side of figure) during the innate immune response. ⁽⁶²⁾ Monocytes, attracted by cytokines released by neutrophils (bottom; red), polarise into either M1 or M2 macrophages (top right) depending on factors such as G-CSF in the local environment of tissue injury and the degree of phagocytosis of neutrophils by macrophages (middle area of figure).	17
Figure 2.7: Cellular mechanisms of NLRP3 activation in the cytosol. ⁽⁷⁶⁾ Caspase-1 signalling following DAMP receptor activation (left) results in caspase-1 activation, which in turn cleaves pro-IL-1 β and pro-IL-18 which is released as active IL-1 β and IL-18 . Receptors for IL-1 β and IL-18 on adjacent immune cells (e.g. Killer Cells (KC); right) are then bound, initiating transcription and release of IL-6 and TNF, further propagating inflammation.	20

Figure 2.8: Mechanisms of the resolution of acute gout attacks.⁽¹⁰⁷⁾ MSU crystals phagocytosed by macrophages (left) or neutrophils (right) results in the initiation of inflammation. NETosis (right) results in sequestration of MSU crystals and the inactivation of pro-inflammatory cytokines.....24

Figure 2.9: Parallel oxidation-reduction cycles for bilirubin and GSH proposed by Sedlak and Snyder.⁽³⁹⁾27

Figure 2.10: Hypothesised mechanisms of UCB oxidation via direct interaction with superoxide (left) vs loss of hydride anion (right).⁽¹²⁵⁾29

Figure 2.11: Chemical structure of BV plus HPLC/ESI-MS/MS chromatogram and product ion spectra for the 583 m/z BV ion indicating that the 297 m/z ion is the major fragment.⁽¹³⁶⁾.....36

Figure 2.12: Differences in structure (circled) of UCB and its internal standard, mesobilirubin (MBR).⁽¹³⁹⁾ The vinyl groups on the terminal pyrroles have been substituted for ethyl groups, resulting in a +4[H] increase in the mass, while keeping similar organic properties.37

Figure 4.1: Extracted ion chromatogram of intestinal contents obtained from a rat receiving 1 (27 mg/kg), 180 mins after i.d. administration (TOP) and an animal administered saline (BOTTOM). The red chromatogram represents UV absorbance at 440 nm and serves as a point of reference for identified ions. The green chromatogram represents the extracted ion chromatogram for m/z 663.2230 ±0.5 and 581.2420 ±0.5. The 581.2420 m/z ion (1) only appears at 9.78 minutes. The compounds eluting at 4.26 min and 8.76 m min were presumed to be BV metabolites (3 and 2 respectively).44

Figure 4.2: Mass spectra (left) and UV spectra (right) of each identified peak in Figure 4.1. The 663.2233 and 663.2205 m/z ions were observed to be the major abundant ion under peaks 2 and 3, with these peaks exhibiting a λ_{max} of 440 nm and 416 nm respectively. The 380 nm peak (1) demonstrates a mass and absorbance spectra consistent with 1.45

Figure 4.3: Extracted ion chromatogram (left; 663.2169 m/z ±0.5) and MS spectra (right) of intestinal contents obtained from a rat receiving 1 (27 mg/kg), 180 mins after i.d. administration. The 663.2178 and 663.2174 m/z ions were observed to be the major abundant ion under peaks 2 and 3, respectively (green MS spectra, top right). 1 was also identified with an m/z of 581.2442 (blue spectra, bottom right). As previously mentioned, the m/z for 1_{calculated} is 581.2406 [M-H], implying a ppm mass accuracy of <7 ppm.45

Figure 4.4: Extracted Ion Chromatogram (left) and mass spectra (right) of *C. youngae* culture treated with 1 (663.2130 m/z ±0.5; C+BV; blue; TOP), 1 without culture (581.2406m/z ±0.5; NC+BV; purple; MIDDLE)

and the *C. youngae* culture without 1 added (581.2406 and 663.2130 m/z \pm 0.5; C+NB; black; BOTTOM). The 581.2407 and 581.2409 m/z ions were the major abundant ions under peak 1 [M-H]⁻ (<1 ppm mass accuracy), and the 663.2122 and 663.2116 m/z ions were the major abundant ion under peaks 2 and 3, respectively.46

Figure 4.5: Chromatogram and related spectra of synthesised 2 (BRS; high resolution mass spectrometry mode). The red chromatogram represents UV absorbance at 440 nm and serves as a point of reference for identified ions. The superimposed chromatogram represents extracted ion chromatograms for 663.2130 and 581.2406 m/z \pm 0.5. It should be noted that the 581.2451 m/z ion only appears at 9.7 minutes. The 663.2150 and 663.2158 m/z ions were observed to be the major abundant ion under peaks (2) and (3) at 440 nm and 412 nm respectively.47

Figure 4.6: Comparison of fragmentation spectra for samples containing 2. The spectra show CID fragmentation at 20V from multiple product ion scans, displayed to 2 decimal places for the targeted ~663.2150 m/z [M-H]⁻ ion collected from 1 treated rat duodena (A), from 1 treated bacterial assay (B) and from bilirubin-10-sulfonate chemical synthesis (C). Fragmentation of the 581.24 m/z ion (1) found in the bacterial assay control (no culture with 1 added) is shown (D) for comparison. Major fragments of 239.12/285.12/493.26/537.25/ 581.24 m/z were found in high abundance in all spectra. Note the m/z in this figure are displayed to 2 decimal places for clarity and ease of comparison.48

Figure 4.7: Putative structure for sulfonated BV (bilirubin-10-sulfonate; 2) with CID fragmentation pathway. The 663.215 m/z ion [M-H]⁻ first loses H₂SO₃. As a result of this neutral loss, the product ion 581.252 m/z [M-H-H₂SO₃]⁻ implies the formation of 1. The product ions then follow a similar fragmentation pattern as 1. Note the m/z in this figure are displayed to 3 decimal places, to demonstrate accurate mass of the fragments.49

Figure 4.8: FRAP analysis of 2 (BRS), ASC, 1 (BV) and BRDT (0-100 μ M; n = 3) in both aqueous (left) and serum (right). Aqueous 2 reduces 3.819 molar equivalents of Fe³⁺-TPTZ, while ASC reduces 1.963 molar equivalents. In serum, 2 only reduces 3.069 molar equivalents while there is little difference between aqueous ASC and serum ASC (1.963 vs 1.991 molar equivalents, respectively). Related tetrapyrroles (1 and BRDT) both had more reductive potential than 2 (p<0.05) in serum, however there was no significant difference in the reductive potential between aqueous 1 and 2. One way ANOVA and Fisher's LSD was used to make multiple comparisons, p<0.05 was considered significant.50

Figure 4.9: Formation of BRS (2) over time, after addition of BV (1) to duodenal chyme.59

Figure 4.10: ¹H NMR (400 MHz, DMSO-*d*₆): δ10.21 – 10.08 (m, 2 H, 2 × COOH); 6.81 – 6.72 (m, 1H, H-18α);
6.52 (dd, 1H, *J*_{3α,3β cis} 17.5, *J*_{3α,3β trans} 11.5 Hz, H-3α); 6.14 (dd, 1H, *J*_{3β cis,3β trans} 2.7 Hz, H-3β *cis*); 6.07 (br s, 2
H, H-5, H-15); 5.61 – 5.57 (m, 2 H, H-18β); 5.24 (dd, 1 H, H-3β *trans*); 5.19 (s, 1H, H-10); 4.13 – 2.90 (br s,
4 H, 4 × NH); 2.70 – 2.45 (m, 6 H, H8α, H-8β, H12α); 2.20 – 1.93 (m, 11 H, H-7α, H-12β, H-13α, H-17α);
1.85 (s, 3 H, H-2α). ¹³C NMR (100 MHz, DMSO-*d*₆): δ178.1, 172.0, 171.2, 171.2 (C-1, C-8γ, C-12γ, C-19);
142.7, 140.9, 130.8, 130.0, 129.8, 129.6, 127.8, 127.5, 124.6, 123.6, 123.5, 123.4, 123.3, 122.7, 122.7,
122.2, 121.7, 121.5, 117.9 (C-2, C-3, C-3α, C-3β, C-4, C-5, C-6, C-7, C-8, C-9, C-11, C-12, C-13, C-14, C-15,
C-16, C-17, C-18, C-18α, C-18β); 101.0, 100.3 (C-5, C-15); 54.8 (C-10); 36.1 (C-8β, C-12β); 21.6 (C-2α);
20.4 (C-8α); 20.4 (C-12α); 10.0, 10.0, 9.8 (C-7α, C-13α, C-17α). HRMS calculated for C₃₃H₃₅N₄NaO₉S [*M*-
Na], 663.212477; found ESIMS (*m/z*): 663.2150 [*M*-Na]⁻. (<5 ppm mass accuracy)..... 60

Figure 5.1: Effect of i.v. treatment with BRS (A, B; n=6) and BV (C, D; n=5) on the plasma concentration (left
panels) of BRS, BV and UCB; and total bile pigment excretion rate (right panels; BDG, BMG, BV and BRS
in stacked columns; left column is compound treatment and right column is compound treatment)
over 180 minutes. Data points in A and C correspond with plasma concentrations at 0, 5, 10, 15, 20, 30,
60, 90, 120 and 180 minutes. 73

Figure 5.2: Effects of i.p. treatment with BRS (A, B) and BV (C, D) on the plasma concentration (left panels) of
BRS, BV and UCB; and total bile pigment excretion rate (right panels; BDG, BMG, BV and BRS in
stacked columns; left column is compound treatment and right column is compound treatment). Data
points in A and C correspond with plasma concentrations at 0, 15, 30, 60, 90, 120, 150 and 180
minutes. 76

Figure 5.3: Effects of i.d. treatment with BRS (A, B) and BV (C, D) on the plasma concentration (left panels) of
BRS, BV and UCB; and total bile pigment excretion rate (right panels; BDG and BMG stacked columns;
left column is compound treatment and right column is compound treatment). Data points in A and C
correspond with plasma concentrations at 0, 15, 30, 60, 90, 120, 150 and 180 minutes. 78

Figure 5.4: Cumulative biliary excretion of bile pigments after i.v. (A), i.p. (B) and i.d. (C) administration of
BRS and BV. For neatness, SEM bars on the cumulative excreted dose data in each graph are shown in
one direction. 80

- Figure 6.1:** A representative scanning electron microscope image of monosodium urate crystals used to induce sterile inflammation within the air pouch model.97
- Figure 6.2:** Effects of 27 mg kg⁻¹ i.p. pre-treatment of BRS (n=6, orange) and BV (n=5, blue) on leukocyte infiltration (A) and neutrophil infiltration (B) following MSU administration (25 mg in 5 mL sterile saline) to a 6 day old air pouch model of acute inflammation. Ibuprofen (8.11 mg kg⁻¹ i.p. molar equivalent to BRS) was administered as a positive control (IBU n=5, grey), and PBS (3.5 mL, i.p.) was administered as a negative control (MSU only n=5, black). The sham group (SHAM, white) was pre-treated with 3.5 mL PBS i.p. and received 5 mL of saline into the pouch instead of MSU. * denotes significant difference (p < 0.05) compared to MSU only, † denotes significant difference (p < 0.05) compared to BRS at the same timepoint and ‡ denotes significant difference (p < 0.05) compared to BV for the same time point. From 6-48 h, the sham group was significantly lower than MSU only (not shown with symbol for neatness). Data are presented as mean ± SEM.104
- Figure 6.3:** Effects of 27 mg kg⁻¹ i.p. pre-treatment of BRS (n=6, orange) and BV (n=5, blue) on monocyte infiltration (A) and lymphocyte infiltration (B) following MSU administration (25 mg in 5 mL sterile saline) to a 6 day old air pouch model of acute inflammation. Ibuprofen (8.11 mg kg⁻¹ i.p., molar equivalent to BRS) was administered as a positive control (IBU n=5, grey), and PBS (3.5 mL, i.p. n=3) was administered as a negative control (MSU only, n=5, black). * denotes significant difference (p < 0.05) compared with VEH, † denotes significant difference (p < 0.05) compared to BRS. From 12-48 h, the sham group was significantly lower than MSU only (not shown with symbol for neatness). Data are presented as mean ± SEM.....105
- Figure 6.4:** Effects of 27 mg kg⁻¹ i.p. pre-treatment of BRS (n=6, orange) and BV (n=5, blue) on concentrations of IL-6 (A), MCP-1 (B), GM-CSF (C) and IL-18 (D) in pouch exudate following MSU administration (25 mg in 5 mL sterile saline) to a 6 day old air pouch model of acute inflammation at the 6 h time point. * denotes p < 0.05 (ANOVA) compared with MSU only (black). Data are presented as mean ± SEM.107
- Figure 6.5:** Effects of 27 mg kg⁻¹ i.p. pre-treatment with MSU only (n=5, black), BRS (n=6, orange) and BV (n=5, blue) on concentrations of chloramine expressed in nmol chloramine per mg of protein in pouch exudate following MSU administration (25 mg in 5 mL sterile saline) into the 6 day old air pouch at the 24 h time point. No significant differences were detected between groups. Data are presented as mean ± SEM.....108

Figure 6.6: Effects of 27 mg kg⁻¹ i.p. pre-treatment with MSU only (n=5, black), BRS (n=6, orange) and BV (n=5, blue) on concentrations of protein carbonyl (nmol carbonyl per mg of protein) in pouch exudate following MSU administration (25 mg in 5 mL sterile saline) into the a 6 day old air pouch. Data are presented as mean ± SEM..... 109

Figure 6.7: Effects of 27 mg kg⁻¹ i.p. pre-treatment of BRS (n=6, A, left) and BV (n=5, B, right) on serum concentrations of BRS, BV and UCB. Data is omitted where compound concentrations were not detectable. Data are presented as mean ± SEM..... 110

Figure 6.8: Effects of 27mg kg⁻¹ i.p. BRS pretreatment of (n=6) on exudate BRS concentrations. BV and MSU only treatment had no quantifiable bile pigment concentrations..... 111

Figure 6.9: Concentrations of cytokines in pouch exudate at 6 h were determined using a multiplexed bead-based flow cytometric immunoassay..... 119

List of Tables

Table 1: Recent studies measuring anti-inflammatory cytokines in BV and UCB in rodent models of inflammation/wound healing	32
Table 2: Pharmacokinetic parameters in the systemic venous circulation after i.v., i.p. and i.d. administration of BRS and BV.	74

List of Abbreviations and Symbols

AA	Arachidonic Acid
%	Percentage
~	Approximately
Δ	delta
$^{\circ}\text{C}$	Degrees Celsius
μ	micro
A	alpha
AggNET	Aggregated NETs
amu	Atomic Mass Units
APR	Acute Phase Response
AUC ₁₈₀	Area Under the Curve over 180 minutes
BDG	Bilirubin Diglucuronide
BMG	Bilirubin Monoglucuronide
BP	Bile Pigment
BPC	Base Peak Chromatogram
BRDT	Bilirubin Ditaurate
BRS	Bilirubin-C10-sulfonate
BV	Biliverdin
BVR	Biliverdin Reductase
C	Carbon
C ₀	Theoretical concentration at time 0
CID	Collision Induced Dissociation
CO	Carbon monoxide
C _{peak}	Peak concentration
CV	Coefficient of Variation
CVD	Cardiovascular Disease
CXCL1	Chemokine ligand-1
γ	gamma
DAMP	Damage Associated Molecular Pattern
deg	Degrees

DMSO	Dimethyl Sulfoxide
DNA	Deoxyribonucleic Acid
e.g.	Example
EDTA	Ethylenediaminetetraacetic Acid
EIC	Electron Ion Chromatogram
ESI	Electrospray Ionisation
EU	Endotoxin Unit
FRAP	Ferric Reducing Ability of Plasma
G	Gauge
g	Gram/s
G-CSF	Granulocyte Colony Stimulating Factor
GM-CSF	Granulocyte/Monocyte Colony Stimulating Factor
GS	Gilbert's Syndrome
H ₂ O ₂	Hydrogen Peroxide
HCl	Hydrochloric acid
HO	Haem Oxygenase
HO-1	Haem Oxygenase-1
HOCl	Hypochlorous acid
HPLC	High Performance Liquid Chromatography
HSO ₃ ⁻	Bisulfite
i.d.	Intraduodenal or intraduodenally
i.e.	In other words
i.p.	Intraperitoneal or intraperitoneally
i.v.	Intravenous or intravenously
IBU	Ibuprofen
ICAM-1	Intercellular Adhesion Molecule-1
ID	Internal Diameter
IFN	Interferon
Ig	Immunoglobulin
IL	Interleukin
iNOS	Inducible nitric oxide synthase

IRI	Ischemia Reperfusion Injury
IU	International Unit
k	kilo
K_a	Dissociation constant
K_{dist}	Distribution constant
K_{elim}	Elimination constant
L	Litre
LAL	Limulus Amebocyte Lysate
LCMS	Liquid Chromatography Mass Spectrometry
LDL	Low Density Lipoprotein
LHS	Left Hand Side
LOD	Limit of Detection
LOQ	Limit of Quantification
LPS	Lipopolysaccharide
m	milli
M	Molar
m/z	Mass to Charge ratio
mBRS	Meso Bilirubin-C10-Sulfonate
mBV	Meso Biliverdin
MCP-1	Monocyte Chemoattractant Protein-1
M-CSF	Macrophage Colony stimulating factor
MeOH	Methanol
mg	milligram
Milli-Q	Ultrapure water
min	Minute(s)
MIP	Macrophage Inflammatory Protein
MP	Mobile Phase
MPO	Myeloperoxidase
mRNA	Messenger RNA
MRP2	Multidrug Resistance Protein-2
MSU	Monosodium Urate

mUCB	meso Unconjugated Bilirubin
n	nano
N ₂	Nitrogen
NaBV	Sodium biliverdinate
NaCl	Sodium chloride
NADPH	Nicotinamide Adenine Dinucleotide
NaOH	Sodium Hydroxide
NLRP3	Nucleotide-binding-domain Like Receptor Protein 3
nm	nanometres
NMR	Nuclear Magnetic Resonance
NO	Nitric Oxide
O ₂	Oxygen
O ₂ ⁻	Superoxide
OATP	Organic Anion Transporting Polypeptide family
OD	Outside Diameter
p	pico
PBS	Phosphate Buffered Saline
pH	Potenz-hydrogen
PK	Pharmacokinetics
Q-TOF	Quadrupole – Time of Flight
R	Receptor
R ²	Correlation coefficient
RBC	Red Blood Cell
RHS	Right Hand Side
RNA	Ribo-Nucleic Acid
RNS	Reactive Nitrogen Species
ROS	Reactive Oxygen Species
RPM	Revolutions Per Minute
RT	Room Temperature
s.c.	Subcutaneous
S ₄ O ₆ ²⁻	Tetrathionate

SD	Standard Deviation
Sec	Second(s)
SEM	Standard Error of the Mean or Scanning Electron Microscope
SIM	Single Ion Monitoring
SOD	Superoxide Dismutase
β	Beta
t_0	Time 0/baseline
$t_{1/2\beta}$	Elimination half life
$t_{1/2\alpha}$	Distribution half life
TGF- β	Tumour Growth Factor- β
TLR4	Toll-Like Receptor-4
TMS	Tandem Mass Spectrometry (also referred to as MS/MS)
TNFR	TNF receptor
TNF	Tumour Necrosis Factor
TPTZ	Tripyridyl Triazine
UA	Uric Acid
UCB	Unconjugated Bilirubin
UDP	Uridine Phosphate
UGT1A1	Uridine Glucuronosyl Transferase 1A1
UHPLC-MS	Ultra High Pressure Liquid Chromatography coupled to Mass Spectrometry
V	Volts
VCAM-1	Vascular cell adhesion molecule-1
V_d	Volume of distribution
vs	Versus
W	Watts
λ	lambda
λ_{max}	Maximal light absorption

Authorship Statement

ALL PAPERS INCLUDED ARE CO-AUTHORED

Acknowledgement of Papers included in this Thesis

Section 9.1 of the Griffith University Code for the Responsible Conduct of Research (“Criteria for Authorship”), in accordance with Section 5 of the Australian Code for the Responsible Conduct of Research, states:

To be named as an author, a researcher must have made a substantial scholarly contribution to the creative or scholarly work that constitutes the research output, and be able to take public responsibility for at least that part of the work they contributed. Attribution of authorship depends to some extent on the discipline and publisher policies, but in all cases, authorship must be based on substantial contributions in a combination of one or more of:

- conception and design of the research project
- analysis and interpretation of research data
- drafting or making significant parts of the creative or scholarly work or critically revising it so as to contribute significantly to the final output.

Section 9.3 of the Griffith University Code (“Responsibilities of Researchers”), in accordance with Section 5 of the Australian Code, states:

Researchers are expected to:

- Offer authorship to all people, including research trainees, who meet the criteria for authorship listed above, but only those people.
- accept or decline offers of authorship promptly in writing.
- Include in the list of authors only those who have accepted authorship
- Appoint one author to be the executive author to record authorship and manage correspondence about the work with the publisher and other interested parties.
- Acknowledge all those who have contributed to the research, facilities or materials but who do not qualify as authors, such as research assistants, technical staff, and advisors on cultural or community knowledge. Obtain written consent to name individuals.

Included in this thesis are papers in *Chapters 4, 5 and 6* which are co-authored with other researchers. My contribution to each co-authored paper is outlined at the front of the relevant chapter. The bibliographic details (if published or accepted for publication)/status (if prepared or submitted for publication) for these papers including all authors, are:

(Where a paper(s) has been published or accepted for publication, you must also include a statement regarding the copyright status of the paper(s).

Chapter 4: Published – Open Access - <https://doi.org/10.1038/s41598-019-39548-w>

This article is licensed under a Creative Commons Attribution 4.0 International License, which permits use, sharing, adaptation, distribution and reproduction in any medium or format, as long as you give appropriate credit to the original author(s) and the source, provide a link to the Creative Commons

license, and indicate if changes were made. The images or other third party material in this article are included in the article's Creative Commons license, unless indicated otherwise in a credit line to the material.

Chapter 5: Prepared and submitted for publication in European Journal of Pharmaceutical Sciences

Chapter 6: Prepared and submitted for publication in European Journal of Pharmaceutical Sciences

Appropriate acknowledgements of those who contributed to the research but did not qualify as authors are included in each paper.

(Signed) _____ (Date) 10/02/20

Ryan G. Shiels

(Countersigned) (Date) 09/02/2020

Supervisor: Andrew Bulmer

Thesis Organisation

This thesis has been divided into three main studies. Chapter 4 contains study one and describes the discovery of a novel biliverdin (BV) metabolite, titled “Unprecedented Microbial Conversion of Biliverdin into Bilirubin-10-sulfonate” (published). Once we were able to identify and synthesise bilirubin-10-sulfonate (BRS), we tested its pharmacokinetics. Chapter 5 contains study two (submitted for publication) titled “Pharmacokinetics of Bilirubin-10-sulfonate and Biliverdin: the potential therapeutic administration of a novel tetrapyrrole” and investigates the pharmacokinetics of BV and BRS in Wistar rats. This study found that BRS had a favourable pharmacokinetic profile, and thus we tested BRS for the first time in a rat pouch model of sterile inflammation. Chapter 6 contains the third study (submitted for publication) entitled “Biliverdin and bilirubin sulfonate inhibit monosodium urate induced sterile inflammation in the rat” and investigates the anti-inflammatory properties of BV and BRS following monosodium urate induced inflammation in the rat. This study demonstrated the anti-inflammatory effects of BRS and BV in this model and indicates that BRS may prove beneficial in the treatment of monosodium urate induced sterile inflammation.

Chapter One: A General Introduction

Historically, biliverdin (BV) and bilirubin (UCB; unconjugated bilirubin), also known as bile pigments, have been viewed as waste products from the physiological degradation of haem. However, a recent paradigm shift in the last decade has occurred in this field, asserting multiple beneficial physiological effects of BV and the haem catabolic pathway.⁽²⁻⁸⁾

The current body of knowledge regarding bile pigment metabolism indicates that BV is chemically reduced to UCB via a cytosolic enzyme biliverdin reductase (BVR) prior to excretion. Recently, an additional route of BV metabolism may have been discovered in rats

following intraduodenal administration of BV.⁽¹⁾ Following BV administration, three unknown metabolites were discovered in the blood, bile, urine and duodenum, which clearly differed from that of UCB. For example, all compounds eluted well before UCB (i.e. <10 mins, when UCB elutes at 20 mins) during HPLC analysis. The unidentified compound spectral characteristics also differed from that of UCB (i.e. λ max 420-450 nm, versus 450 nm for UCB). This revealed a very exciting and novel finding, suggesting an additional metabolic pathway for BV exists *in vivo*. Furthermore, this pathway of BV metabolism may partly explain some of BV's pharmacological effects after oral administration, and this information could be used to guide the development of a therapy for treatment of inflammatory pathology.

Biliverdin and UCB are formed after trauma (i.e. during bruising when haemoglobin enters the tissues and is broken down by sentinel/infiltrating macrophages). Trauma is accompanied by an initial inflammatory and wound healing response.⁽⁹⁾ The function of inflammation is to remove invading pathogens and damaged cells, and to assist in stimulating an appropriate regenerative/healing response. However, when inflammation becomes chronic or pathologic (i.e. repeated trauma or insult), it can cause significant damage to tissues with the resulting fibrosis potentially leading to organ dysfunction. Chronic inflammation is implicated in the pathogenesis of many diseases including cardiovascular disease, cancer as well as liver and kidney failure.⁽¹⁰⁾ Drugs that can reduce or eliminate chronic inflammation are highly valued and sought after in the current pharmaceutical market, because incurable chronic conditions including cystic fibrosis and rheumatoid arthritis are underpinned by chronic inflammation and are poorly managed using existing therapies.⁽¹¹⁾ A new class of anti-inflammatory pharmaceuticals could significantly reduce the social and economic burden of these diseases world-wide.

The administration of BV or its metabolites to humans could theoretically assist in preventing and treating disease. However, before assessing the anti-inflammatory potential of BV metabolites in animals and humans, these molecules must be isolated and characterised. This thesis aimed to identify and characterise these novel BV metabolites, and investigate their pharmacokinetics and therapeutic potential in an animal model of sterile inflammation.

Chapter Two: A Review of the Literature

2.1 Evolution of Haem

In order for multi-cellular life to flourish, eukaryotes are believed to have developed a highly efficient process to transport oxygen between cells in order for mitochondria to use this oxygen as a terminal electron receptor in the process of creating ATP via oxidative phosphorylation through electron transport, the endpoint of aerobic cellular respiration.⁽¹²⁾ Haem is synthesised in the mitochondria and cytosol of erythrocytes (red blood cells; RBCs) which are themselves produced in bone marrow⁽¹³⁾ and this haem is then bound to globin chains and stored in RBCs. Each RBC contains 200-300 million molecules of haemoglobin, and the process of oxygen delivery in humans is accomplished by roughly 60 - 90 trillion red blood cells that circulate throughout the body every minute.⁽¹³⁾ With a finite lifespan approximating 115 days⁽¹⁴⁾, senescent RBCs contribute approximately 75% of all physiological haem, with the remainder sourced via ineffective erythropoiesis and heme-containing enzymes.⁽¹⁵⁾

2.2 Haem Catabolism

While regularly exposed to different forms of insult, including mechanical to oxidative stress, mature RBCs lack nuclei and thus cannot synthesise regenerative capacity of other mammalian cells. This leaves them susceptible to irreversible damage and potential rupture⁽¹⁶⁾, resulting in an average lifespan of 120 days. As haem itself is toxic, mammals have evolved a metabolic pathway to catabolise haemoglobin which serves as a protective mechanism, to avoid toxicity and tissue damage associated with RBC lysis.⁽¹⁷⁾ In cases of severe or persistent haemolysis, an increase in haem transport to the kidney induces cell death via oxidative injury, demonstrating the importance of degrading excess haem.⁽¹⁸⁾

The reticulo-endothelial system, involving hepatic Kupffer cells and splenic macrophages, capture old or damaged RBCs along with free haemoglobin and catabolise the globin component of haemoglobin, resulting in the release of free haem. Haem Oxygenase-1 (HO-1) is the inducible isoform of Haem Oxygenase (HO) and is responsible for the catabolism of free haem via oxidative cleavage of the haem group, resulting in the release of biliverdin (BV; a linear tetrapyrrole or bile pigment), carbon monoxide (CO; either bound by haemoglobin or acting as a substrate for soluble guanylate cyclase⁽¹⁹⁾) and ferrous iron.⁽²⁰⁾ In addition to HO-1, an array of carrier proteins such as haptoglobin and haemopexin can bind haem with high affinity and subsequently transport it to the liver for catabolism and excretion, assisting with removal of excess haem.⁽²¹⁾

2.3 Bile Pigment Metabolism and Excretion

In mammals, the central methine bridge at carbon 10 on BV is reduced to unconjugated bilirubin (UCB; Figure 2.1, C10 bridge identified by γ) by cytosolic biliverdin reductase-a (BVR-A)⁽²²⁾ and this lipophilic UCB then diffuses out of the cell and binds to circulating albumin and is delivered to the liver where it is actively and passively absorbed into hepatocytes as a complex with albumin, prior to its conjugation and excretion in bile (Figure 2.2).⁽²³⁾

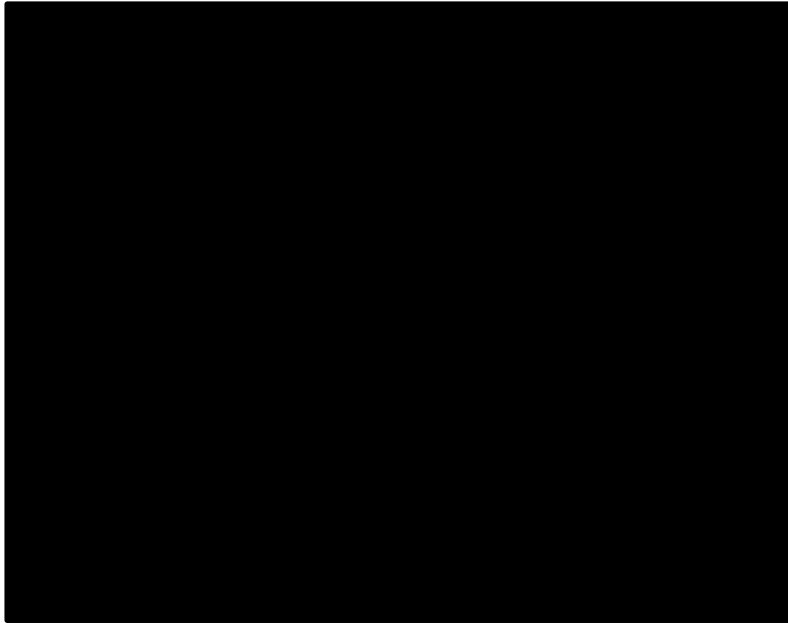


Figure 2.1: Catabolism of haem by haem oxygenase to biliverdin and unconjugated bilirubin.⁽¹⁷⁾

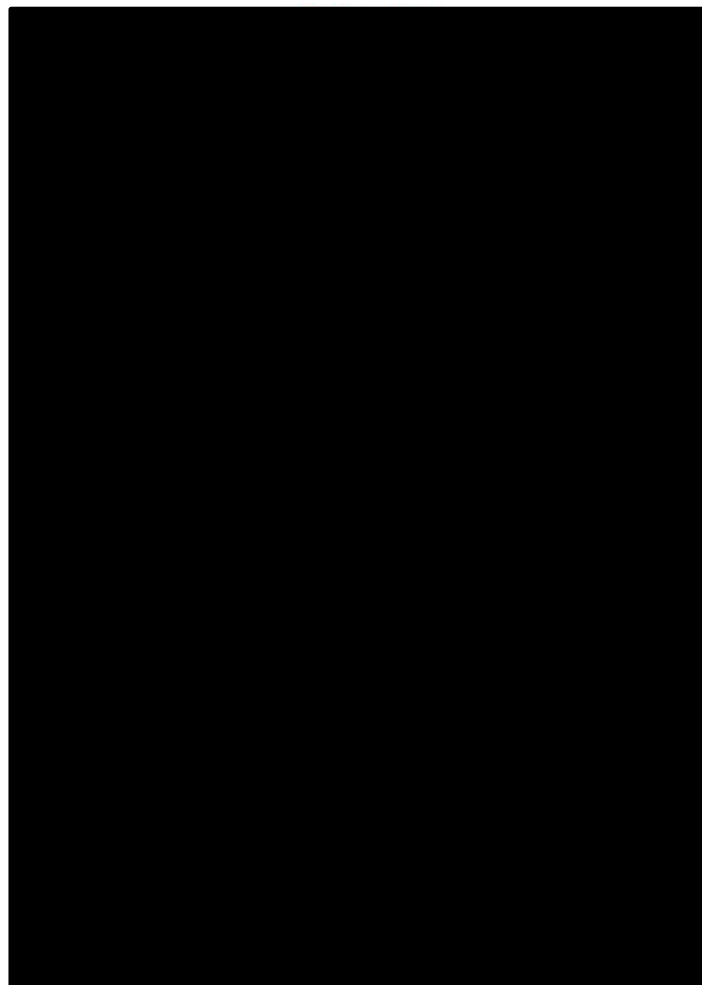


Figure 2.2: Human metabolic pathways of haem and its metabolites BV/UCB.⁽²⁴⁾ Haem liberated from cells via RBC catabolism (1) is metabolised to BV, where BVR converts it to

UCB prior to binding with albumin. It is then transported to the liver (2), where hepatic uptake occurs (3). UCB is then conjugated (4) to bilirubin mono and di glucuronide (BMD/BDG) prior to biliary excretion, ending in excretion via faeces (5). Enterohepatic circulation also occurs (6) in the intestine as bacterial β -glucuronidase deconjugated BMG/BDG forming UCB which is then able to be reabsorbed by the intestine (back to (2)).

Prior to its excretion in the bile, UCB is bound to ligandin and Z protein, transported to the endoplasmic reticulum (ER) and glucuronidated by uridine glucuronosyltransferase 1A1 (UGT1A1).⁽²⁵⁾ Following its glucuronidation, multidrug resistance-related protein 2 (MRP2) transports the conjugated bilirubin (mono and di-glucuronides) into the bile canaliculus, consuming ATP in the process.⁽²⁵⁾ These bilirubin conjugates are then excreted into the duodenum via the common biliary duct⁽²⁶⁾ where β -glucuronidases found in both *Clostridia* spp. & *Bacteroides fragillis* deconjugate some bilirubin glucuronide in the distal ileum and colon, forming UCB.^(27, 28) Unconjugated bilirubin is then either re-absorbed via the enterohepatic circulation or is oxidised/reduced in a multi-step process yielding a plethora of linear tetrapyrroles (Figure 2.3) which contribute to the colouration of stool and urine.⁽²⁸⁾ In mammals, this pathway allows for the safe and effective catabolism and excretion of haem. Additionally, these linear tetrapyrroles may become trapped in the gall bladder, most abundantly in the form of calcium hydrogen bilirubinate, leading to the formation of black or brown gallstones.⁽²⁹⁾

Interestingly, the haem catabolic pathway in birds, reptiles and many fish share many similarities with mammals with one important distinction; the haem catabolic pathway terminates with BV instead of UCB in these animals.⁽³⁰⁻³²⁾ Conjugated BV has also been reported to be present in the bile of some fish⁽³⁰⁾, although it is excreted intact in mammals.⁽¹⁾

A key difference between these animals is that mammals generally give birth to live young, whereas birds, reptiles and fish tend to lay eggs which are exposed to atmospheric oxygen during gestation. Mammals however, give birth to live young and have acquired an additional NADPH-consuming metabolic step in order to reduce the C10 bridge of biliverdin to form bilirubin.^(15, 22) Interestingly, concentrations of UCB are elevated in human neonates (86–103 μM average in neonatal serum⁽³³⁾ vs 8.6–17.1 μM in adults) and this is hypothesised to protect the lungs from injury, based upon UCB's potent antioxidant effects, during the transition from placental to air breathing in the first minutes of life.^(34, 35)

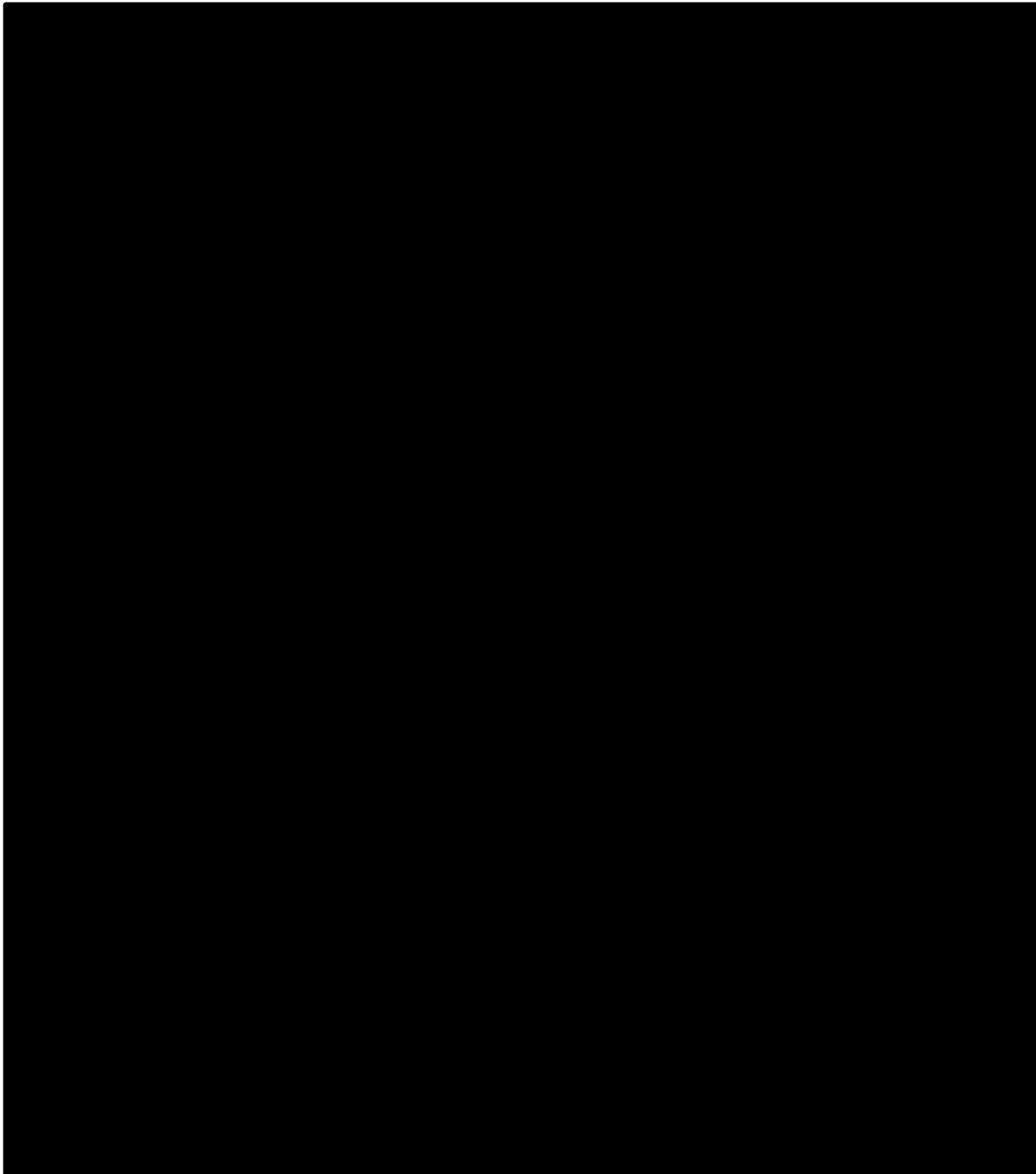


Figure 2.3: Structures and masses resulting from the sequential reduction/oxidation of UCB by the intestinal microflora.⁽²⁸⁾

2.4 Recent Discoveries in Bile Pigment Metabolism

Recent research regarding bile pigment metabolism in the larval American bullfrog (*Rana catesbiana*) is of particular interest. It does not produce UCB or bilirubin glucuronides, but rather it forms a related polar linear tetrapyrrole, bilirubin-10-sulfonate (BRS) from BV.⁽³⁶⁾ Intriguingly, BRS is reportedly excreted intact in the bile of the frog, but not in the rat.⁽³⁶⁾ The authors further report that i.v. administration of BV or frog haemoglobin to bullfrogs leads to

biliary excretion of BRS suggesting hepatic formation of BRS occurs by the enzymatic addition of HSO_3^- anion to BV in the frog liver. Furthermore, the bullfrog exhibits great tolerance against freezing⁽³⁷⁾, and bullfrog tadpoles (*Lithobates catesbeiana*) exhibit high tolerance towards Paraquat toxicity, which catalyses the formation of reactive oxygen species (ROS), specifically superoxide anions.⁽³⁸⁾ This is of particular note given the antioxidant status of bile pigments, including bilirubin and biliverdin.⁽³⁹⁻⁴³⁾

Unfortunately, no further literature regarding BRS *in vivo* has been published since the short 1995 report. Furthermore, the published data presented above is mentioned briefly in the source article with little data available⁽³⁶⁾, representing a gap in the literature regarding this compound relating to its formation, pharmacokinetics and therapeutic benefit in mammals.

2.5 Oxidative Stress

Reactive Oxygen Species (ROS) such as superoxide radicals (O_2^-), hydrogen peroxide (H_2O_2), hydroxyl radicals ($\cdot\text{OH}$), and singlet oxygen ($^1\text{O}_2$) are generated as metabolic by-products by biological systems⁽⁴⁴⁾, for example, during cellular aerobic respiration. These ROS, produced during physiological and pathophysiological processes, cause damage to important cellular structures including proteins, lipids and nucleic acids and thus is it imperative that biological systems maintain adequate antioxidant defences.⁽⁴⁵⁾ It is also important to address ROS subtypes, as antioxidant compounds may be either a selective or general ROS scavenger. For example, abundant antioxidants such as glutathione and cysteine reportedly show poor reactivity toward O_2^- whereas bilirubin readily scavenges it.⁽⁴⁰⁾

Underpinning human inflammatory disease is the excessive generation of O_2^- by neutrophils, which form part of the innate immune system.⁽⁴⁶⁾ Known as the acute phase response (APR) and characterised initially by oedema caused by the infiltration of plasma proteins and

leukocytes into the affected tissue, this process results in the 'respiratory burst'. Here O_2^- , generated by NADPH oxidase occurs following phagocytosis by infiltrating neutrophils and macrophages, is transformed into other ROS such as H_2O_2 via superoxide dismutase (SOD). This H_2O_2 is used by myeloperoxidase (MPO) to produce hypochlorite (ClO^-) in the presence of Cl^- further contributing to oxidant production and the potential for cellular injury.^(47, 48) During the APR, ROS are also released into the extracellular space, causing collateral damage to host tissues and propagating further inflammation, with the potential to create a vicious cycle, if not resolved.⁽⁴⁶⁾

2.6 Inflammation

Physiologically, inflammation is considered a mechanism of innate immunity which occurs in response to tissue damage or microbial infection and serves, in an acute setting (up to 2 weeks), to remove the initial insult. This protects the host against further insult and initiates healing in order to restore homeostasis within the biological organism.⁽⁴⁴⁾ When repeated insult occurs or inflammation otherwise fails to resolve in a timely fashion, chronic inflammation is the result and the healing process is impaired causing progressive fibrosis of the affected area. Pathophysiologically, diseases with chronic inflammation at their root, such as atherosclerosis, chronic respiratory diseases, neurological disease, cancer, obesity, and diabetes, are the most significant cause of death in the modern world.⁽⁴⁹⁾

2.7 Initiation of Inflammatory Response

Immune cells of the innate immune system reside in tissues and include macrophages, mast cells, fibroblasts and dendritic cells. Also included are circulating leukocytes such as

neutrophils and monocytes.⁽⁵⁰⁾ These cells express both intracellular and surface receptors that detect both pathogen-associated molecular patterns (PAMPs) generally associated with microbial organisms, and damage-associated molecular patterns (DAMPs) that are released from injured cells.⁽⁵¹⁾ Cells undergoing lytic cell death (e.g. necrosis or pyroptosis) release their internal contents, including DAMPs (e.g. ATP, ROS, uric acid, and interleukin-1 α (IL-1 α)), into the extracellular fluid (ECF) where they activate local and circulating immune cells (Figure 2.4).⁽⁵²⁾ Once activated by DAMPs, often referred to as 'danger signals' or 'alarmins'⁽⁵³⁾, DAMP receptors initiate pro-inflammatory signalling cascades in leukocytes that in turn cause the release of pro-inflammatory cytokines promoting recruitment and chemotaxis of leukocytes to the affected region.⁽⁵¹⁾ Inflammatory responses triggered by DAMPs occur independently of microbial or pathogen invasion and this type of inflammation is referred to as sterile inflammation.⁽⁵³⁾

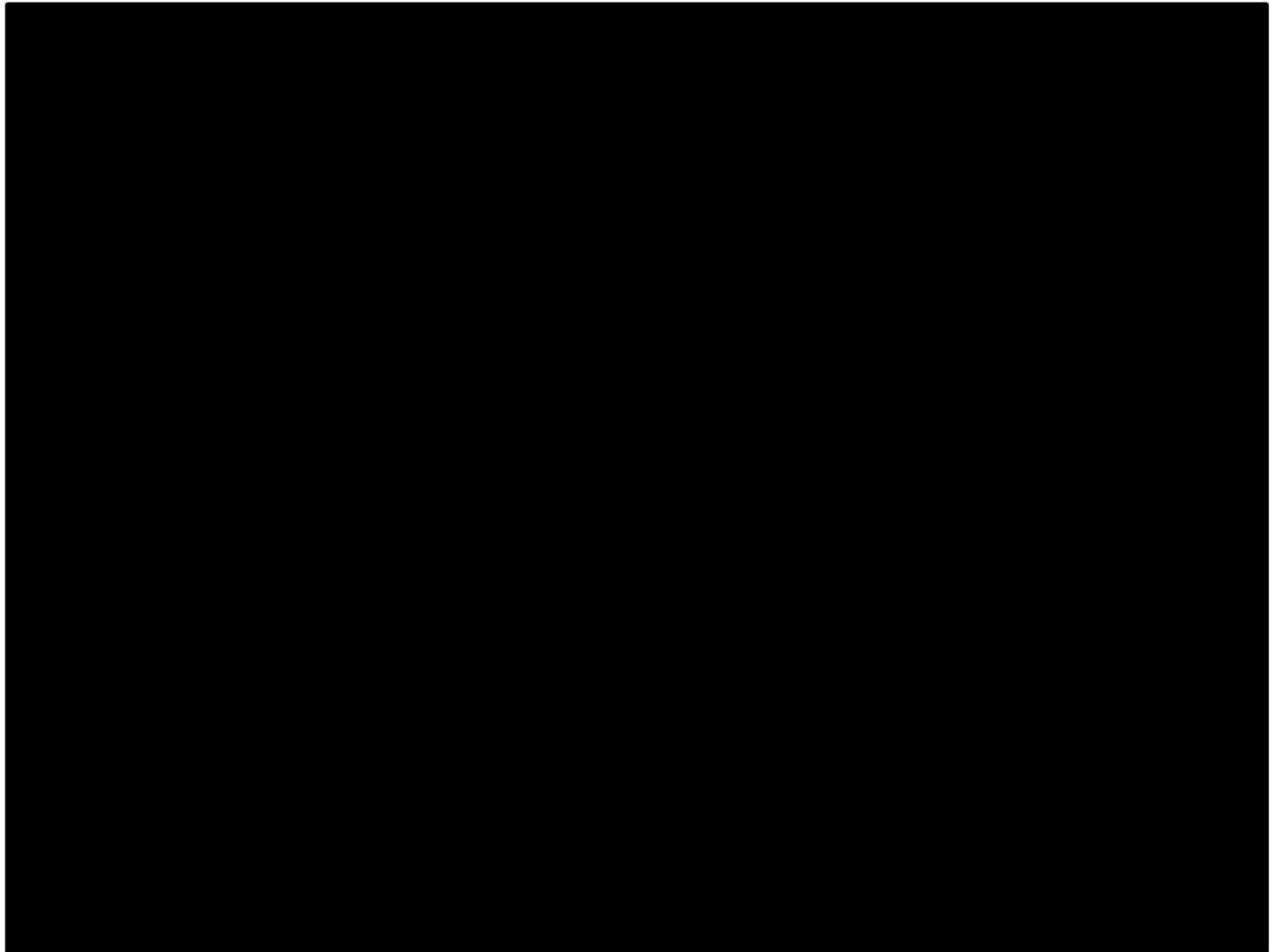


Figure 2.4: Damage associated molecular patterns (DAMPs) activate various immune cells, initiating pro-inflammatory signalling cascades observed in sterile inflammation.⁽⁵³⁾

Recent studies propose additional genetically encoded mechanisms of controlled cell death, referred to as pyroptosis and necroptosis.⁽⁵⁴⁻⁵⁶⁾ It is reported that these cell suicide mechanisms involve lytic cell death⁽⁵⁷⁾ and differ from necrosis because they are controlled by molecular signalling. While necroptosis is reportedly a backup cell death defence mechanism activated when apoptosis fails (e.g. during pathogen infection)⁽⁵⁸⁾, pyroptosis is a primary cellular response following the sensing of DAMPs.⁽⁵⁷⁾ Interestingly, pyroptosis appears to be a controlled lytic cell-suicide mechanism facilitating further DAMP release in order to directly activate immune cells and initiate a potent inflammatory response.⁽⁵⁷⁾

Pyroptosis is reportedly initiated via the NLRP3 inflammasome, which is discussed later in this literature review (Section 2.10).

2.8 Immune Cells

The acute sterile inflammation response predominantly involves the actions of immune cells such as neutrophils and macrophages as well as non-immune cells including endothelial cells (Figure 2.4).

Neutrophils

Continuously produced in the bone marrow and derived from hematopoietic stem cells that are controlled by granulocyte/macrophage colony stimulating factor (GM-CSF)⁽⁵²⁾, neutrophils are polymorphonuclear cells that circulate in blood and have a half-life of 6-11 hours. These cells wait until they are activated by inflammatory signals such as DAMPs prior to beginning the process of intravascular migration (or extravasation) where they first tether to and roll along the endothelium mediated by selectins.⁽⁵⁹⁾ Endothelial cells, themselves activated by DAMPs (figure 2.4b), express adhesion molecules such as ICAM-1⁽⁶⁰⁾ which allow neutrophils to firmly adhere to the endothelium and migrate to the site of inflammation along a chemokine gradient and crossing the endothelial layer in the process.⁽⁶⁰⁾ Once at the site of inflammation, neutrophils perform phagocytosis, release proteases, antimicrobial peptides, cytokines, ROS and MPO (Figure 2.5), potentiating and amplifying the innate immune response.⁽⁶¹⁾ While these actions serve to destroy invading pathogens, they also damage surrounding tissues in models of sterile inflammation.⁽⁵³⁾

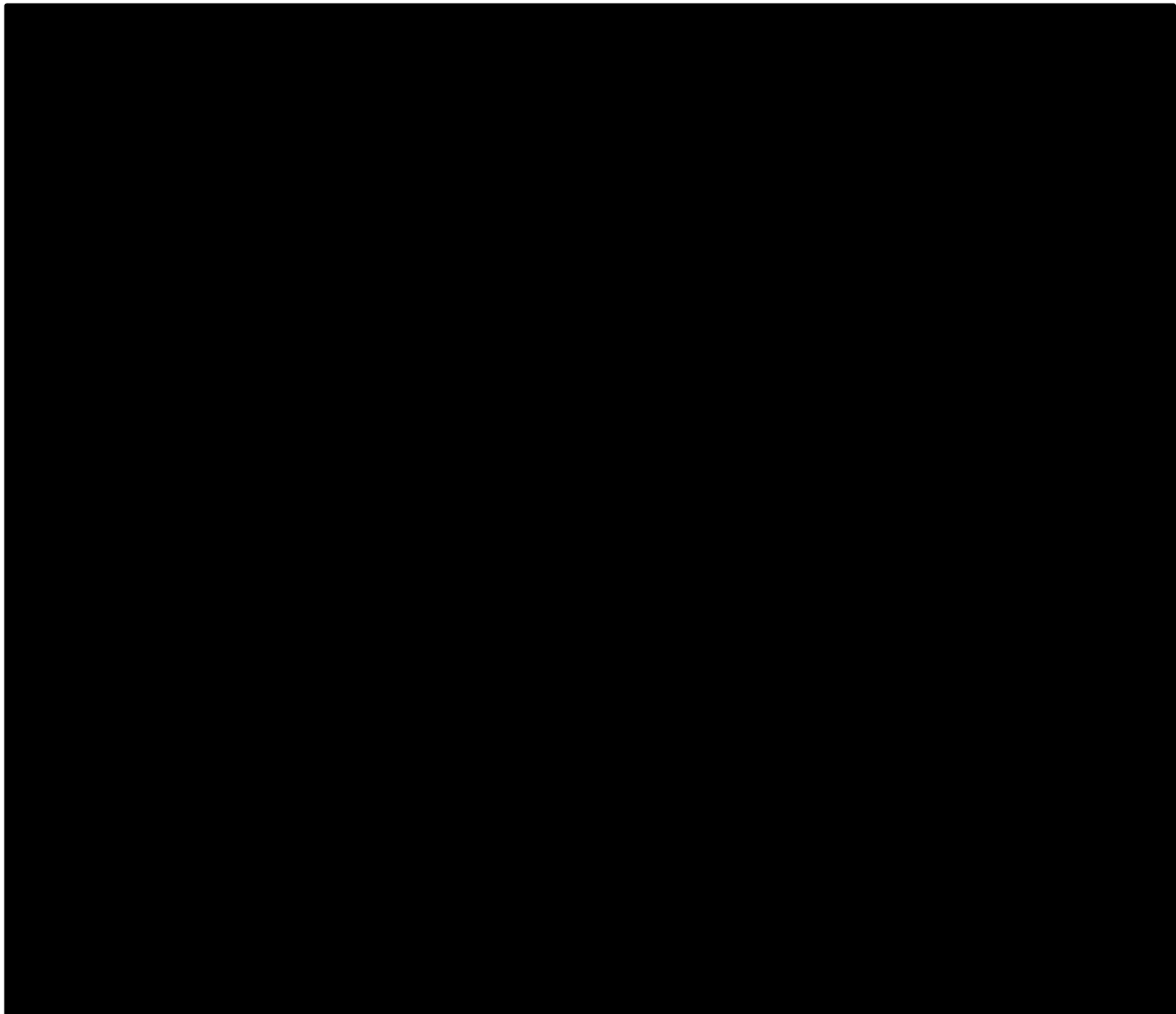


Figure 2.5: Mechanisms of neutrophils in the acute phase of inflammation.⁽⁶¹⁾ Neutrophils are developed in bone marrow (top left), released into circulation where they patrol until they are stimulated by cytokines, and as a result undergo extravasation into the affected tissue (middle right). There they produce intra and extracellular ROS via MPO release, perform phagocytosis, NETosis, and participate in downstream signalling via further cytokine release.

Macrophages

Macrophages originate from monocytes that differentiate when stimulated by colony stimulating factors (GM-CSF, G-CSF and M-CSF).⁽⁶²⁾ Existing within tissues and circulation, monocytes are recruited to sites of inflammation following neutrophil infiltration and the release of chemoattracting factors such as cathepsin G and azurocidin.^(62, 63) Additionally, neutrophil infiltration also upregulates the expression of adhesion molecules (ICAM-1, VCAM-

1, e-selectin) on endothelial cells which serve to facilitate the movement of monocytes to the inflamed tissue.^(62, 64) Macrophages are polarised into two phenotypic states, the pro-inflammatory phenotype 'M1' and the anti-inflammatory phenotype 'M2'.⁽⁶²⁾ The polarisation state of macrophages is dependent on local environmental factors, such as cytokine concentrations (e.g. IL-10, GM-CSF, IL-4, IFN- γ), anatomical location and disease state (Figure 2.6).⁽⁶⁵⁾ During the acute inflammatory response, initial infiltration by neutrophils is associated with increased GM-CSF concentrations and the activation of M1 macrophages that express inducible nitric oxide synthase (iNOS, a generator of ROS), and also secrete pro-inflammatory cytokines such as TNF, IL-6 and IL-1 β .⁽⁶²⁾ In contrast, M2 macrophages secrete IL-10 and TGF- β which are associated with the resolution of inflammation; however, they are still capable of pro-inflammatory cytokine release following phagocytosis of monosodium urate and subsequent initiation of NLRP3 inflammasome signalling in cases of gouty arthritis.⁽⁶⁶⁾ Additionally, tissue-resident macrophages also include the M2 phenotype, yet can become pro-inflammatory when encountering DAMPs such as MSU.

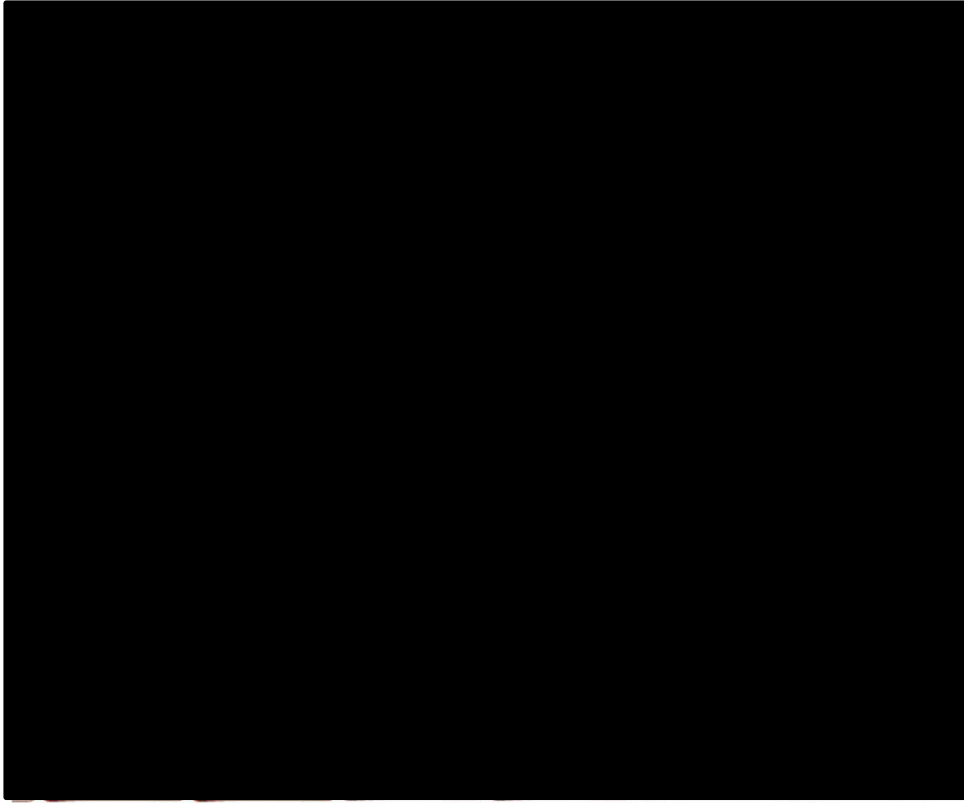


Figure 2.6: Interactions between neutrophils (left hand side of figure) and macrophages (right hand side of figure) during the innate immune response.⁽⁶²⁾ Monocytes, attracted by cytokines released by neutrophils (bottom; red), polarise into either M1 or M2 macrophages (top right) depending on factors such as G-CSF in the local environment of tissue injury and the degree of phagocytosis of neutrophils by macrophages (middle area of figure).

Endothelial Cells

Lining all blood vessels, endothelial cells also play a functional role in the inflammatory response, mediating chemotaxis and increasing vascular permeability in response to tissue injury.⁽⁶⁷⁾ When activated, endothelial cells and tissue-resident macrophages express CXCL1⁽⁶⁸⁾ and CXCL2⁽⁶⁹⁾ which act as chemokines. They are concentrated at the site of tissue injury creating a gradient for leukocytes to migrate along thereby assisting in the direction of chemotaxis toward the site of injury. Upon activation, endothelial cells within post-capillary venules, also upregulate expression of adhesion molecules (e.g. ICAM-1, VCAM-1 and e-

selectin)⁽⁷⁰⁾ which induce leukocytes to roll along the endothelium. The rolling decreases their velocity, and they eventually cross the endothelial layer into the site of injury once firmly adhered to and arrested by integrin.⁽⁷¹⁾ During this process, vasodilators such as nitric oxide, histamine and prostaglandins also act on endothelial cells and smooth muscle cells, disrupting the tight gaps between cells and allowing leukocytes along with plasma proteins into the site of injury.⁽⁷⁰⁾ Pro-inflammatory cytokines (e.g. IL-1 and TNF) released by activated innate immune cells (e.g. NLRP3 inflammasome signalling), increase the expression of adhesion molecules on endothelial cells in the acute phase.⁽⁷²⁾ Persistent inflammatory signalling results in chronic inflammation which disrupts the resolution of inflammation, causing oxidative damage, chronic tissue injury, promoting endothelial cell dysfunction and subsequent formation of scar tissue, leading to fibrosis, necrosis and organ dysfunction.^(70, 72) Specifically, altered or inappropriate vascular response to nitric oxide is a manifestation of endothelial dysfunction caused by persistent inflammatory signalling and results in a change in vascular tone which is an important contributor to the pathophysiology of atherosclerosis.⁽⁷³⁾

2.9 Cytokine Signalling and Chemotaxis

Cytokines are produced by cells and are released as part of the inflammatory cascade. Acting as either pro-inflammatory or anti-inflammatory signalling messengers, these peptides activate receptors on the target cell thereby promoting the production and release of further cytokines, however they also have a short lifespan.⁽⁷⁴⁾ The interleukin-1 family of cytokines which are described within the literature to significantly influence disease pathogenesis include IL-1 α , IL-1 β , IL-18, and IL-33.⁽⁷⁵⁾ However, other cytokines such as tumour necrosis factor (TNF) interferon gamma (IFN- γ), colony stimulating factors (CSF, G-CSF, GM-CSF), monocyte chemoattractant protein (MCP-1) are also important pro-inflammatory mediators.⁽⁷⁴⁾

Notably, Interleukin-1 signalling induces the production of secondary inflammatory cytokines (IL-6, TNF, KC, and GM-CSF), while IL-10 inhibits the release of TNF, IL-6 and IL-1 by activated macrophages.^(74, 76)

2.10 NLRP3 Inflammasome

Inflammasomes are protein complexes that act as a sensor of PAMPs and DAMPs in the cytoplasm and include the NLRP3 inflammasome.⁽⁷⁷⁾ Upon activation, the inflammasome activates caspase-1 and induces the formation of IL-1 β and IL-18, along with the cleavage of gasdermin D, which induces pyroptosis.⁽⁷⁷⁾ Briefly, pyroptosis results in the formation of pores in the cell membrane of 10-14 nm in diameter, causing swelling and lysis, and thus release of DAMPs including cytokines.^(77, 78) The NLRP3 inflammasome is activated by a wide range of DAMPs, including haem⁽⁷⁹⁾ and monosodium urate crystals as observed in clinical gout in mammals⁽⁸⁰⁾ and its activation stimulates the innate immune response as previously mentioned above. However, inappropriate inflammasome activation is linked to inflammatory disease and thus the activation of NLRP3 is a tightly regulated process that involves complex cell signalling regulation.⁽⁷⁶⁾

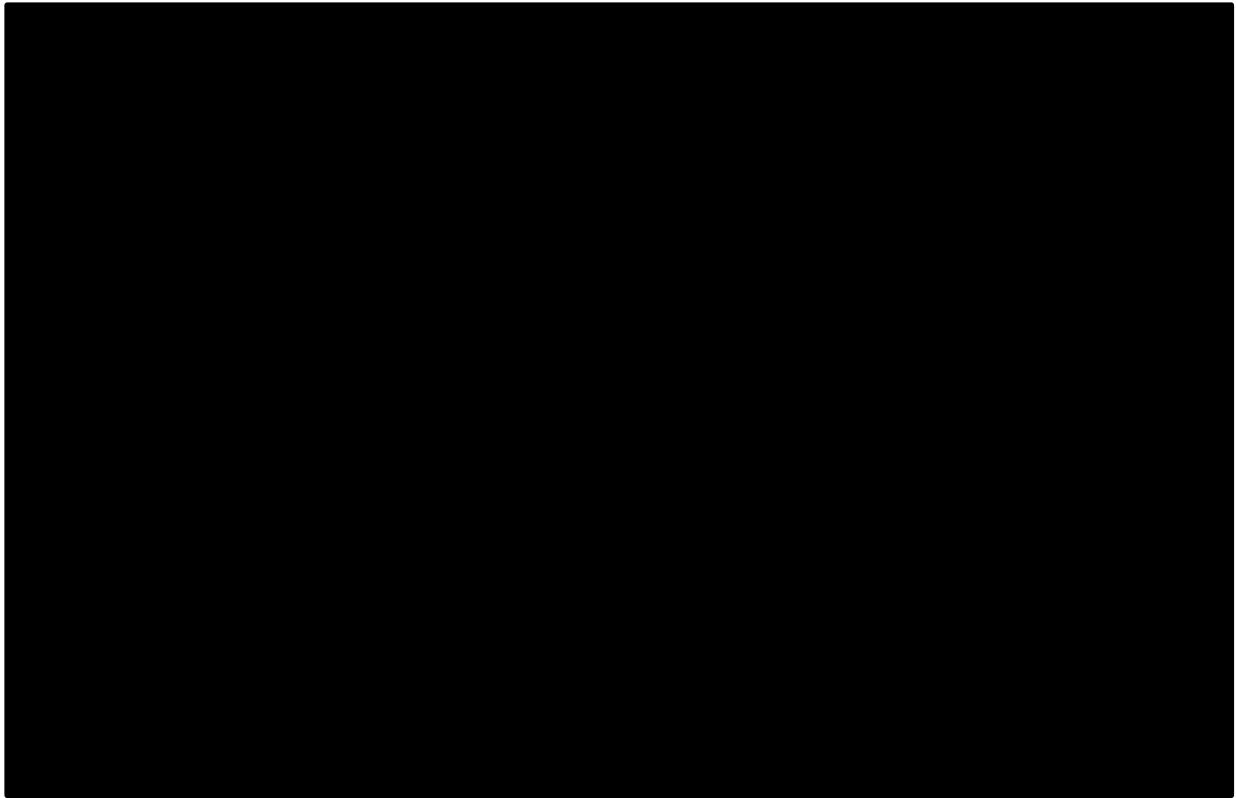


Figure 2.7: Cellular mechanisms of NLRP3 activation in the cytosol.⁽⁷⁶⁾ Caspase-1 signalling following DAMP receptor activation (left) results in caspase-1 activation, which in turn cleaves pro-IL-1 β and pro-IL-18 which is released as active IL-1 β and IL-18 . Receptors for IL-1 β and IL-18 on adjacent immune cells (e.g. Killer Cells (KC); right) are then bound, initiating transcription and release of IL-6 and TNF, further propagating inflammation.

2.11 Inflammation in gout

The pathologic formation of monosodium urate crystals in small joints, commonly referred to as gout, is strongly linked with elevated blood uric acid levels. Monosodium urate crystals are DAMPs and stimulate the activation of the NLRP3 inflammasome, resulting in painful bouts of acute inflammation.⁽⁸¹⁾ Interestingly, the loss of uricase activity during the evolution of hominids has rendered humans and higher primates incapable of degrading uric acid to water soluble allantoin, the final metabolic product of purine metabolism in non-primate mammals, fish and reptiles.⁽⁸²⁾ Therefore, while the NLRP3 inflammasome is evolutionary conserved across species, the formation of monosodium urate crystals is not. Thus, the study of sterile inflammation in non-primate animal models following activation of the NLRP3 inflammasome by monosodium urate crystals is attractive, as there is little chance of control animals

spontaneously developing gout-like symptoms. Gouty arthritis is a common and clinically relevant sterile inflammatory condition, with limited treatment options. Bile pigments have not yet been investigated in such conditions/models but could represent an attractive treatment option considering the combination of both the compounds' antioxidant and anti-inflammatory activity, compared with current NSAID therapy which employs anti-inflammatory activity alone.

2.12 Monosodium urate monohydrate crystal-induced inflammation in vivo: sterile inflammation in the rat

The monosodium urate (MSU) air pouch model of inflammation is a well-documented method of inducing sterile inflammation in *in vivo* animal models.⁽⁸³⁻⁹²⁾ The subcutaneous injection of sterile air in rodents on day 1 followed by a second injection on day 6 causes mechanical disruption of the subcutaneous tissue resulting in the formation of a pseudosynovial membrane consisting mainly of mononuclear cells, fibroblasts, mast-cells and small blood vessels.⁽⁹³⁾ This membrane also resembles synovium with many features of a synovial membrane.^(85, 89, 94) Administration of an inflammatory agent such as MSU monohydrate (crystals) into the resulting pseudosynovial cavity induces an acute inflammatory response^(84, 89, 90) which mimics the inflammatory response seen in human gout, and has successfully been employed to demonstrate the anti-inflammatory capacity of potential therapeutic compounds.^(88, 89, 93, 95)

Mechanisms of MSU crystal-induced Inflammation

It is well documented that MSU crystals are potent pro-inflammatory stimuli⁽⁹⁶⁾ and induce, amplify and sustain an acute inflammatory response⁽⁹⁷⁾ characterised by inflammatory

cytokine production and leukocyte infiltration.⁽⁹⁸⁾ This response is likely caused by multiple mechanisms, including direct activation of leukocytes, membrane lysis and activation of the NLRP3 inflammasome.^(77, 81, 97) Initially, the response involves activation and subsequent pyroptosis^(77, 78) of mast cells and resident monocytes, followed by activation of vascular endothelial cells⁽⁹⁹⁾, which leads to vasodilation, resulting in increased blood flow and permeability to plasma proteins as well as leukocyte infiltration to the affected tissue. In the initial stage, mast cells are reported to release TNF and IL-1 β ⁽⁹⁹⁾ which in turn induce endothelial cells to express adhesion molecules, E-selectin, intercellular adhesion molecule-1 (ICAM-1) and vascular cell adhesion molecule-1 (VCAM-1); all of which promote the transmigration of leukocytes.⁽⁹⁷⁾

Amplification of the inflammatory response occurs as infiltrating leukocytes, along with plasma immunoglobulins (IgG) and complement proteins, interact with MSU crystals either by phagocytosis or direct interaction with receptors on the cell surface. MSU crystal phagocytosis is also increased following opsonisation by either complement or IgG proteins, adding to the amplification of the response. At this stage, the inflammatory response is also driven by IL-6 and IL-18⁽¹⁰⁰⁾ and this intense neutrophil infiltration and activation is a well-reported characteristic of gout and is reported to be the main cellular mechanism by which tissue injury occurs.⁽¹⁰¹⁾ The consequence of intense neutrophil activation is the excessive generation of reactive oxygen species (ROS) and reactive nitrogen species (RNS) from the release of MPO, iNOS/NO and activation of NADPH oxidase. Interestingly, urate is also a physiological substrate of MPO and is oxidised to the urate radical.⁽¹⁰²⁾ A synergistic effect between IFN- γ and MSU crystal exposure has also been reported to increase iNOS expression and NO production leading to increased nitrosative stress.⁽¹⁰³⁾

During the acute phase of the inflammatory response, inflammatory cytokines monocyte chemoattractant protein-1 (MCP-1), interferon-gamma (IFN- γ), interleukin-6 (IL-6), interleukin-1 β (IL-1 β), myeloperoxidase (MPO), macrophage inflammatory protein-1 α (MIP-1 α), TNF, chemokine ligand 1 and 2 (CXCL-1 and CCL-2 respectively), interleukin-8 (IL-8), and macrophage inflammatory protein-2 (MIP-2) increase in MSU crystal air pouch inflammation models.^(88-91, 93, 103-105) Therefore, therapeutic approaches generally aim to inhibit the release of these compounds and, if successful, also reduce leukocyte invasion.

Resolution of gouty inflammation

Acute gout is characterised as a self-limiting inflammation, with acute gout attacks reported to spontaneously resolve within 7-10 days of initiation.⁽¹⁰⁶⁾ Multiple mechanisms are proposed for this resolution including release of anti-inflammatory cytokines (IL-10, IL-37 and TGF β)⁽¹⁰⁷⁾ by neutrophils, and neutrophilic cannibalism (i.e. the phagocytosis of dying neutrophils by live ones). Interestingly, via a process called NETosis, chromosomal DNA released following neutrophil death following phagocytosis of MSU form neutrophil extracellular traps (NETs).^(107, 108) In areas of high neutrophil density, NETs aggregate, forming aggNETs which capture and degrade cytokines via serine proteases⁽¹⁰⁸⁾ and aggregate MSU, forming tophi containing trapped MSU crystals. This is further evidenced by studies reporting that MSU administration in cases of mice with impaired NETosis resulting in uncontrolled production of pro-inflammatory cytokines and a persistent inflammation.⁽¹⁰⁸⁾ There is some disagreement regarding impaired murine NETosis, with a further study asserting that neutrophils are not required for resolution of acute gouty arthritis in mice.⁽¹⁰⁹⁾ In reply to this, the original authors published a further study demonstrating that although MSU crystal aggregates can be formed by cell types other than neutrophils, the degradation of

inflammatory mediators contributes to the control of MSU-crystal-induced inflammation in vivo.⁽¹¹⁰⁾ Despite these observations, neutrophilic cannibalism and the release of anti-inflammatory cytokines all contribute to the resolution of MSU induced inflammation (Figure 2.7).^(107, 108, 110-112)

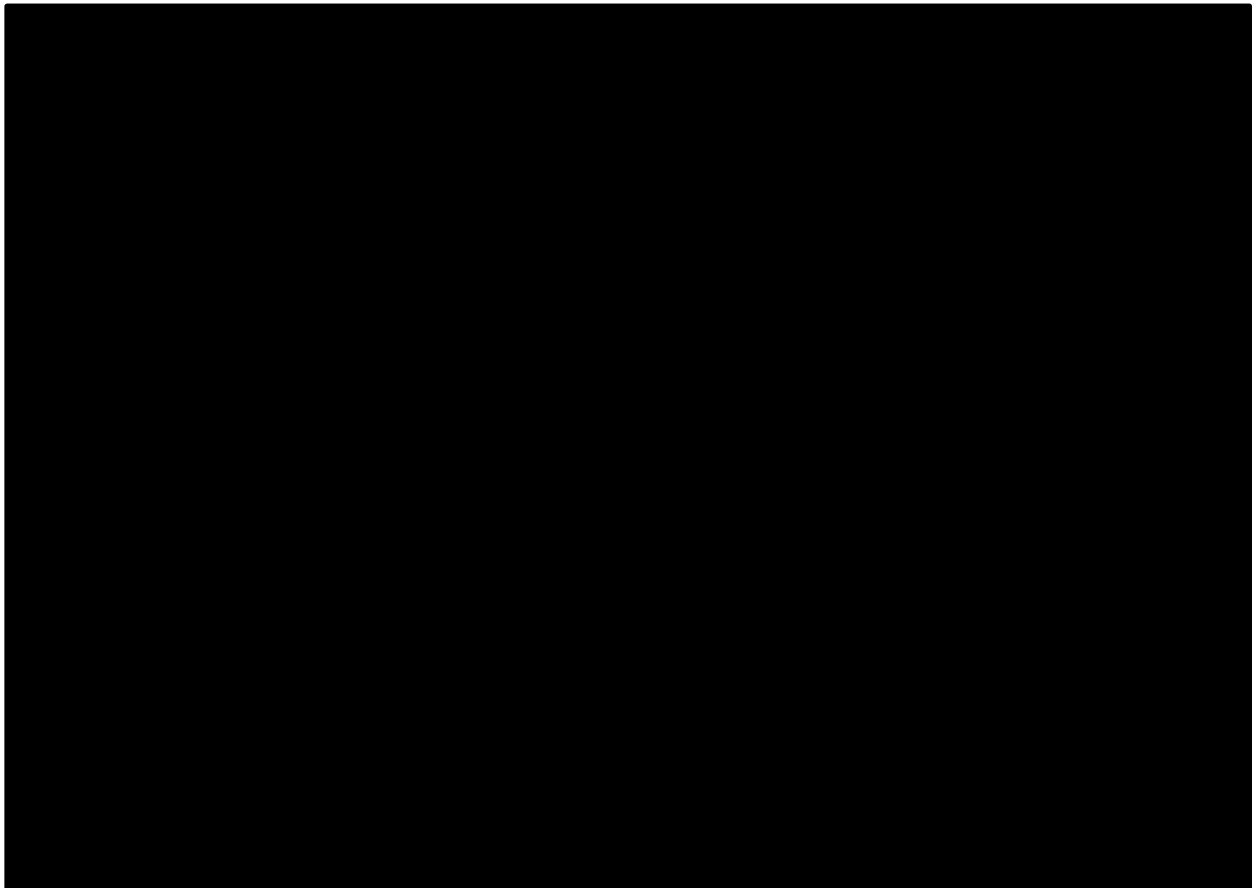


Figure 2.8: Mechanisms of the resolution of acute gout attacks.⁽¹⁰⁷⁾ MSU crystals phagocytosed by macrophages (left) or neutrophils (right) results in the initiation of inflammation. NETosis (right) results in sequestration of MSU crystals and the inactivation of pro-inflammatory cytokines.

2.13 Bile Pigments and Linear Tetrapyrroles

From a precursor for phycobilin synthesis in cyanobacteria and algae⁽¹¹³⁾, to a part of the haem catabolic pathway/anti-inflammatory mechanism in mammals^(28, 42), linear tetrapyrroles (or bile pigments when relating to animals) appear vital for the survival of all organisms that synthesise them.

The abundance of tetrapyrroles in mammalian (e.g. BV and haem when bound to Fe^{++} ion), cyanobacterial (e.g. phycobilin) and plant (chlorophyll; bound to Mg^+ ion) metabolism suggest that many species in the kingdom of life have common, evolutionarily conserved, enzymatic metabolic pathways for tetrapyrrole metabolism. The mammalian haem metabolic pathway likely shares a common ancestor with the chlorophyll (Chl) metabolic pathway found in the chloroplasts of plants & algae as well as in cyanobacteria. In plants, the process of degreening involves the conversion of Chl to linear tetrapyrroles known as chlorophyll catabolites. This process also mediates the ripening of fruits.⁽¹¹⁴⁾

The ability of early Hominidae to tell the difference in colour between ripe and unripe fruit may have also conferred an evolutionary nutritional advantage. The levels of affinity/repulsion towards ripening fruit as well as colour of urobilin and stercobilin (the tetrapyrroles which give faeces and urine their colour) may have resulted in an evolutionary selective pressure in terms of the anti-oxidant/anti-inflammatory properties of these tetrapyrroles, the avoidance of disease (avoiding rotten fruit, faeces etc) and the identification of better sources of nutrition. Enteric bacteria also metabolise (via β -glucuronidase, oxidise and reduce) mammalian bilirubin, which is excreted from the liver and into the gut.⁽²⁸⁾ These compounds are then either excreted in the faeces (stercobilins) or reabsorbed into the circulation and excreted in urine (urobilins). Whether bacterial metabolism of BV in the gut exists, however, remains undocumented.

2.14 Bile pigments as antioxidants

Canonically, BV and UCB were dismissed as simple waste products of haem catabolism, needing to be excreted. However, recent studies report that they possess antioxidant and anti-inflammatory properties.⁽¹¹⁵⁾ In fact, UCB and BV reportedly possess antioxidant

properties *in vitro*^(6, 115) and UCB prevents the oxidation of human plasma and lipids following copper exposure.⁽²⁾ A recent meta-analysis demonstrates the existence of an inverse, reliable and dose-dependant relationship between serum UCB and atherosclerotic risk in men.⁽¹¹⁶⁾ Biliverdin too has reported antioxidant properties, with a recent study reporting UCB and BVs antioxidant capability in multiple test systems (Trolox Equivalent Antioxidant Capacity (TEAC), Oxygen Radical Absorbance Capacity (ORAC) and Ferric Reducing Ability of Plasma (FRAP)) with UCB reported as having more antioxidant capacity than BV.⁽¹¹⁷⁾ It is theorised that UCB, due to its lipophilic nature, is also more effective at scavenging free radicals within lipids, whereas BV may confer more protection to proteins and other polar structures.⁽¹¹⁷⁾ Mechanistically, these findings are further supported by *in vitro* and *ex vivo* findings regarding the capacity of UCB to inhibit lipid peroxidation.^(2, 8) The oxidation of macromolecules including lipids is thought to represent a key event in the process of atherogenesis.⁽¹¹⁸⁾ Therefore, UCB's ability to prevent lipid oxidation, by its action as a lipophilic antioxidant, is assumed to exert protection from cardiovascular disease, *in vivo*.⁽³⁾ These findings have importantly contributed to redefining the physiological importance of bilirubin.⁽¹¹⁹⁾

Despite this, bilirubin's status as a physiological relevant antioxidant is a point of contention in the literature.⁽⁴⁰⁾ It has been proposed that BV is formed following UCB oxidation and is recycled by BVR back to UCB in cultured cells⁽³⁹⁾, thereby magnifying UCB antioxidant effects by a factor of 10000. This led the authors to theorise that BVR could perpetuate a cycle allowing relatively low levels of UCB to provide physiologically relevant levels of protection. To test the importance of BVR reduction of BV to UCB, they depleted cells of BVR using RNA interference, which tripled the levels of ROS and significantly increased cell death. Based on this result, the authors concluded that UCB potently protects cells against lipid peroxidation

in a cyclic manner akin to the glutathione cycle (Figure 2.4).⁽³⁹⁾ Considering that UCB is lipophilic, the BVR cycle represent another system that is used to protect the human organism from lipid oxidation (e.g. occurring within cell membranes).

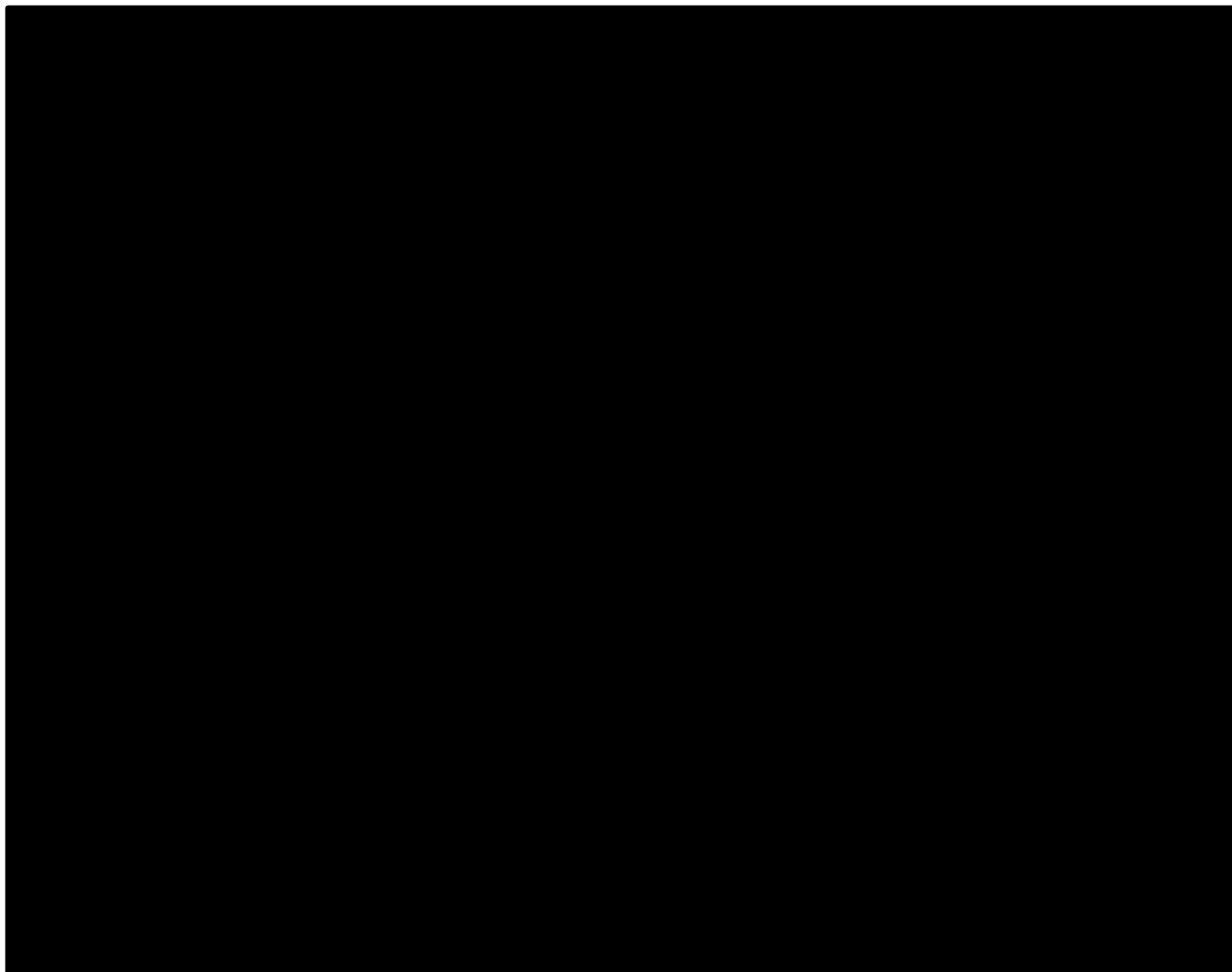


Figure 2.9: Parallel oxidation-reduction cycles for bilirubin and GSH proposed by Sedlak and Snyder.⁽³⁹⁾

The physiologic relevance of the BVR recycling mechanism of protection has since been disputed by McDonagh⁽¹²⁰⁾ and Maghzal et al.⁽¹²¹⁾, the former reporting that the degradation of bilirubin, rather than dehydrogenation to biliverdin, predominates in the reaction of bilirubin with peroxy radicals, and the latter finding that only stoichiometrically modest yields of BV follow UCB oxidation irrespective of the conditions and oxidants used. Interestingly, they note that albumin bound UCB gives the most favourable BV yield. In published letters since, Sedlak and Snyder defended their findings⁽¹²²⁾, asserting that certain technical aspects

accounted for the unsupported findings and maintain that BVR has pathophysiologic and physiologic importance, citing clinical studies where bilirubin is reported to protect against cardiovascular and cerebrovascular disease. The final published letter in response by Stocker and Maghzal⁽¹²³⁾ again disagree with Sedlak and Snyder, and assert that non-enzymatic antioxidants GSH, ascorbic acid and tocopherol are present at concentrations several orders of magnitude greater than UCB.⁽¹²¹⁾

Most recently, Vasavda et al. reported that mice lacking bilirubin are particularly vulnerable to $O_2^{\cdot-}$ compared with other tested reactive oxidants and electrophiles.⁽⁴⁰⁾ They also report that major antioxidants such as glutathione and cysteine exhibit little to no reactivity toward $O_2^{\cdot-}$ and that UCB readily scavenges $O_2^{\cdot-}$. These authors went on to assert that the unique reactivity of UCB to $O_2^{\cdot-}$ may underlie a relevant physiologic role despite its lower abundance compared with other antioxidants *in vivo*. Research investigating the murine bilirubin oxidase sheds further light on this disputed mechanism, hypothesising that direct interaction of UCB and the anion $O_2^{\cdot-}$ forms a bilirubin peroxyradical (and subsequently degrades to dipyrroles) whereas the oxidation of UCB to BV begins with removal of an H^- anion from the C10 bridge of UCB, forming a positively charged intermediate which then spontaneously donates a H^+ to the surrounding aqueous environment, resulting in BV formation (Figure 2.5). While this study was conducted in murine cells, the authors also hypothesise the findings potential relevance to humans. This study is interesting as it proposes that the mechanism of UCB oxidation determines whether BV is formed and thereby able to participate in the proposed redox cycling and also highlights the complexity and importance of the C10 bridge of these bile pigments, especially as the C10 bridge is also the site of bisulfite addition in the formation of BRS.⁽¹²⁴⁾

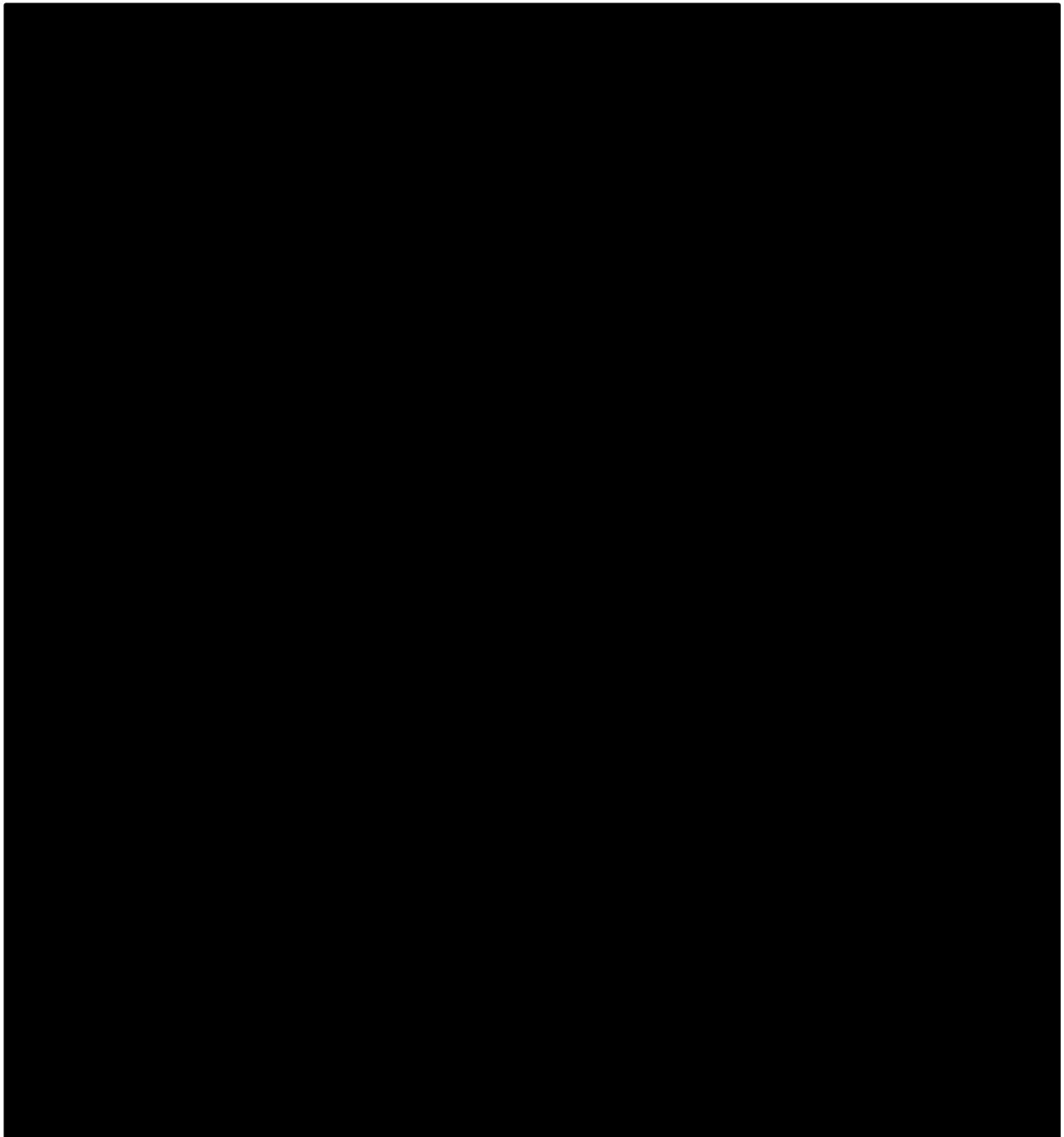


Figure 2.10: Hypothesised mechanisms of UCB oxidation via direct interaction with superoxide (left) vs loss of hydride anion (right).⁽¹²⁵⁾

The action of BV on BVR in the antioxidant cycle and the downstream signalling following BVR activation⁽²²⁾ potentially explains the puzzling evolutionary development of the energy consuming enzymatic reaction which converts BV (a non-toxic, readily excretable compound) into UCB (which is potentially cytotoxic and requires conjugation prior to active hepatic transport/elimination) in mammals as previously mentioned. This extra metabolic step is

costly in terms of NADPH in comparison to with the direct hepatic excretion of BV in fish and birds⁽¹²⁶⁾, however, the ability of new metabolic pathways to confer evolutionary benefits as a result of their processes is a commonly acknowledged process⁽¹²⁷⁾ and therefore some evolutionary advantage was likely conferred by this additional energy consuming step in pigment metabolism.

2.15 Gilbert's Syndrome – UCB elevation in humans

Gilbert's syndrome is a condition presenting with a mildly elevated circulating UCB concentration, and interestingly it is associated with protection of individuals against oxidative processes and cardiovascular disease.⁽¹¹⁶⁾ An autosomal recessive disorder, Gilbert's syndrome (GS) is endemic within the population (3-17%) and is caused by a reduction uridine glucuronosyltransferase 1A1 (UGT1A1) function, via a polymorphic mutation of the UGT1A1 gene promoter, which reduces gene induction and induces a ~60% deficiency in enzyme activity.⁽⁵⁾ Given that the primary function of UGT1A1 is to conjugate UCB, this deficiency results in elevated circulating UCB (>17.1 μM ; normal concentration $\sim 10 \mu\text{M}$).⁽²⁾ Of particular relevance is the inverse relationship between serum UCB and the atherosclerotic (and presumably inflammatory related) processes. In fact GS individuals have a 10.1% lower incidence of cardiovascular disease (CVD) and their lipid profile is significantly improved compared to control individuals.^(5, 116) Additionally, GS plasma has a greater antioxidant capacity, demonstrated by improved resistance to copper induced lipid oxidation.⁽⁴²⁾ Additional findings also indicate that individuals with elevated UCB, have a decreased serum lipid concentration (LDL and total cholesterol) with the remaining blood cholesterol also being protected from oxidation. It is likely that both reduced total and LDL cholesterol and improved resistance to lipoprotein oxidation underpins the protection conferred from development of

cardiovascular disease in these persons.⁽¹¹⁸⁾ It should also be pointed out here that this was an *ex vivo* assay and thus may not be relevant *in vivo*, and is a limitation of this interpretation.

The benefits of Gilbert's Syndrome along with a lack of major side effects associated with the condition lend support to the idea of bilirubin and related tetrapyrroles having potential as therapeutic molecules.

2.16 Bile pigment anti-inflammatory effects

Biliverdin and UCB are formed following events that liberate haem including trauma (e.g. tissue injury), and are accompanied by initial inflammatory and wound healing responses.⁽⁹⁾

While administration of BV or its metabolites to humans could assist in the treatment of inflammatory pathologies, the pharmacokinetics of its metabolites and the anti-inflammatory potential of BV and its metabolites must be investigated further in animal models to justify its potential use in clinical medicine. Since 2004, the use of BV and UCB in rodent models of sterile inflammation and wound healing to demonstrate their anti-inflammatory ability has been well documented. Many studies use expression or concentration of pro-inflammatory cytokines as a measure of anti-inflammatory capacity of bile pigments and these are listed below (Table 1).

Table 1: Recent studies measuring anti-inflammatory cytokines in BV and UCB in rodent models of inflammation/wound healing

Model	Compounds	Species	Cytokines increased/decreased	Tissue analysed	Study outcomes
Open excision type wound (10 days) - sterile ⁽¹²⁸⁾	i.p. UCB (30 mg kg ⁻¹)	Male wistar rats (140-160g)	TNF - significant decrease, 145 (control) vs 65 (treatment) pg/mg protein IL-10 - significant increase, 872 (control) vs 1485 (treatment) pg/mg protein	Granulation tissue of excision wound	Bilirubin possesses significant pro-healing modulation of pro-inflammatory/anti-inflammatory cytokines and adhesion molecule and an improvement in the quantity of extracellular matrix in the granulation tissue
Open excision-type wound - loose subcutaneous tissue - sterile ⁽¹²⁹⁾	UCB (0.3% ointment)	Adult male Wistar rats (180 to 220 g) induced with diabetes	TNF - significant decrease (3day), 3000 (control) vs 2000 (treatment) pg/mg protein IL-1 β - mRNA expression decreased, cytokine itself was not measured IL-10 1400 (control) vs 600 (treatment) pg/mg protein	Granulation tissue of excision wound	Bilirubin treatment accelerated the timely progression of wound healing by modulating expression of a number of cytokines and growth factors
Intraportal islet transplantation graft ⁽¹³⁰⁾	i.p. injection of bilirubin (~ 1 mg kg ⁻¹)	Adult inbred male Lewis rats (200-250 g) induced with diabetes	IL-1 β - significant decrease - 135 (control) vs 101 (treatment) pg/mL in treated (6H) TNF - significant decrease - 119 (control) vs 87 (treatment) pg/mL (3H) MCP (CCL-2) - 66 (control) vs 43 pg/mL (treatment) (24H)	Serum obtained from tail vein bleeds	Nonspecific inflammatory response is the major cause for failure of islet grafts, i.p. UCB administration reduced inflammatory markers.
Syngeneic transplantation of small bowel ⁽¹³¹⁾	i.p. BV (50 mg kg ⁻¹) 3H before and after transplant	Inbred male Lewis rats (200–250 g)	IL-6 - significant decrease - 1585 (control) vs 604 (treatment) pg/mL IL-1 β and TNF mRNA significantly decreased In muscularis externa stripped from small bowel	Serum 3H after reperfusion of transplant	After a single IP injection of biliverdin, serum bilirubin peaked to 1.07 \pm 0.5 mg/dL at 30 minutes and then returned toward control levels by 2 hours.

The pharmacokinetics and anti-inflammatory capacity of Bilirubin Sulfonate: A novel biliverdin metabolite

Model	Compounds	Species	Cytokines increased/decreased	Tissue analysed	Study outcomes
LPS induced lung injury ⁽¹³²⁾	BV (3 mg kg ⁻¹)	Adult Sprague-Dawley rats (225-250 g)	Significant decrease in IL-6 - 3.2 (control) vs 1.4 (treatment) ng/mL Significant increase in IL-10 - 2.8 (control) vs 8 (treatment) pg/mL	Bronchial Alveolar Lavage	BV protects against lethal endotoxic shock. BV exposure prevents LPS-induced lung injury.
Trinitrobenzenesulfonic acid (TNBS) induced colitis	UCB (40 μM) intra-gastric gavages	Adult male Sprague-Dawley rats (~180 g)	TNF sig. decrease in UCB treatment vs untreated at 3 and 7 days IL-1β significantly decreased in UCB treatment vs untreated at 1 and 3 days	Colon	Unconjugated bilirubin ameliorates the inflammation and digestive protease increase in TNBS-induced colitis.
Liver cold ischemia model followed by ex vivo reperfusion. ⁽¹³³⁾	BV (10 or 50 μmol L ⁻¹) in perfusate	Male Sprague-Dawley rats (250–300 g)	mRNA expression: iNOS, TNF, IL-1β and IL-6 was significantly decreased in BV treatment	Liver	BV attenuates IRI in rat models of prolonged cold ischemia followed by ex vivo reperfusion.
HO-2 null mouse phenotype in corneal epithelial injury ⁽¹³⁴⁾	i.p. BV (20 mg kg ⁻¹) plus 10uL of 100uM BV applied topically, both applied once daily	HO-2-null mice with a C57BL/6 × 129/Sv genetic background	KC (CXCL-1) decreased significantly 4 days post injury in BV treated mice	Cornea	Biliverdin accelerates wound healing and reduces the number of inflammatory cells and the levels of proinflammatory proteins.

From a mechanistic perspective, recently published literature cites biliverdin reductase (BVR) as a critical regulator of the innate immune response in the context of acute inflammation.⁽²²⁾ Interestingly, a lack of BVR results in an enhanced proinflammatory phenotype, and in macrophages the authors report that BVR, when binding its substrate BV, promotes IL-10 (an anti-inflammatory cytokine) secretion as well as inhibition of TLR4 expression.⁽²²⁾ A follow-up study then reported that knockdown of BVR in macrophages suppressed pro-inflammatory cytokine release (TNF) and also showed that the protection provided by BV in a model of sterile hepatic injury requires the activity of BVR and nitric oxide.⁽¹³⁵⁾ The authors speculate that inflammatory processes and increased oxidative stress cause the induction of HO-1, and BVR (activated by BV) helps to maintain the balance between the expression of anti-inflammatory (IL-10) and proinflammatory mediators (TNF), thereby protecting against unrestrained inflammation.⁽²²⁾

Novel Biliverdin Metabolites – an Alternative Metabolic Pathway

Despite the emerging therapeutic potential of BV, UCB and BVR, very little research has explored the metabolism of BV *in vivo*. In 2011, Bulmer et al. explored the pharmacokinetics of intraduodenal BV administration and reported that BV was poorly absorbed from the intestine⁽¹⁾, with a bioavailability of < 1%. Serendipitously, the authors discovered three separate compounds were formed within the duodenal milieu and they were potently absorbed into the blood and subsequently excreted into urine and bile. These poorly characterised compounds absorbed light between 420-450 nm, indicating that their C10 bridge may be cleaved or reduced, similar to UCB.⁽¹⁾ Based upon these results it is reasonable to conclude that the uncharacterised compounds, or enzymes involved in their formation, induce potent antioxidant and/or anti-inflammatory effects *in vivo* that are not induced by BV *per se*. Additionally, this finding suggests that an alternate BV metabolic pathway existed, in addition to the commonly accepted reduction of BV to UCB.

2.17 Intestinal Bacterial Tetrapyrrole Metabolism

Intraduodenally administered BV results in its rapid and complete metabolism within three hours.⁽¹⁾ Intestinal metabolism of structurally related tetrapyrroles is documented, however, it is limited to study of bilirubin metabolism, because bilirubin and not BV is excreted normally

in bile.⁽¹⁾ It is possible that one or more of the BV metabolites reported by Bulmer in 2011 was a previously reported metabolite of UCB⁽⁶⁾ alternatively, it was equally likely that the metabolites formed were entirely novel products. Although intraduodenal administration reduced the bioavailability of BV, the metabolised products were potentially absorbed and may have been responsible for the protection observed after BV administration in other studies.⁽¹⁾ However, enteric biliverdin metabolites have not been isolated or characterised. Considering this gap in scientific knowledge, analysing, isolating and characterising these compounds may lead to important discoveries regarding an alternate metabolic pathway for BV metabolism in addition to the discovery of a new generation of anti-inflammatory compounds for treatment of diseases that involve inflammatory pathophysiology.

2.18 Analysis of bile pigments

Many analytical methods exist for the quantification of bile pigments, ranging from the simple colourmetric reaction with diazotised sulfanilic acid (the 'diazo' reaction) to mass spectrometric methods for example. This literature review will now focus on contemporary methods used to analyse biliverdin and related compounds for their quantification and characterisation in various matrices.

Previous studies^(1, 136) have used HPLC to identify and quantify bile pigments with a mobile phase comprising of 0.1M of *n*-dioctylamine (95 methanol:5 H₂O) and a reverse phase C18 column with the absorption of light recorded using a photo diode array detector, reporting pure biliverdin with a peak in light absorption (λ_{max}) of 375 nm. These data are supported by numerous other reports that have also quantified/separated bile pigments including biliverdin from pure and crude samples, using gradient and isocratic separations, using a variety of organic gradients to facilitate the separation of sample components.^(1, 42)

Furthermore, liquid chromatography coupled to mass spectrometry has also been employed to identify biliverdin within complex solutions. For example, Gorchein et al.⁽¹³⁶⁾ used a gradient HPLC separation and a Q-TOF spectrometer to ionise biliverdin in positive ion mode. They report that biliverdin had a m/z of 583 (molar mass 582.7). Furthermore, biliverdin was fragmented using MS/MS analysis, showing that biliverdin fragments across its central C10 bridge, liberating a fragment with a m/z of 297 (right hand side; RHS, Figure 2.11).⁽¹³⁶⁾

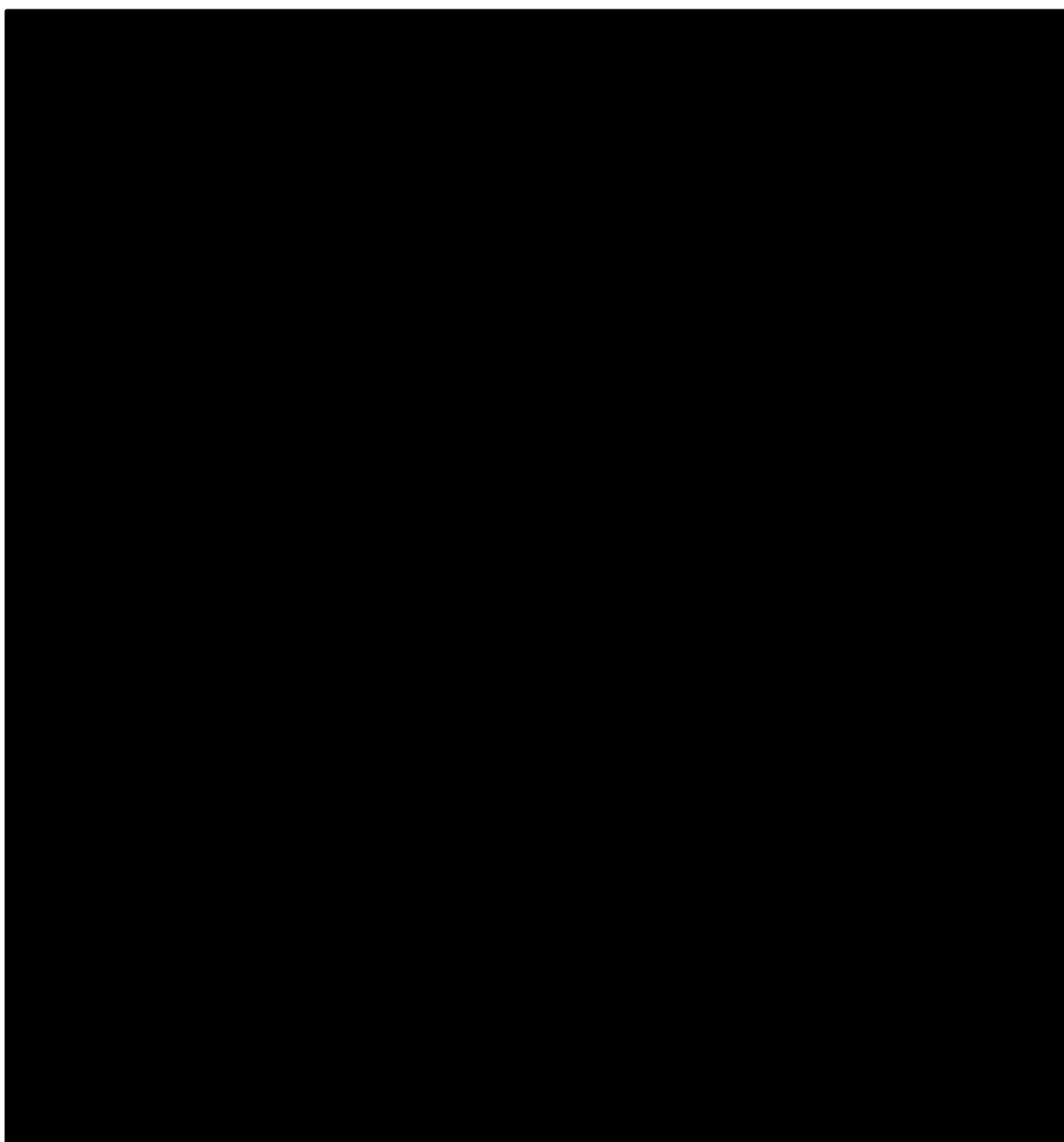


Figure 2.11: Chemical structure of BV plus HPLC/ESI-MS/MS chromatogram and product ion spectra for the 583 m/z BV ion indicating that the 297 m/z ion is the major fragment.⁽¹³⁶⁾

Additional analytical methods have been employed via both LCMS and HPLC.^(1, 137) While there are ease of use advantages for HPLC, LCMS is superior in its selectivity and sensitivity. In previous studies, biliverdin has been measured using its deuterated internal standard, biliverdin-d4⁽¹³⁸⁾ which is the gold standard of quantification. Interestingly, in cases where a deuterated standard is either unavailable or not cost effective, compounds with similar organic structures and properties can be used as internal standards. One such example is the use of meso-bilirubin (MBR) as an internal standard for UCB.⁽¹³⁹⁾ In this case, MBR shares structural similarity (Figure 2.12) and is able to control for losses during extraction and analysis.⁽¹³⁹⁾ Another study uses both MBR and meso-biliverdin (MBV) as internal standards during the LCMS analysis of UCB and BV respectively⁽¹⁴⁰⁾ demonstrating that the use of meso analogues as internal standards for the LCMS quantification of tetrapyrrolic bile pigments is valid and effective.

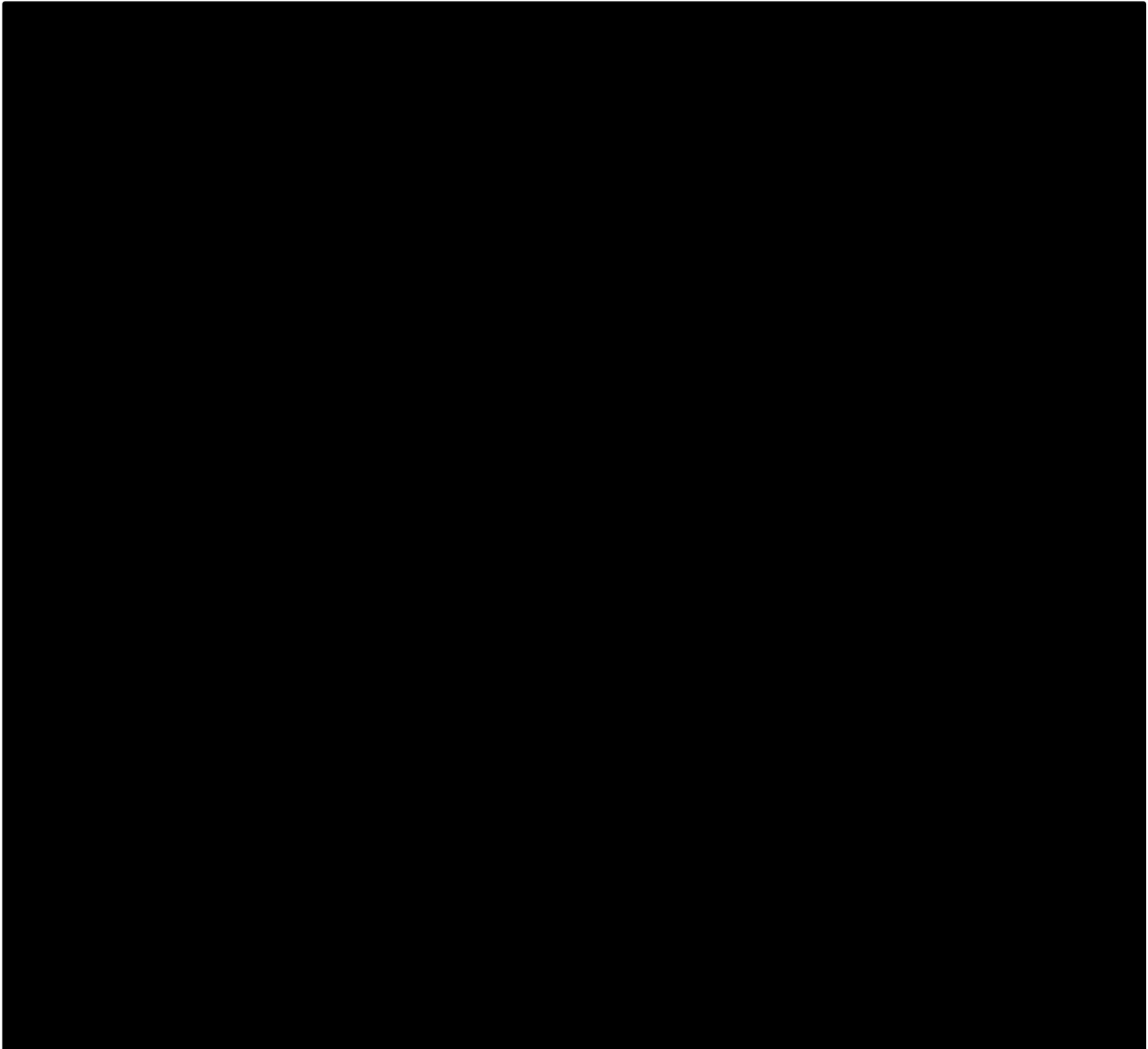


Figure 2.12: Differences in structure (circled) of UCB and its internal standard, mesobilirubin (MBR).⁽¹³⁹⁾ The vinyl groups on the terminal pyrroles have been substituted for ethyl groups, resulting in a +4[H] increase in the mass, while keeping similar organic properties.

2.19 Conclusion

The catabolism of haem, induced after tissue injury and during homeostatic turnover of red blood cells, is a highly conserved and energy consuming pathway which has further evolved during mammalian evolution. The evolution of the haem catabolic pathway in mammals is believed to have occurred to minimise haem toxicity and protect the body by producing bile pigments, which have potent antioxidant capacity and could modulate inflammatory responses. Importantly, the chemical reduction of biliverdin by biliverdin reductase, likely amplifies both biliverdin and bilirubin's effect, by allowing for oxidation-reduction cycling. This, in combination with biliverdin's activation of kinase signalling by BVR, likely protects from sterile inflammation, as demonstrated by biliverdin administration and BVR knockout studies. Collectively, these data emphasise the importance of endogenous bile pigments in protecting against oxidant and inflammatory mediated injury and suggest the haem catabolic and bile pigment synthetic pathway could be used therapeutically to inhibit injurious responses in vivo.

The recent discovery of novel BV metabolites that are potently absorbed following intraduodenal administration⁽¹⁾ heralds the possibility of an alternate biliverdin metabolic

pathway mediated by enteric bacteria. This serendipitous discovery raises highly pertinent questions regarding whether biliverdin *per se* is the responsible anti-inflammatory agent in administration studies. Furthermore, questions arise as to the identity, pharmacokinetics, and anti-inflammatory capacity of these metabolites in mammals. Answers to these questions will help to further understand the importance of bile pigments in human physiology and their importance in the prevention and possible treatment of disease. The ever-present and unrelenting scourge of oxidative stress and inflammatory disease continues to plague humanity, and the discovery of novel, safe and effective anti-inflammatory therapies is vital to lessen the burden of disease globally. Therefore, a sizeable gap in literature is revealed here, presenting an exciting opportunity to explore the identity, pharmacokinetics and anti-inflammatory potential of these novel bile pigment metabolites. It was hypothesised that these novel bile pigment metabolites ameliorate the immune response to a sterile inflammatory stimulus.

Chapter Three: Aims & Hypotheses

This thesis aims to investigate the therapeutic potential of the novel BV metabolite, bilirubin-10-sulfonate. Overall, the aim was to identify the novel BV metabolite and explore its pharmacokinetics and its anti-inflammatory capacity in clinically relevant animal models.

3.1 Study One (Chapter Four)

The aim of this chapter was to elucidate the principal metabolite formed after intraduodenal administration of biliverdin, to determine whether bacteria could be responsible for its transformation and evaluate its antioxidant activity. It was hypothesised that enteric bacteria caused the conversion of biliverdin to the unknown metabolite via addition at the C10 bridge.

3.2 Study Two (Chapter Five)

The aim of this study was to quantify the absorption and pharmacokinetics of biliverdin versus bilirubin-10-sulfonate in rats after i.v., i.d. and intraperitoneal (i.p.) administration as well as to determine their biliary excretion. It was hypothesised that biliverdin and bilirubin-10-sulfonate would be absorbed from the peritoneal and intestinal cavities, and that there would be significant differences in half life and maximum serum concentration between BRS and BV.

3.3 Study Three (Chapter Six)

The aim of study three was to evaluate the potential therapeutic potential of intraperitoneal pre-treatment of bilirubin-10-sulfonate and biliverdin in a subcutaneous air pouch model of inflammation within rodents. It was hypothesised that i.p. pre-treatment of rats with biliverdin and bilirubin-10-sulfonate would have significantly decreased leukocyte infiltration, cytokine concentrations and oxidative stress markers compared with placebo treatment when challenged with monosodium urate crystals as an inflammatory stimulus.

Chapter Four: Unprecedented Microbial Conversion of Biliverdin into Bilirubin-10-sulfonate

Foreword:

This manuscript details the identification and chemical structure of BRS following its initial discovery following intraduodenal administration of biliverdin to rats. The anti-inflammatory and antioxidant properties of BV are well documented in literature^(22, 117, 131, 133, 134, 141-146), and this manuscript compares the antioxidant potential of BRS to BV. This led to the identification of BRS as the lead compound for further pharmacokinetic testing. The manuscript also details the synthesis of BRS and identifies analytical methodology required for the analysis of this compound.

This chapter has been published by Scientific Reports as an original investigation. The abbreviations, formatting and referencing of this document have been altered slightly to more closely reflect the formatting of other chapters and published work in this thesis.

Statement of Contribution to a Co-Authored Published Paper

This chapter is in the form of a co-authored published paper. The bibliographic details of the co-authored published paper are:

Shiels, R.G., Vidimce, J., Pearson, A.G., Matthews, B., Wagner, K-H., Battle, A.R., Sakellaris, H. and Bulmer, A.C. Unprecedented Microbial Conversion of Biliverdin into Bilirubin-10-sulfonate. *Sci Rep* **9**, 2988 (2019). <https://doi.org/10.1038/s41598-019-39548-w>

Appropriate acknowledgements of those who contributed to the research but did not qualify as authors are included in the paper.

My contribution to the published paper involved:

- Experimental design and planning
- Development and validation of the analytical methods
- Data acquisition and statistical analysis
- Manuscript preparation, critical review and submission

(Sign) _____

First Author
Ryan Shiels

(Date) 11th February 2020

(Sign)

(Date) 11th February 2020

Corresponding Author and Supervisor
Associate Professor Andrew Bulmer

Unprecedented Microbial Conversion of Biliverdin into Bilirubin-10-sulfonate

Ryan G. Shiels¹, Josif Vidimce¹, Andrew G. Pearson¹, Ben Matthews¹, Karl-Heinz Wagner²,

Andrew R. Battle³, Harry Sakellaris¹ and Andrew C. Bulmer^{1*}

¹School of Medical Science, Griffith University, Gold Coast, Queensland, Australia

²Department of Nutritional Sciences, University of Vienna, Vienna, Austria

³Translational Research Institute (TRI), Institute for Biomedical Innovation, School of Biomedical Sciences, Queensland University of Technology, Brisbane, Queensland, 4102, Australia.

*a.bulmer@griffith.edu.au

Abstract

Biliverdin (BV) possesses antioxidant and anti-inflammatory properties, with previous reports identifying protection against oxidant and inflammatory injury in animal models. Recent reports indicate that intra-duodenal administration of BV results in the formation of an uncharacterised metabolite, which is potently absorbed into the blood and excreted into the bile. This compound may be responsible for protection against inflammatory responses. This study aimed to identify novel, enterally-derived BV metabolites and determine the source of their metabolic transformation. Rat duodena and bacterial cultures of *Citrobacter youngae* were treated with BV and subsequently analysed via high performance liquid chromatography/high resolution tandem mass spectrometry to identify and characterise metabolites of BV.

A highly abundant metabolite was detected in duodenal wash and bacterial culture supernatants with a 663.215 m/z (3 ppm mass accuracy) and a composition of C₃₃N₄O₉H₃₆S, which conformed to the predicted structure of bilirubin-10-sulfonate (BRS) and possessed a λ_{\max} of 440 nm. Bilirubin-10-sulfonate was then synthesised for comparative LCMS/MS analysis and matched with that of the biologically formed BV metabolite. This report confirms the formation of a previously undocumented metabolite of BV in mammals, indicating that a new metabolic pathway likely exists for BV metabolism requiring enteric bacteria, *Citrobacter youngae*. These data may have important implications with regard to understanding and harnessing the therapeutic efficacy of oral BV administration.

Introduction

Mammalian catabolism of haem by haem oxygenase-1 (HO-1) forms the linear tetrapyrrole biliverdin (BV; **1**), which is chemically reduced by biliverdin reductase (BVR) to unconjugated bilirubin (UCB). Previously, these tetrapyrroles were thought to be waste products; however, recently these compounds were found to protect from oxidant-mediated damage. Specifically, both the induction of HO-1 and the administration of **1** and related tetrapyrroles confer protection in animal models of ischemia-reperfusion injury.^(41, 144) Administration of **1** protects from ischemia-reperfusion injury (IRI) in the liver during transplantation in swine.⁽¹⁴¹⁾ Furthermore, oral administration of **1** protects from Forssmann reagent induced anaphylaxis in guinea pigs⁽⁷⁾ and its intravenous (i.v.) administration after haemorrhagic shock and

subsequent resuscitation protects against acute lung injury (ALI).⁽¹⁴³⁾ Given that **1** is rapidly reduced to UCB *in vivo*⁽¹⁾, it is possible that either of these molecules conferred protective effects in these models.

Intriguingly however, intraduodenal (i.d.) administration of **1** in rats leads to rapid and complete metabolism of **1** and the absorption of uncharacterised metabolites, found in the duodenum, serum, bile and urine.⁽¹⁾ These metabolites, which are more polar than **1** and UCB, were hypothesised to possess a rubinoid structure (λ_{\max} 420-450 nm) suggesting modification or reduction at the C10 bridge of **1**. These observations suggested that oral administration of **1** instead leads to the formation of a novel active metabolite that may confer protection against anaphylaxis as reported previously.⁽¹⁴⁷⁾ The aim of this study was to identify and characterise the metabolites formed after i.d. administration of **1**⁽¹⁾ and to determine whether bacteria could be responsible for its transformation. We then sought to synthesise this compound and evaluate its antioxidant activity.

Results

Given that the retention time and optical characteristics of novel BV metabolites have been published previously⁽¹⁾, the composition of these molecules was confirmed using tandem mass spectrometry. Figure 4.1 shows UV and MS chromatograms of duodenal contents taken from an anaesthetised rat 180 mins after administration of i.d. saline or **1**.

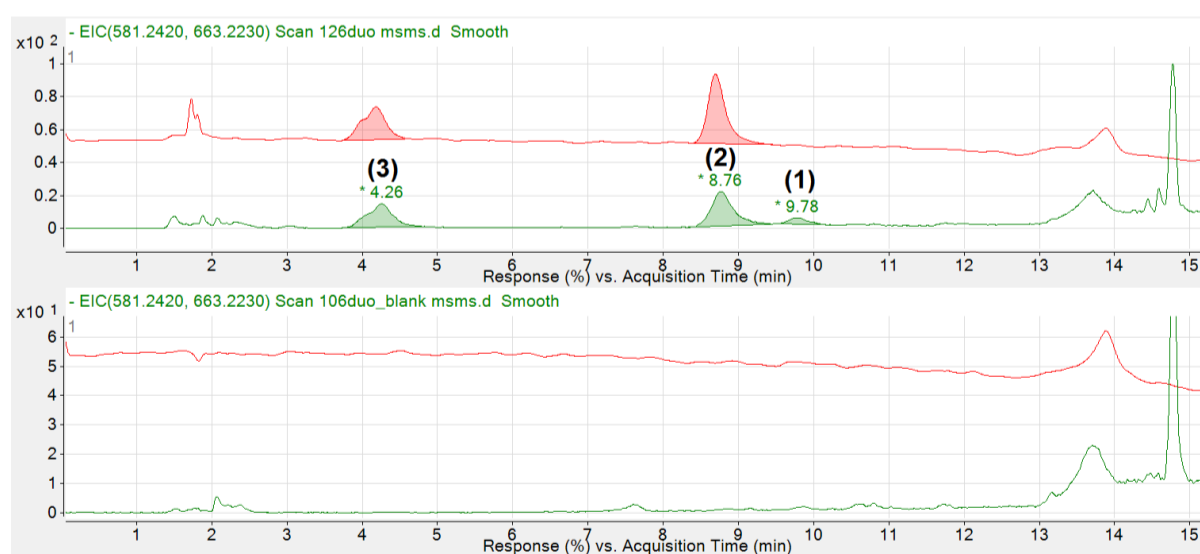


Figure 4.1: Extracted ion chromatogram of intestinal contents obtained from a rat receiving **1** (27 mg/kg), 180 mins after i.d. administration (TOP) and an animal administered saline (BOTTOM). The red chromatogram represents UV absorbance at 440 nm and serves as a point of reference for identified ions. The green chromatogram represents the extracted ion chromatogram for m/z 663.2230 \pm 0.5 and 581.2420 \pm 0.5. The 581.2420 m/z ion (**1**) only appears at 9.78 minutes. The compounds eluting at 4.26 min and 8.76 min were presumed to be BV metabolites (**3** and **2** respectively).

The three prominent peaks in **1** treated duodenal samples identified in Figure 4.1 (peaks **1-3**) were then analysed for their UV and mass spectra and are displayed in Figure 4.2 below.

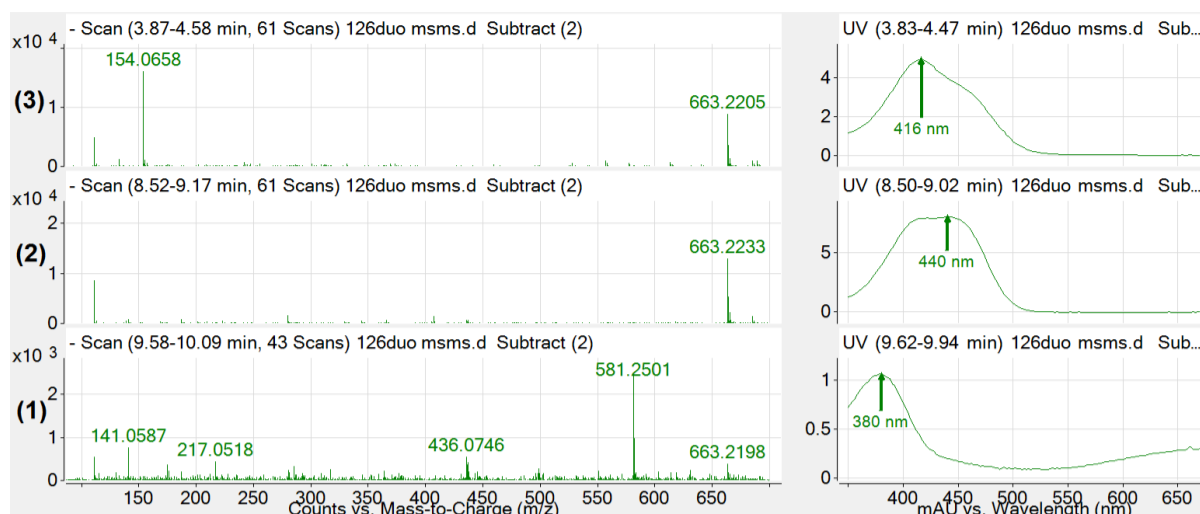


Figure 4.2: Mass spectra (left) and UV spectra (right) of each identified peak in Figure 4.1. The 663.2233 and 663.2205 m/z ions were observed to be the major abundant ion under peaks 2 and 3, with these peaks exhibiting a λ_{max} of 440 nm and 416 nm respectively. The 380 nm peak (1) demonstrates a mass and absorbance spectra consistent with 1.

The m/z difference between $[M-H]^-$ ions for **1**_{observed} (581.2501) and **1**_{calculated} (581.2406) was 0.0095, or 16.3 parts per million (ppm). In order to improve the mass accuracy, the PDA was removed from the flow path, the method was optimised, and the instrument was cleaned and re-calibrated. Figure 4.3 shows MS chromatograms and mass spectra of the same BV treated duodenal sample as analysed in Figures 4.1 and 4.2, targeting the 663.2169 m/z ion for fragmentation and employing a longer, shallower gradient with a lower flow rate to optimise separation and ionisation conditions.

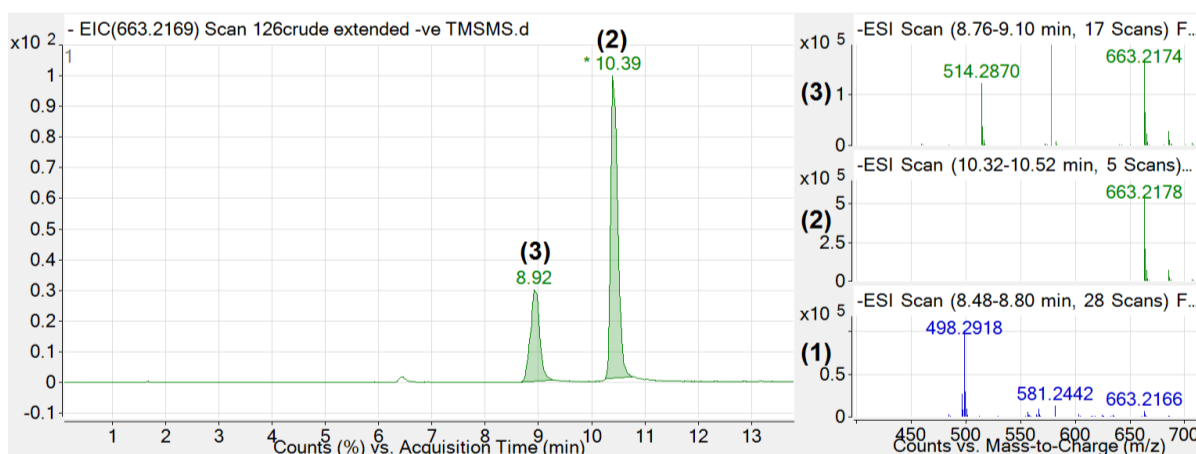


Figure 4.3: Extracted ion chromatogram (left; 663.2169 m/z \pm 0.5) and MS spectra (right) of intestinal contents obtained from a rat receiving **1 (27 mg/kg), 180 mins after i.d. administration. The 663.2178 and 663.2174 m/z ions were observed to be the major abundant ion under peaks 2 and 3, respectively (green MS spectra, top right). **1** was also identified with an m/z of 581.2442 (blue spectra, bottom right). As previously mentioned, the m/z for **1**_{calculated} is 581.2406 $[M-H]^-$, implying a ppm mass accuracy of <7 ppm.**

To determine the possible source of **1** metabolism, *C. youngae*, a non-pathogenic facultative anaerobe commonly found within the gut, was cultured and treated with **1** (C+BV), without *C. youngae* culture but with **1** (NC+BV), or with *C. youngae* and nutrient broth solvent control (C+NB) for 18 hours. The supernatant was then extracted and analysed by LCMS/MS. In order to ensure adequate separation between **1** and **2**, chromatographic separation for the

following bacterial culture analyses was achieved isocratically (30%A and 70%B). Representative MS chromatograms and spectra for these samples are displayed below (Figure 4.4).

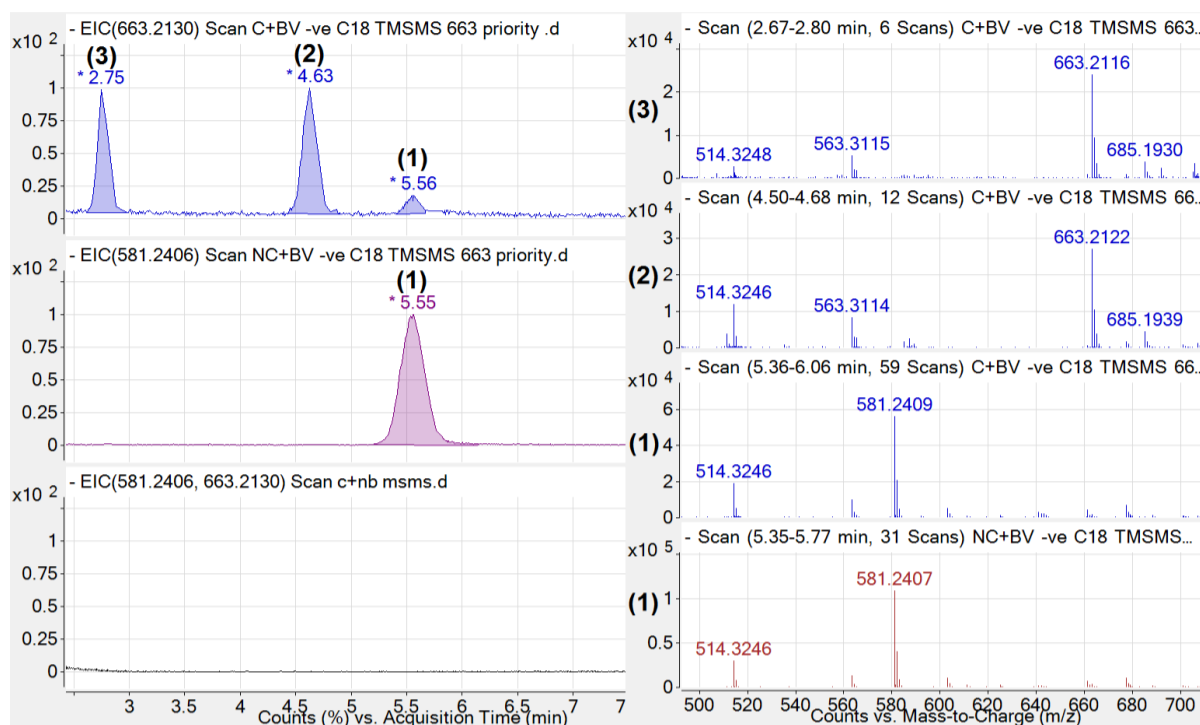


Figure 4.4: Extracted Ion Chromatogram (left) and mass spectra (right) of *C. youngae* culture treated with 1 (663.2130 m/z \pm 0.5; C+BV; blue; TOP), 1 without culture (581.2406m/z \pm 0.5; NC+BV; purple; MIDDLE) and the *C. youngae* culture without 1 added (581.2406 and 663.2130 m/z \pm 0.5; C+NB; black; BOTTOM). The 581.2407 and 581.2409 m/z ions were the major abundant ions under peak 1 [M-H]⁻ (<1 ppm mass accuracy), and the 663.2122 and 663.2116 m/z ions were the major abundant ion under peaks 2 and 3, respectively.

Having identified previously uncharacterised compounds 2 and 3, UV, mass and fragmentation spectra (see Figures 4.3, 4.4 and 4.6) demonstrated that BV metabolites formed in duodenal chyme matched that of BV treated *C. youngae*. To confirm that these compounds were formed from duodenal chyme itself, 1.2 mg/mL of BV was added to fresh duodenal contents and incubated in a petri dish at 37 °C for 30 minutes. Upon addition of BV to duodenal chyme, the BV concentration decreased by \sim 35 μ M (\sim 22%) while 2 increased by \sim 40 μ M, suggesting a 1:1 stoichiometric reaction (Figure 4.9). Furthermore, incubation of BV without duodenal chyme did not result in the production of 2.

During collision induced dissociation (CID) of the 663.217 m/z ion (Figure 4.7), a shift from 663.217 m/z [M-H]⁻ to 581.244 m/z [M-H-H₂SO₃]⁻ was observed, with the loss of 81.973 mass units occurring, equivalent to the neutral loss of H₂SO₃. This assisted in a prediction that the novel BV metabolites 2 and 3 were bilirubin-10-sulfonate (BRS). In order to confirm this prediction, a bilirubin-10-sulfonate synthesis was performed (purity >95%, yield = 53%).

Chemical synthesis and purification of **2** confirmed that the predicted metabolite of **1** had a similar mass to that of bilirubin-10-sulfonate, confirmed by using high resolution mass spectrometry (663.2150 m/z $[M-H]^-$). The in source fragmentation from ESI, observed during high resolution mass spectrometry analysis of synthesised **2** (Figure 4.5; bottom), suggests that a neutral loss of 81.9727 mass units occurred from the parent 663.2178 m/z ion (Figure 4.5; bottom), equal to the mass of H_2SO_3 ($<1\text{ ppm}$ mass accuracy). Synthesised **2** was also analysed by NMR, confirming expected shifts in ^1H and ^{13}C assignments (Figure 4.10). LCMS analysis of synthesised **2** is shown in Figure 4.5 and Figure 4.6 includes Fragmentation analysis displayed with spectra from a duodenal sample and a *C. youngae* culture sample both treated with **1**.

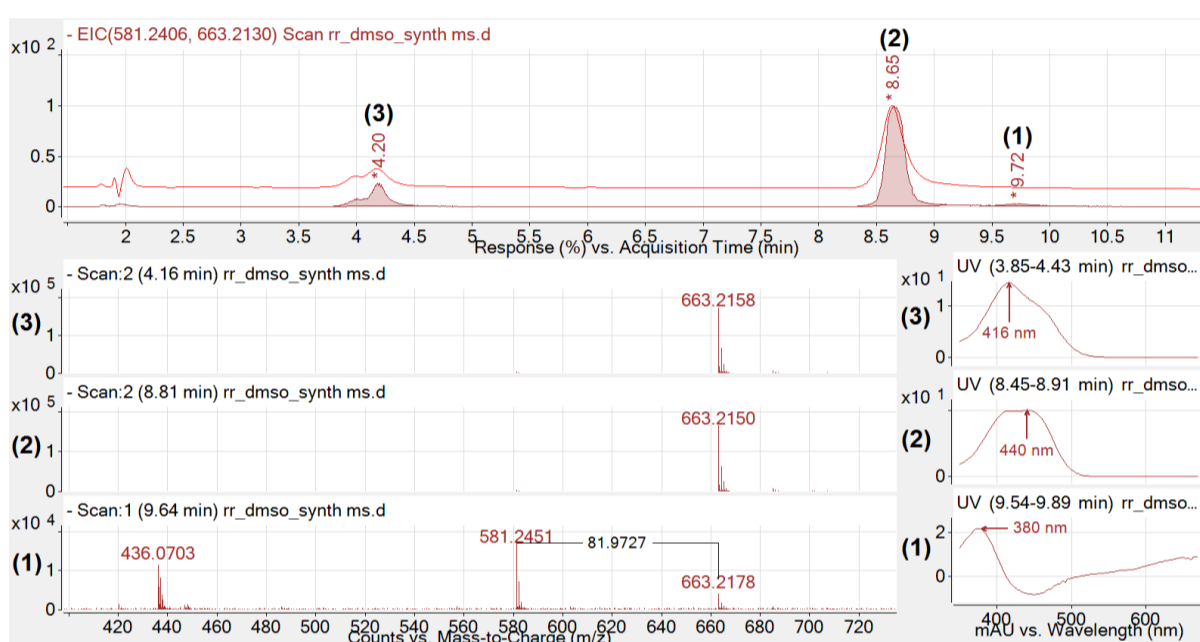


Figure 4.5: Chromatogram and related spectra of synthesised **2 (BRS; high resolution mass spectrometry mode). The red chromatogram represents UV absorbance at 440 nm and serves as a point of reference for identified ions. The superimposed chromatogram represents extracted ion chromatograms for 663.2130 and $581.2406\text{ m/z} \pm 0.5$. It should be noted that the 581.2451 m/z ion only appears at 9.7 minutes. The 663.2150 and 663.2158 m/z ions were observed to be the major abundant ion under peaks (2) and (3) at 440 nm and 412 nm respectively.**

As displayed in Figure 4.5, the 380 nm peak (1) demonstrates a 581.2426 m/z ion corresponding to BV (1) while peaks with a λ_{max} of 440 nm and 412 nm show abundant 663.2150 and 663.2158 m/z ions corresponding to that of BRS (2 and 3). The bottom chromatogram shows the 663.2178 m/z ion in low abundance; note the m/z difference between 1 and 2 equalled 81.9727 corresponding to the mass of H_2SO_3 (calculated monoisotopic mass of 81.9724; $<4\text{ ppm}$ mass accuracy). Some peak tailing occurred within this analysis, explaining the presence of both 581.2451 and 663.2150 m/z ions within the 9.55-9.91 min peak in Figure 4.5.

In order to confirm the identity of BV metabolites in duodenal and bacterial samples, CID of **2** was performed (Figure 4.6).

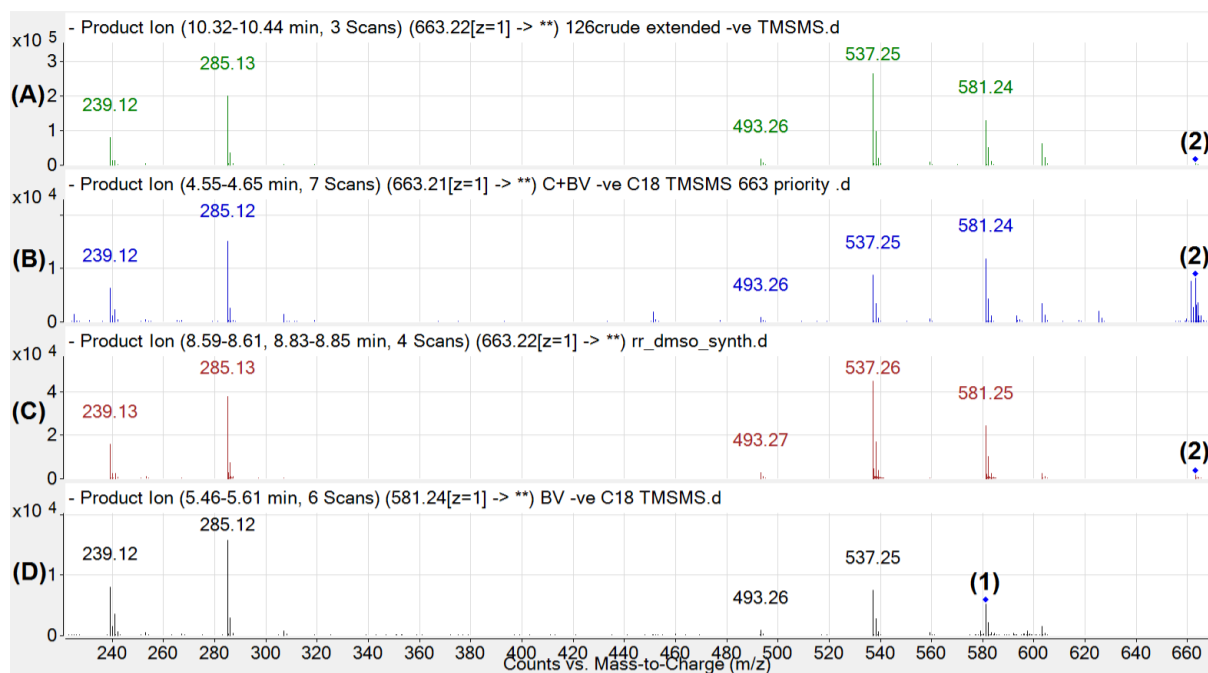


Figure 4.6: Comparison of fragmentation spectra for samples containing **2.** The spectra show CID fragmentation at 20V from multiple product ion scans, displayed to 2 decimal places for the targetted ~ 663.2150 m/z $[M-H]^-$ ion collected from 1 treated rat duodena (A), from 1 treated bacterial assay (B) and from bilirubin-10-sulfonate chemical synthesis (C). Fragmentation of the 581.24 m/z ion (1) found in the bacterial assay control (no culture with 1 added) is shown (D) for comparison. Major fragments of 239.12/285.12/493.26/537.25/ 581.24 m/z were found in high abundance in all spectra. Note the m/z in this figure are displayed to 2 decimal places for clarity and ease of comparison.

The data presented above confirmed that **2** in all samples were identical, a graphical representation of the proposed fragmentation scheme of **2** was proposed.

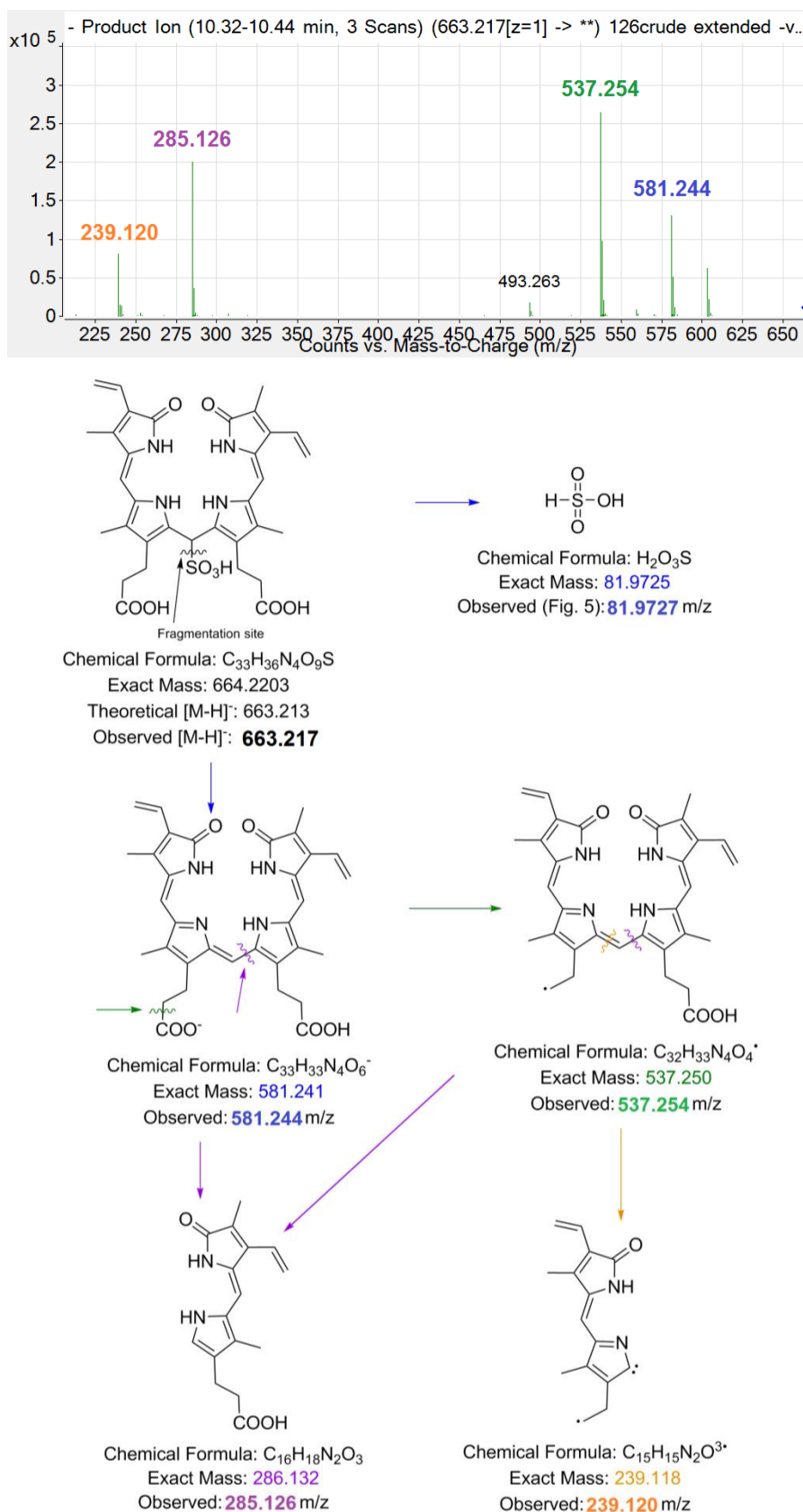
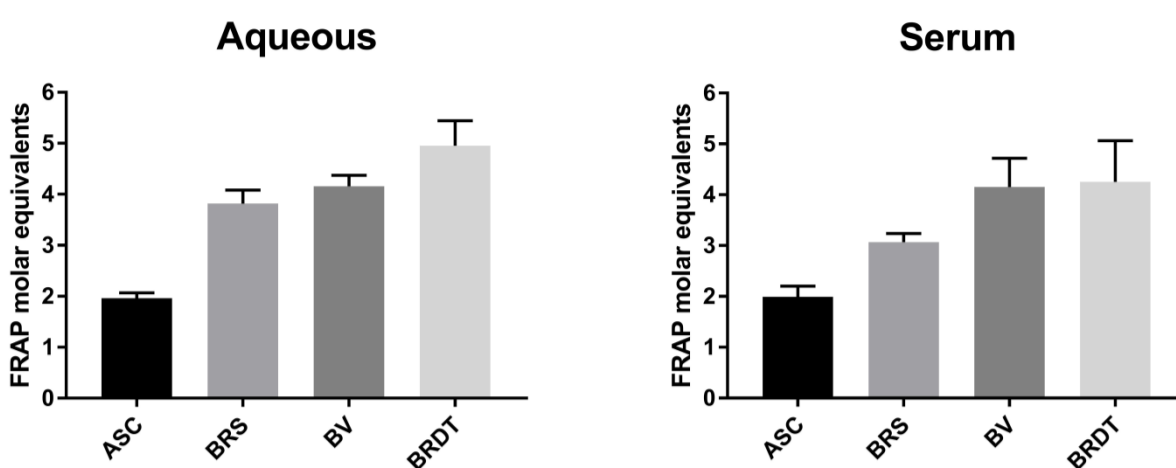


Figure 4.7: Putative structure for sulfonated BV (bilirubin-10-sulfonate; 2) with CID fragmentation pathway. The 663.215 m/z ion [M-H]⁻ first loses H₂SO₃. As a result of this neutral loss, the product ion 581.252 m/z [M-H-H₂SO₃]⁻ implies the formation of 1. The product ions then follow a similar fragmentation pattern as 1. Note the m/z in this figure are displayed to 3 decimal places, to demonstrate accurate mass of the fragments.

To determine whether 2 had reductive potential, we tested its ability to reduce ferric-tripyridyltriazine (Fe³⁺-TPTZ) to the ferrous form (Fe²⁺-TPTZ)⁽¹⁴⁸⁾ alongside ascorbate (ASC), biliverdin (BV; 1) and bilirubin ditaurate (BRDT) in the ferric reducing capacity of plasma (FRAP) assay (see Figure 4.8).



	Mean Diff.	Significant?	P Value
ASC vs BRS	-1.855	Yes	<.001
ASC vs BV	-2.194	Yes	<.001
ASC vs BRDT	-2.989	Yes	<.001
BRS vs BV	-0.3384	No	0.208
BRS vs BRDT	-1.134	Yes	0.002
BV vs BRDT	-0.7954	Yes	0.012

	Mean Diff.	Significant?	P Value
ASC vs BRS	-1.078	Yes	0.033
ASC vs BV	-2.162	Yes	<.001
ASC vs BRDT	-2.26	Yes	<.001
BRS vs BV	-1.084	Yes	0.032
BRS vs BRDT	-1.181	Yes	0.023
BV vs BRDT	-0.09774	No	0.821

Figure 4.8: FRAP analysis of 2 (BRS), ASC, 1 (BV) and BRDT (0-100 μ M; n = 3) in both aqueous (left) and serum (right). Aqueous 2 reduces 3.819 molar equivalents of Fe^{3+} -TPTZ, while ASC reduces 1.963 molar equivalents. In serum, 2 only reduces 3.069 molar equivalents while there is little difference between aqueous ASC and serum ASC (1.963 vs 1.991 molar equivalents, respectively). Related tetrapyrroles (1 and BRDT) both had more reductive potential than 2 ($p < 0.05$) in serum, however there was no significant difference in the reductive potential between aqueous 1 and 2. One way ANOVA and Fisher's LSD was used to make multiple comparisons, $p < 0.05$ was considered significant.

As displayed in Figure 4.8, 2 reduces 3.819 and 3.069 molar equivalents of Fe^{2+} -TPTZ in aqueous and serum preparations respectively. For reference, ascorbate has been previously reported to reduce 2 molar equivalents and in this assay it appears to have reduced 1.963 and 1.991 equivalents (aqueous and plasma media), indicating that the assay functioned as intended.

DISCUSSION

We show for the first time a new metabolic pathway for BV (1) in mammals, which is likely related to bacterial metabolism of 1 within the gut. Metabolism of 1 to 2 was observed *in vivo* and was confirmed in *in vitro* bacterial cultures of *C. youngae*. Formation of 2 was confirmed using HPLC, showing expected shifts in retention times and change in λ_{max} from 385 to 420-450 nm due to reduction of the C10 bridge of 1. Furthermore, high resolution liquid chromatography-mass spectrometry determined with high confidence the product of 2, with fragmentation spectra demonstrating removal of sulfonate and the consequent formation of 1, which was fragmented into its dipyrrolic halves (Figure 4.7).

Previous reports demonstrate the formation of a BV metabolite upon i.d. administration of **1**, with chromatographic evidence suggesting the compound formed was more polar than **1** and possessed a reduced C10 bridge (λ_{\max} 420-450 nm). This report sought to identify the product formed by performing additional chromatographic investigations and high-resolution tandem LCMS analysis in two independent models (*in vivo* and bacterial culture experiments). LCMS analysis revealed that two novel compounds (**2**, **3**) with differing retention times, similar UV spectra, m/z 663.215 and a similar fragmentation spectra were observed in the **1** treated rat duodenum and the **1** treated *C. youngae* culture. These data suggest that intraduodenal administration of **1** is associated with the formation of **2** and that **2** is also formed when **1** is exposed to the facultative anaerobe *C. youngae*.

HPLC and LCMS/MS confirmed the identity of **2** as bilirubin-10-sulfonate⁽³⁶⁾ in both bacterial and duodenal samples, and NMR analysis (Figure 4.10) verified the physico-chemical nature of chemically synthesised BRS, which shared an identical mass and CID spectra to **2** and **3**. We expect that **2** is the major biological metabolite of **1**, with the formation of **3** occurring over time when **2** is solubilised in aqueous or methanolic solution, under normal lighting conditions at room temperature.

Our previously published⁽¹⁾ HPLC method used to detect BV metabolites required an *n*-dioctylamine containing mobile phase, which is incompatible with LCMS.⁽¹⁾ Thus, a new method was developed in order to analyse these compounds via mass spectrometry. We then observed that during both ionisation and fragmentation (Figure 4.5 and Figure 4.6 respectively), the sulfonate group (H_2SO_3) at the C10 bridge of **2** was cleaved, followed by the detection of a BV 581.242 m/z ion (**1**). The neutral loss of H_2SO_3 has been reported previously (i.e. intestinal sulfonation of gambogic acid in the rat) and the subsequent neutral loss of H_2SO_3 in negative ion mode for both ESI and CID of the sulfonated compound during MS/MS analysis.⁽¹⁴⁹⁾ The 581.242 m/z ion observed in both **1** $[\text{M}-\text{H}]^-$ and **2** $[\text{M}-\text{H}-\text{H}_2\text{SO}_3]^-$ both follow similar CID for BV as previously described in the literature.⁽¹⁵⁰⁾ Interestingly, the CID spectra for **1** and **2** also feature a 285.126 m/z ion as a prominent fragment, and this fragment has been reported in the literature as a prominent fragment for UCB under similar CID conditions⁽¹⁵¹⁾ indicating that all 3 compounds have this dipyrrole moiety in common (Figure

4.7). Chemically prepared and biologically formed **2** both exhibit similar fragmentation patterns (Figure 4.6), and therefore it is possible that **1** may be metabolised into **2** in the duodenum and transported to the blood where it could contribute to reductive potential and potentially be oxidised to become **1**.⁽¹⁵²⁾ We confirmed that **2** contributes to reductive capacity of serum, reducing 3 molar equivalents of (Fe³⁺-TPTZ) in the FRAP assay. Therefore, future investigation into the pharmacokinetics of **2** is warranted, in addition to studying the efficacy of its administration in disease models that induce oxidative damage.

The broad specificity of anaerobic bacterial enzymes found in the human gastrointestinal tract for bile pigments has been previously demonstrated⁽¹⁵³⁾ and it has been suggested that bilirubin reducing enzymes serve for the disposal of electrons produced by fermentolytic processes performed by these bacteria, however, the mechanisms of biliverdin/bilirubin metabolism are poorly understood.

Citrobacter youngae is widely distributed in water, soil, food, and the intestinal tract of humans and animals. It stands among several genera of the family *Enterobacteriaceae* found in mammals and respire tetrathionate (S₄O₆²⁻), which is formed in the intestinal mucosa of vertebrates as a result of the oxidation of thiosulfate (S₂O₃²⁻; an endogenous luminal sulfur compound) by reactive oxygen species (ROS) during gut inflammation.⁽¹⁵⁴⁾ The reduction of tetrathionate is catalyzed by a membrane bound electron transport chain (containing tetrathionate reductase).⁽¹⁵⁵⁾ This process results in the reduction of tetrathionate into two molecules of thiosulfate which is in turn reduced further to sulfite (SO₃²⁻) and hydrogen sulfide (H₂S) via disproportionation which can provide energy for growth.⁽¹⁵⁶⁾ It is quite interesting to note that octahaem tetrathionate reductase in *Shewanella oneidensis* contains eight covalently attached haem groups⁽¹⁵⁷⁾, which highlights the complicated interplay between mammalian haem metabolism, the use of O₂ in mitochondria as a final electron acceptor, and the bacterial respiration of sulfates and inflammatory processes, all of which involve the structure of cyclical and linear tetrapyrroles. Based upon our limited knowledge of tetrapyrrole bacterial metabolism, we hypothesised that bacteria might sulfonate biliverdin (**1**) via the generation of bisulfite ions which are added to biliverdin at the C10 bridge, forming bilirubin sulfonate (**2**).

It is possible that *C. youngae* either enzymatically, or through the process of sulfite production occurring at the membrane during tetrathionate reduction and subsequent disproportionation into sulfites and sulfides, could catalyse the formation of **2** from **1**. We note the **2** synthesis method adopted here involved addition of sodium hydrogen sulfite to **1**⁽¹²⁴⁾, lending credibility to the idea that sulfite production from bacteria may occur via a similar mechanism and result in the formation of **2**.

While there are no reports identifying the presence of endogenous **2** production in mammals, **2** has been identified in the bullfrog. McDonagh⁽³⁶⁾ reported that the larval American bullfrog *Rana catesbeiana* does not produce UCB or bilirubin glucuronides, but rather forms a related polar linear tetrapyrrole, BRS (**2**) from BV (**1**). McDonagh also reports that **2** is excreted intact in the bile of the frog, but not in the rat.⁽³⁶⁾ This may occur because frogs lack hepatic expression of BVR⁽³⁶⁾, meaning that **1** was available for hepatic metabolism (to **2**). Further, i.v. administration of **1** or frog haemoglobin to bullfrogs leads to biliary excretion of **2**, suggesting the hepatic formation of **2** occurs by the enzymatic addition of HSO₃⁻ anion to **1** in the frog liver.⁽³⁶⁾ Interestingly, the bullfrog exhibits great tolerance against freezing⁽³⁷⁾, and bullfrog tadpoles (*Lithobates catesbeiana*) exhibit high tolerance towards Paraquat toxicity, which catalyses the formation of ROS, specifically superoxide anions.⁽³⁸⁾ Given the antioxidant capacity of related tetrapyrroles⁽¹¹⁷⁾, **2** may form part of the antioxidant defence network in the bullfrog. We confirmed the reductive potential of **2**, demonstrating that one molecule of **2** scavenges 3.819 equivalents of FRAP oxidant (aqueous), similar to that of BRDT, supporting a conclusion that **2** may support antioxidant defence mechanisms *in vivo*.

This study suggests that oral administration of **1**, which reportedly induces protection against Forssmann anaphylaxis in Guinea pigs⁽¹⁴⁷⁾, may instead result in **2** formation (as demonstrated in Wistar rats⁽¹⁾). **2** is rapidly absorbed and accumulates within the blood after the administration of **1**⁽¹⁾ and, therefore, might represent an active metabolite of **1** and potentially protect against hypersensitivity reactions. We demonstrate that **2**, **1** and related tetrapyrroles reduce Fe³⁺-TPTZ radical species and therefore may serve as a protective mechanism against inflammatory/anaphylactic mechanisms as previously reported.^(7, 158, 159) Therefore, **2** should be tested in models of inflammation, with **1**, to discriminate relative efficacies. If **2** is

determined to be efficacious, the pharmacokinetics of various **2** formulations could be tested in addition to titrating the necessary dose to maximise the efficacy of treatment.

This manuscript is the first to report gastroenteric BV (**1**) metabolism and provides details as to the nature of this metabolite, the source of its formation and its reductive potential. These results carry importance because they may assist in explaining the anti-inflammatory effects of **1** in addition to assisting in rational drug design of anti-inflammatory drugs.

Methods:

Reagents and Materials:

Biliverdin hydrochloride was obtained from Frontier Scientific (Utah, USA). All other reagents were obtained from Sigma-Aldrich, unless otherwise stated. BV standards were stored at -30 °C (in DMSO) and biological samples were stored at -80 °C. Prior to injection, 40 µL of either standard (~50 µM) or sample was added to 120 µL of mobile phase (50:50 20 mM ammonium acetate in 100% HPLC grade methanol: 20 mM ammonium acetate in HPLC grade H₂O), except for duodenal samples where 120 µL of pure methanol (duodenum) was used instead of mobile phase in the same ratios.

Synthesis of bilirubin-10-sulfonate (BRS; **2)**

In a dark room and in vessels covered in foil, biliverdin.HCl (10 mg) was dissolved in 10 mL of ethanol. With the mixture, 1 mL of NaHSO₃ solution (0.4 g; 1.92 mmol) was added and this mixture was vortexed for 30 seconds at time points 0, 15, 30 and 45 minutes. After the 45th minute, the mixture was centrifuged for 5 minutes at 4500 rpm, and the supernatant was added to 10 mL of saturated Na₂SO₄ with 5 µL of glacial acetic acid then added. The mixture was then vortexed for 30 seconds and centrifuged again for 5 minutes at 4500 rpm. The supernatant was then diluted at a ratio of 1:2 (supernatant:dH₂O). Under light vacuum, the mixture was passed through a C18 hypersep SPE cartridge (Thermo Fisher Scientific, Australia; 300 mg packing) that had been conditioned with 15 mL of methanol, followed by 15 mL of pure dH₂O. Following the addition of the mixture, 35 mL of dH₂O was passed through the column. Bilirubin-10-sulfonate was eluted from the SPE cartridge using 5 mL of methanol. Pure product was obtained after removal of methanol via centrifugal evaporation at room

temperature (below 30 °C). The pure product was then analysed by mass spectrometry (ESI-MS, 663.215 m/z, Figure 4.5).

High Performance Liquid Chromatography/Mass Spectrometry – a method for the simultaneous detection of 1 & 2 present in biological matrices and sample assays.

Bacterial assays, intestinal samples and standards were analysed for **1** and structurally related tetrapyrroles using HPLC-ESI/MS/MS (Agilent, California, USA). Biliverdin (**1**), bilirubin-10-sulfonate (BRS; **2**), and a primary bilirubin-10-sulfonate breakdown product (**3**) were detected using a photodiode array (380 nm, 440 nm and 412 nm respectively), in a single run. HPLC-ESI/MS/MS (LCMS/MS) analysis was performed on an Agilent 1290 HPLC (with PDA) coupled in series to an Agilent 6530 Q-TOF operating in negative ion mode using Agilent Jet Stream ESI ion source. Separation was achieved using a reverse phase C18 column (GraceSmart C18 150 x 4.6 mm, 3 µm, Grace Davidson, Australia; column oven set at 45 °C) and a flow rate of 1.0 mL·min⁻¹. The initial mobile phase consisted of 50% mobile phase B (20 mM ammonium acetate in 100% HPLC grade methanol) and 50% mobile phase A (20 mM ammonium acetate in 100% HPLC grade H₂O). A linear gradient was applied: 0-3 minutes, 50% B; 3-11 min, from 50% to 65% B; 11-12 min, from 65% to 95% B; from 12-15 min, 95% B. After 15 minutes, 50% B was run for a minimum of 7 minutes to re-equilibrate the column between analyses. Reference ions at 68.995758, 119.036320, 301.998139 and 966.000725 m/z were continually introduced into the detector along with the eluent to provide accurate reference mass correction. ESI operating conditions were: drying and sheath gas (N₂, purity >98%), drying gas temperature 325 °C, drying gas flow 10 L/min, nebulizer gas pressure 40 psig, sheath gas temperature 325 °C, sheath gas flow 12 L/min, capillary voltage 4kV with the MS and MS/MS acquisition range set from 70 – 700 m/z. The nozzle, fragmentor, skimmer and octopole RF voltages were set at 2000, 130, 65 and 750 V, respectively. Nitrogen (purity >99.999%) was used as the collision gas for MS/MS analysis, with collision-induced dissociation (CID) voltages set at 10, 20 and 40 V. Data were collected via targeted MS/MS analysis with a scan rate of 3 spectra/sec. A 663.2150 m/z ion was identified as the ion in highest abundance correlating with the UV peaks of unknown metabolites and was targeted as the precursor ion for CID, along with the 581.2425 m/z ion which eluted with the UV peak of **1**. **1** and **2** were also detected in series (prior to MS/MS analysis) using a photodiode array (PDA; 380 nm and 440

nm, respectively) in a single run. Agilent MassHunter software was used for UV and MS data analysis.

Prior to analysis, duodenal wash or bacterial assay samples were defrosted at 22 °C and were prepared by adding 120 µL of pure methanol to 40 µL of the sample and centrifuged (21500 × *g*; 10 min). The supernatant from each sample was then passed through a 0.22 micron PTFE syringe filter (Shimadzu, Australia), and 20 µL of the filtrate was injected via the autosampler for analysis.

Duodenal administration of 1 to rats

Rats were administered biliverdin hydrochloride as documented previously.⁽¹⁾ To prepare a duodenal sample, 1 mL of sterile phosphate buffered saline was washed through the duodenum via syringe and collected. It was then centrifuged (21500 × *g*; 10 min) and the supernatant was aliquoted and immediately transferred to a –80 °C freezer for later analysis.

Bacterial metabolism of 1

To test whether *C. youngae* metabolised **1**, 100 µL of a 1 mM solution of **1** or equivalent volume of diluent (2% DMSO + 98% 100 mM TRIS-HCl 7.6 pH) was added to a *C. youngae* culture at 1 : 1 ratio and was incubated at 37 °C for 60 mins. The reaction was quenched with 800 µL of –20 °C methanol (MeOH) at 0, 20, 40 and 60 mins, in order to determine the effect of time on **1** metabolism. To ensure consistency and repeatability between experiments the culture broths were inoculated for a period of 18 hrs, the bacterial content of which was standardised to 0.28 OD by measuring optical density with a spectrophotometer (POLARstar, Germany) at 600 nm. After completion of the assays, the samples were centrifuged (30000 × *g*; 80 seconds) and the supernatant was aliquoted and immediately transferred to a –80°C freezer for later analysis.

Appropriate control assays were prepared in the same manner, with one excluding **1** (culture with no **1**) and another not including bacterial culture including **1** (no culture with **1**).

Duodenal chyme metabolism of 1

To confirm that the duodenal content, and potentially bacteria therein was responsible for forming **1**, an 8 cm length of duodenum, cut 2 cm distal to the pyloric sphincter, was removed

from a naïve Wistar rat. To one end of the freshly excised duodenum, a 5 mL syringe was attached and 5 mL of phosphate buffered saline was washed through it with the resulting liquid collected in a petri dish. A control sample of 5 mL PBS added directly to a second petri dish prepared at the same time. A 500 μ L sample was collected prior to the addition of sodium biliverdinate from both petri dishes and analysed for its BV and BRS concentration. To both dishes, 500 μ L of 1.2 mg/mL sodium biliverdinate was then added and both dishes were incubated in the dark at 37 °C. At 1, 5, 15 and 30 minutes, a 500 μ L sample was collected. 40 μ L of each sample was immediately prepared for analysis of BRS and BV via LCMS.

FRAP assay

The ferric reducing ability of plasma (FRAP) was determined by the method of Benzie and Strain⁽¹⁴⁸⁾ and performed on a COBAS Integra 400 analyser (Roche Diagnostics, Australia). Three independent dose response experiments were conducted, with each concentration of each bile pigment tested in duplicate in each experiment. The sodium salt of biliverdin was prepared as previously published.⁽¹⁾ All other compounds were solubilised in distilled H₂O at stock solutions of 4 mM and were diluted further for experimental testing (final concentrations 0-100 μ M). All solutions were covered in foil and lights dimmed during experimental testing. All solutions were made in either ddH₂O or human plasma obtained with informed consent from a single healthy donor and repeated in triplicate, with all methods carried out in compliance with relevant guidelines and regulations. Reductive equivalents were determined by fitting a linear regression to the dose response relationship with the slope of that relationship quantifying the reducing equivalents per mole of bile pigment.

NMR analysis

¹H and ¹³C NMR spectra were recorded at 298 K on an Avance 300 MHz spectrometer (300 and 75 MHz, respectively; Bruker BioSpin). ¹H-¹H correlation spectroscopy (COSY) and ¹H-¹³C heteronuclear single quantum coherence (HSQC) were used to confirm ¹H and ¹³C assignments. Signals are reported as chemical shift (δ in ppm) relative to (CD₃)₂SO (¹H NMR: δ =2.50 ppm; ¹³C NMR: δ = 39.52 ppm). Coupling constants (*J*) are reported in Hz and can be found in Figure 4.10.

Additional information

Author contribution statement

A.C.B. provided rat duodenum samples and assisted in data analysis. Both A.C.B. and R.G.S performed HPLC and LCMS method development and analysis, developed the bilirubin-10-sulfonate synthesis method and wrote the manuscript text. B.M. assisted in LCMS/MS analysis and elucidation of fragmentation data. J.V. performed the bacterial analysis. A.P. assisted with the synthesis and NMR analysis. H.S. assisted with microbiological studies. A.R.B. assisted with research design and interpretation of data. K.H.W assisted with concept, design and final approval. All authors contributed to revision of the MS and provided their final approval for manuscript submission.

Competing interests

The author(s) declare no competing interests.

Acknowledgement

The authors acknowledge the assistance of Ben Matthews and the Griffith SmartWater Institute for the Q-TOF analysis. The authors thank Mr Ben Jull for early discussions regarding the nature of biliverdin metabolism. The authors acknowledge the support received through an Australian Government Research Training Program Scholarship as well as the generosity of Patricia Barlow in providing a scholarship. The research was supported by the Griffith Enterprise Innovation Fund, which utilised funding provided by Griffith University and the Queensland Government.

Animal Use

All animal care and experimental procedures complied with the Guidelines of the Australian National Health and Medical Research Council and were approved by the Ethical Committee of the University of Queensland.

Human Tissue

Human blood was obtained with informed consent from all subjects under permission from the Griffith University Human Research Ethics Committee, all methods were carried out in accordance with relevant guidelines and regulations.

Supplementary information

Duodenal chyme metabolism of 1

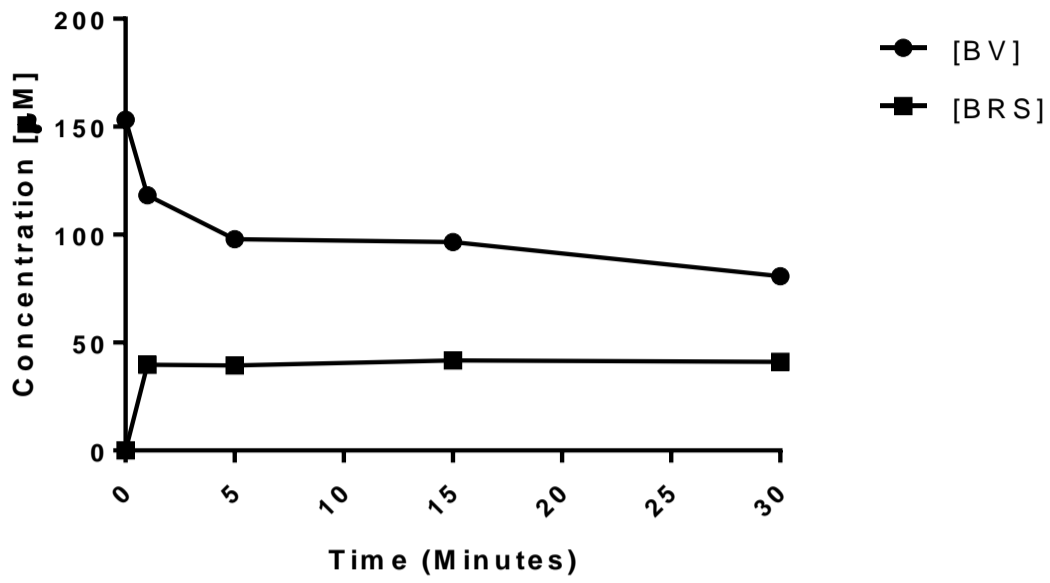


Figure 4.9: Formation of BRS (2) over time, after addition of BV (1) to duodenal chyme.

Sodium bilirubin-10-sulfonate (2)

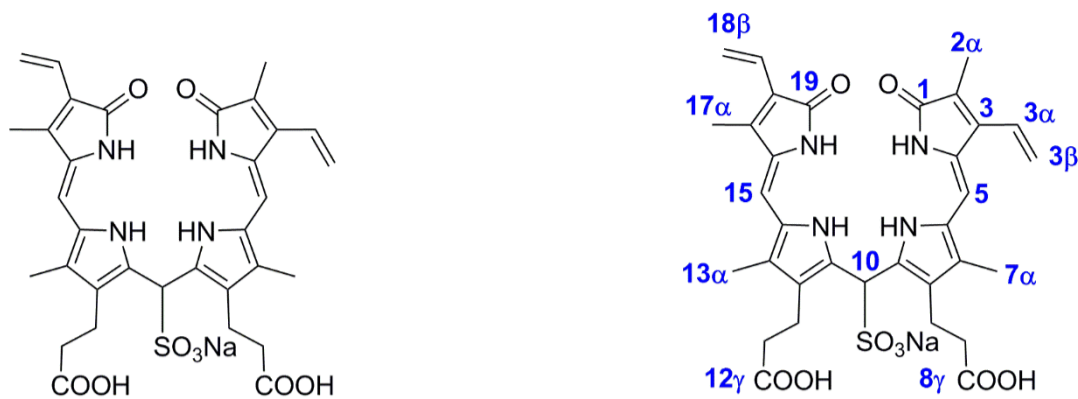


Figure 4.10: ^1H NMR (400 MHz, $\text{DMSO-}d_6$): δ 10.21 – 10.08 (m, 2 H, 2 \times COOH); 6.81 – 6.72 (m, 1H, H-18 α); 6.52 (dd, 1H, $J_{3\alpha,3\beta}$ *cis* 17.5, $J_{3\alpha,3\beta}$ *trans* 11.5 Hz, H-3 α); 6.14 (dd, 1H, $J_{3\beta}$ *cis,3\beta* *trans* 2.7 Hz, H-3 β *cis*); 6.07 (br s, 2 H, H-5, H-15); 5.61 – 5.57 (m, 2 H, H-18 β); 5.24 (dd, 1 H, H-3 β *trans*); 5.19 (s, 1H, H-10); 4.13 – 2.90 (br s, 4 H, 4 \times NH); 2.70 – 2.45 (m, 6 H, H-8 α , H-8 β , H-12 α); 2.20 – 1.93 (m, 11 H, H-7 α , H-12 β , H-13 α , H-17 α); 1.85 (s, 3 H, H-2 α). ^{13}C NMR (100 MHz, $\text{DMSO-}d_6$): δ 178.1, 172.0, 171.2, 171.2 (C-1, C-8 γ , C-12 γ , C-19); 142.7, 140.9, 130.8, 130.0, 129.8, 129.6, 127.8, 127.5, 124.6, 123.6, 123.5, 123.4, 123.3, 122.7, 122.7, 122.2, 121.7, 121.5, 117.9 (C-2, C-3, C-3 α , C-3 β , C-4, C-5, C-6, C-7, C-8, C-9, C-11, C-12, C-13, C-14, C-15, C-16, C-17, C-18, C-18 α , C-18 β); 101.0, 100.3 (C-5, C-15); 54.8 (C-10); 36.1 (C-8 β , C-12 β); 21.6 (C-2 α); 20.4 (C-8 α); 20.4 (C-12 α); 10.0, 10.0, 9.8 (C-7 α , C-13 α , C-17 α). HRMS calculated for $\text{C}_{33}\text{H}_{35}\text{N}_4\text{NaO}_9\text{S}$ [$M\text{-Na}$] $^-$, 663.212477; found ESIMS (m/z): 663.2150 [$M\text{-Na}$] $^-$. (<5 ppm mass accuracy)

Chapter Five: Pharmacokinetics of Bilirubin-10-sulfonate and Biliverdin: the potential therapeutic administration of a novel tetrapyrrole

Foreword: Following the characterisation and identification of BRS documented in Chapter Four, this study sought to determine the pharmacokinetics of BRS alongside BV. This manuscript also identifies the ideal route and timing of administration of BV and BRS, which guided experimental design for Chapter 6 where the anti-inflammatory properties of BRS and BV were investigated.

The abbreviations, formatting and referencing of this document have been altered slightly to more closely reflect the formatting of other chapters and published work in this thesis.

Statement of Contribution to a Co-Authored Paper Submitted for Publication

This chapter is in the form of a co-authored paper currently under consideration. The bibliographic details of the co-authored published paper are:

Shiels, R.G., Hewage, W., Vidimce, J., Pearson, A.G., Wagner, K-H., and Bulmer, A.C. Pharmacokinetics of bilirubin-10-sulfonate and biliverdin: unlocking the therapeutic potential of a novel antioxidant formed by the enteric microbiome. Submitted to *European Journal of Pharmaceutical Science*.

Appropriate acknowledgements of those who contributed to the research but did not qualify as authors are included in the paper.

My contribution to the published paper involved:

- Experimental design and planning
- Development and validation of the analytical methods
- Experimental execution and sample collection
- Data acquisition and statistical analysis
- Manuscript preparation, critical review and submission

(Sign) _____

First Author
Ryan Shiels

(Date) 11th February 2020

(Sign)

(Date) 11th February 2020

Corresponding Author and Supervisor
Associate Professor Andrew Bulmer

Pharmacokinetics of bilirubin-10-sulfonate and biliverdin: unlocking the therapeutic potential of a novel antioxidant formed by the enteric microbiome

Ryan G. Shiels¹, Wenu Hewage¹, Josif Vidimce¹, Andrew G. Pearson¹, Karl-Heinz Wagner²
and Andrew C. Bulmer^{1*}

¹ School of Medical Science and Menzies Health Institute Queensland, Griffith University, Gold Coast, Queensland, Australia

²Department of Nutritional Sciences, University of Vienna, Vienna, Austria

Abstract

Background and Purpose: Biliverdin (BV) administration induces antioxidant and anti-inflammatory effects, with previous reports also identifying anti-anaphylactic potential. Interestingly however, intra-duodenal administration of BV in rats leads to the formation of bilirubin-10-sulfonate (BRS), which might be responsible for BV's purported effects.

Experimental Approach: This study aimed to assess the intravenous, intraperitoneal and intraduodenal pharmacokinetics of BRS and BV in order to assess their therapeutic potential in future studies. Bile and venous blood were intermittently collected before and after administration, which was subsequently analysed using liquid chromatography-mass spectrometry for quantification of bile pigment concentrations.

Key Results: When BRS was administered i.v., BRS had a significantly ($p < 0.05$) longer elimination (146.0 vs 61.3 minutes) and distribution (38.3 vs 6.3 minutes) half-life compared to BV, and significantly reduced ($p < 0.05$) volume of distribution (0.048 vs 0.065 L kg^{-1}). Furthermore, BRS was excreted intact in the bile, whereas BV was excreted after chemical reduction and conjugation. As a consequence, intraperitoneal and intraduodenal administration resulted in significantly greater blood concentrations of BRS ($p < 0.05$) with similar bioavailabilities (i.p. BV 31.9%, BRS 31.6%; i.d. BV 0.08%, BRS 0.14%), over 180 minutes.

Conclusions and Implications: Cumulatively, these data demonstrate that BRS has a superior pharmacokinetic profile when compared to BV, which is a result of its resistance to hepatic metabolism and excretion. These data therefore provide a basis to explore the capacity of BRS to protect from inflammatory pathology.

Introduction

Biliverdin (BV) and unconjugated bilirubin (UCB) are catabolites of haem and protect from oxidant-mediated damage *in vivo*. Specifically, BV administration confers protection in animal models of ischemia-reperfusion injury^(41, 144), including liver transplantation in swine.⁽¹⁴¹⁾ Oral administration of BV potently protects from Forssmann reagent induced anaphylaxis in guinea pigs⁽⁷⁾ and its intravenous (i.v.) administration after haemorrhagic shock and resuscitation protects against acute lung injury (ALI)⁽¹⁴³⁾ suggesting important anti-inflammatory potential. Given that intravenously and intraperitoneally administered BV is rapidly reduced to UCB *in vivo*⁽¹⁾, it remains unclear to what extent each of these molecules contribute to protection in these models.

Intriguingly, intraduodenal (i.d.) administration of BV in rats leads to the formation of a novel antioxidant, bilirubin-10-sulfonate, via addition of bisulfite (HSO_3^-) to BV.⁽¹⁶⁰⁾ This process occurs due to HSO_3^- formation by enteric bacteria, resulting in the rapid and complete transformation of BV to bilirubin-C10-sulfonate (BRS) which is absorbed and found in the duodenum, serum, bile and urine.^(1, 160) Intraduodenal BRS formation from BV now suggests that oral BV administration leads to the formation of BRS that may confer protection against anaphylaxis, as reported previously.⁽¹⁴⁷⁾ There is scarce BRS pharmacokinetic data within the literature. Although McDonagh et al⁽³⁶⁾ reported intact biliary excretion of BRS after i.v. administration bullfrogs, however, this did not occur in rats. This report was very brief with no quantitative data provided. Given that BRS possesses similar reductive capacity to UCB and related bile pigments⁽¹⁶⁰⁾, it is crucial that the pharmacokinetics of BRS be described in order to inform further research regarding its therapeutic potential in models of oxidative stress/inflammation.

The aims of this study were to quantify the pharmacokinetics of BV versus BRS in rats after i.v., i.d. and intraperitoneal (i.p.) administration as well as to determine their biliary excretion.

Methods

Materials

Experimental work was performed under low light conditions, with BV and BRS solutions covered in foil and administered within 10 minutes to minimise degradation. Biliverdin hydrochloride (BV-HCl), bilirubin-10-sulfonate and all other bile pigments including meso compounds were obtained from Frontier Scientific (Utah, USA). All other reagents were obtained from Sigma-Aldrich, unless otherwise stated. Powdered BRS and BV standards were stored at -20 °C, while internal standard solutions and biological samples were frozen in liquid nitrogen and stored at -80 °C.

Sodium biliverdinate synthesis

50 mg of NaOH (1.252 mmol) was added to 400 mL of ethanol and sonicated for 10 minutes at 32 °C. This solution was then added to a flask containing 250 mg of BV-HCl (0.404 mmol). This solution was again sonicated for 10 minutes at 32 °C, then 20 mL aliquots of the 0.625 mg mL⁻¹ BV solution were transferred to 50 mL Falcon tubes, with each containing 12.5 mg of BV. These solutions were then evaporated to dryness (Speedyvac centrifuge vacuum concentrator; LabGear, Australia) at 400 × *g*, 32 °C for 12 hours at a pressure of ~2 millibar. The dry aliquots were sealed, transferred to a -80 °C freezer and prepared immediately prior to use.

Test systems used

Male Wistar rats (10-12 weeks old; 327-437g; Animal Resources Centre, Australia) were fasted for approximately 12 hours (with free access to water) and allocated to ensure similar average animal weights for each group. For i.v. administration (2.7 mg kg⁻¹ body weight) ~1.25 mg of BV/BRS was dissolved in 1 mL of sterile phosphate-buffered saline (PBS; Baxtor, Australia), sonicated for 5 minutes and administered through a syringe filter (0.45 µm, 33 mm, Millex PVDF syringe filter, Australia) into the jugular vein via a cannula, which was followed by a further 3 mL of 0.9% sterile NaCl through the same filter to minimise any loss of compound within the filter. For i.p. and i.d. administration (27 mg kg⁻¹ body weight), 12.5 mg of BV/BRS was dissolved in 4 mL of PBS and sonicated for 5 minutes where the solution was filtered (as above) and the required volume was administered via syringe into the peritoneal cavity for i.p. injections. For i.d. injections, a suture was tied gently around the duodenum, ~2

cm distal to the pyloric sphincter in order to prevent the dose from entering the stomach, and the dose was injected 5 cm distal to the pyloric sphincter over 120 seconds in order to allow the small intestine to fill gradually with the solution. A small drop of super glue gel (Loctite, Australia) was placed over the injection site to prevent escape of the administered fluid or duodenal chyme into the peritoneum. The duodenal suture was removed 5 minutes after compound administration. All solutions were optically clear after sonication.

For vehicle control groups, either 1 mL or 3 mL of PBS was administered (i.v. and i.d./i.p. control groups, respectively).

All animal care and experimental procedures complied with the Guidelines of the Australian National Health and Medical Research Council and were approved by the Griffith University Animal Ethics Committee (Ref: MSC/03/18/AEC).

Compliance with design and statistical analysis requirements relating to animal use

For all treatment groups, n=6 was initially planned with n=5 allocated for vehicle control groups. Due to expected adverse events (i.e. animal sensitivity to anaesthetic), n=5 was achieved in the i.v. BV and i.d. BV groups. Randomisation of treatments within each administration route was performed via generating and assigning random numbers to each animal ID. Blinding was not possible during the treatment process as each compound administered has a distinctive colour (Blue for BV, yellow for BRS), however blinding was achieved during sample analysis, by having the sample preparation and instrument analysis conducted by different operators.

Experimental protocol

Rats were anaesthetised to a surgical plane with i.p. ketamine (50 mg kg⁻¹): xylazine (3 mg kg⁻¹) in a 50:3 ratio until reflexes ceased. The rats' ventral surface was then shaved and prepared for surgery, fitted with a rectal thermometer and placed on a heating pad to maintain a constant body temperature (± 1 °C from the initial reading). The right jugular vein was cannulated with flexible silastic tubing (1.19 OD \times 0.64 ID mm; Dow Corning, USA) and 50 IU mL⁻¹ of warm sterile sodium heparin (100 IU mL⁻¹; Pfizer, USA) was used to flush the cannula after each use. A mid-line laparotomy was performed, and the common bile duct was identified and cannulated with 0.78 OD \times 0.32 ID mm tubing (Microtube Extrusions, Australia). Bile acids were continuously replaced via an infusion pump administering sodium

taurocholate (taurocholic acid sodium salt hydrate; Sigma; 1 nmol minute⁻¹ g⁻¹ body weight) diluted in sterile 0.9% NaCl through a syringe filter and a 3-way valve (Becton Dickinson, USA) attached to the jugular cannula. Bile flow was allowed to equilibrate for 15 minutes after the commencement of sodium taurocholate infusion, and thereafter bile was collected for 15 minutes to approximate baseline bile pigment excretion and bile flow. Bile was collected on ice, in pre-weighed 1.5 mL microtubes (Sarstedt, Australia) and frozen. After compound or vehicle administration, the laparotomy wound was sutured closed and kept moist using 0.9% NaCl and gauze. The animal remained anaesthetised for 180 minutes with occasional i.p. administration of the previously described ketamine:xylazine solution (0.05-0.1 mL). After 180 minutes, the animals were euthanised by removal of the heart. Blood samples of 200 µL were taken from the jugular cannula, and that volume replaced with sterile, pre-warmed saline. The blood was centrifuged (5000 × *g*; 10 minutes) and the 40 µL of the supernatant (plasma) aliquoted and frozen. All frozen samples described above were first snap-frozen in liquid nitrogen, then transferred to a -80 °C freezer for storage.

Bile pigment analysis

Plasma samples were analysed for bile pigments via quantitative UHPLC-MS and bile was analysed for bile pigments via quantitative UHPLC-PDA (LCMS-2020 with SPD-30 PDA, Shimadzu, Japan). UHPLC analysis was performed using a Shimadzu Nexera X2 system and separation of the targeted tetrapyrroles was achieved using a reverse phase C18 column (Vision HT C18HL, 2mm × 100 mm, 1.5 µm, PhaseSep, Australia). The UHPLC column was preceded by a VisionHT C18HL guard column (2mm × 5 mm, 1.5 µm, PhaseSep, Australia) and an UltraShield UHPLC precolumn filter (Restek, 0.2 µm, Shimadzu, Australia), respectively. The column oven and autosampler were set to 45 °C and 4 °C, respectively, and the flow rate was 0.35 mL minute⁻¹.

Plasma analysis

The initial mobile phase consisted of 34% mobile phase B (HPLC grade methanol, Scharlau, Spain) and 66% mobile phase A (10 mM ammonium acetate in 25% HPLC grade methanol and 75% Milli-Q H₂O), representing a 50.5% initial methanol concentration. The gradient program applied for the analytical portion of the analysis was as follows: 0.3 minutes - 50% B; 1.5 minutes - 74% B; 1.8 minutes - 92% B; 3.1 minutes - 92% B. The re-equilibration portion of the analysis ran from 3.1 minutes to 6 minutes at 34% B, with the flow rate increased to 0.42 mL

minute⁻¹ at 3.5 minutes, held until 4.0 minutes, reducing linearly to 0.35 mL minute⁻¹ at 4.4 minutes and remaining so until 6 minutes. The total run time including re-equilibration was 6 minutes, with retention times of 2.17, 2.40 and 2.90 minutes for BRS, BV and UCB, respectively. A 2 µL injection volume was used for all analyses. ESI operating conditions were: Desolvation line temperature 250 °C, heat block temperature 200 °C, nebulizing gas flow 1.5 L minute⁻¹ (N₂), drying gas flow 20 L minute⁻¹ with all detection voltages set via autotune using the manufacturer's tuning solution (Shimadzu, Japan). Data were collected in negative ion mode via single ion monitoring (SIM) of the m/z corresponding with the deprotonated cation [M-H]⁻ of each compound.

External standards

Stock solutions of BRS, BV and UCB were dissolved individually at 8 mM in DMSO, then combined to form a mixed stock solution containing 2 mM of each compound. This mixed stock solution was further diluted with DMSO in order to form working solutions and were made fresh prior to each standard curve. The working solutions contained BRS/BV/UCB at concentrations from ~391nM to 200 µM.

Internal standards

Internal standards (IS) included mesobilirubin-10-sulfonate, mesobiliverdin and mesobilirubin (mBRS, mBV and mUCB, respectively). A mixed IS solution was created by initially dissolving each individual IS at 8mM in DMSO, which were then combined and further diluted with DMSO to form the final IS solution with mBRS/mBV/mUCB concentrations of 80/80/40 µM, respectively. Aliquots of 500 µL of the IS solutions were made, and frozen in liquid nitrogen prior to storage at -80 °C. Prior to use, IS aliquots were defrosted in darkness at room temperature.

Calibration

Calibration standards were prepared by adding 40 µL of working solution to 150 µL of initial mobile phase (34% B as above) and 10 µL of IS solution followed by mixing for 5 seconds via vortex. Prior to injection, the calibration standard was passed through a 0.22 µm syringe filter (PhaseSep, Australia) and 2 µL of the filtrate was injected for analysis.

Sample analysis

Prior to plasma analysis, 10 μL of IS solution was added to 40 μL of plasma, mixed via vortex for 10 seconds before adding 150 μL of 1:4 DMSO:methanol and mixing via vortex again for 10 seconds before being centrifuged ($21500 \times g$; 10 minutes). The supernatant was then passed through a 0.22 μm syringe filter (PhaseSep, Australia) and 2 μL of the resulting filtrate was injected for analysis.

Concentrations of tetrapyrroles found in the plasma were calculated via the internal standard method using AUC integration of single ion monitoring (SIM) mass chromatograms at the relevant m/z to compare each analyte to its meso internal standard. Linear calibration curves ($r^2 > 0.9995$) were generated in Labsolutions software (version 5.87 sp1, Shimadzu, Japan) and the limit of quantification for bile pigments in plasma and bile approximated 300 nM. Extraction efficiency was assessed via analysis of rat plasma spiked with 12.5/50/100 μM of BRS and BV, which was then allowed to incubate in the dark for 30 minutes allowing for an equilibrium in albumin binding to be reached. The extraction efficiency following the 12.5/50/100 μM spike was 95/90/91 % for BRS and 96/89/86 % for BV, meeting the acceptance criteria of 15% for this method.

Bile analysis

Bile analysis was performed via UHPLC using PDA detection. The initial mobile phase consisted of 60% mobile phase B (100% HPLC grade methanol) and 40% mobile phase A (20 mM ammonium acetate 100% dH_2O with 0.005% v/v acetic acid). The gradient program applied for the analytical portion of the analysis was as follows: 1.6 minutes - 60% B; 1.75 minutes - 70% B, 2.4 minutes - 95% B; 3.5 minutes - 95% B. The re-equilibration portion of the analysis ran from 3.5 minutes to 6.5 minutes at 60% B, with the flow rate increased to $0.5 \text{ mL minute}^{-1}$ at 3.75 minutes, decreasing linearly to $0.4 \text{ mL minute}^{-1}$ at 5 minutes then decreasing to $0.35 \text{ mL minute}^{-1}$ and remaining until a minimum of 6.5 minutes. The total run time including re-equilibration was 6.5 minutes, with retention times of 2.17, 2.50, 2.69, 3.2 and 3.27 minutes for bilirubin diglucuronide (BDG), bilirubin ditaurate (BRDT), BRS, BV and bilirubin monoglucuronide (BMG) respectively. A 2 μL injection volume was used for all analysis.

BRDT was used as an external standard for BDG/BMG as previously published.⁽¹⁾ Working solutions were created from $\sim 391 \text{ nM}$ to $800 \mu\text{M}$ as per the plasma analysis method above. Calibration standards were prepared by adding 40 μL of a working solution to 160 μL of initial mobile phase (60% B) and mixing for 5 seconds via vortex. Prior to injection, the calibration

standard was passed through a 0.22 μm syringe filter (PhaseSep, Australia) and 2 μL of the resulting filtrate was injected for analysis.

Prior to bile sample analysis, 160 μL of 1:4 DMSO:methanol was added to 40 μL of bile, mixed via vortex for 10 seconds before being centrifuged ($21500 \times g$; 10 minutes). The supernatant was then passed through a 0.22 μm syringe filter (PhaseSep, Australia) and 2 μL of the resulting filtrate was injected for analysis. Each sample was analysed within 45 minutes of preparation in order to minimise degradation of bile pigments.⁽¹⁾

Bile pigment concentrations were calculated via AUC integration of PDA peaks at the relevant wavelengths (440nm for BRS, 380nm for BV and 451nm for UCB and BRDT). All instrument analysis was performed using LabSolutions Software (version 5.87 sp1, Shimadzu, Japan).

Data and statistical analysis

The peak and theoretical maximum ($t=0$) plasma bile pigment concentrations, AUC of bile pigment concentrations (AUC_{180}), volume of distribution (V_{dist}), distribution ($t_{1/2\alpha}$; K_{dist}) and elimination ($t_{1/2\beta}$; K_{elim}) half-lives and rate constants were calculated using the PK solver⁽¹⁶¹⁾ add-in to perform single compartment analysis in Microsoft Excel.

Bile pigment bioavailability was calculated by dividing the AUC_{180} for i.p. and i.d. by the AUC_{180} for i.v. after correcting the i.v. AUC_{180} for differences in dosage.

In order to approximate net bile pigment excretion, the observed biliary bile pigment concentration for each time point was multiplied by the volume of excreted bile. The vehicle control group's bile pigment excretion for that time point was subtracted from treatment animals, to obtain the delta bile pigment excretion at each time point. These individual amounts were then added together over time and divided by the total bile pigment dose administered to obtain a cumulatively excreted dose through the bile.

Statistical analysis of pharmacokinetic parameters between treatment groups was performed using unpaired t-tests (GraphPad Prism version 8.1.0, USA). If data sets were not normally distributed, then the Mann-Whitney test was performed. Pharmacokinetic data are presented as mean \pm SEM. and a $p < 0.05$ was considered statistically significant.

Plasma bile pigment concentration and total bile pigment excretion over time were analysed via one-way repeated measures ANOVA (RM ANOVA; Bonferroni post hoc). If any dataset

lacked normal distribution, Friedman repeated measures ANOVA on ranks (Dunn's post hoc) was used to determine time points that were different from baseline (t_0). Where missing values were identified, mixed-effects analysis was performed. Repeated measures ANOVA with Holm-Sidak's multiple comparisons test was performed to determine differences in cumulative excreted bile pigment doses across all time points. A t-test or equivalent nonparametric procedures (Kruskal-Wallis ANOVA; Dunn's post hoc) was used to test for significant differences in the cumulative excreted dose at 180 minutes.

Results

Vehicle Control

For each experimental route of administration, the vehicle (PBS) was administered as a control for biliary bile pigment excretion and the baseline AUC for UCB over 180 minutes (AUC_{180}). Basal total bile pigment excretion was not significantly different over 180 minutes between the routes of administration (196.3 ± 19.46 nmol, 238.7 ± 14.18 nmol and 288.8 ± 52.91 nmol for i.v., i.p. and i.d. administration groups, respectively ($p > 0.05$)). Correction for total bile pigment excretion in treatment conditions was performed by subtraction of total bile pigment excretion from each of the respective vehicle groups.

Intravenous administration

Intravenous (i.v.) BRS (2.7 mg kg^{-1} of body weight) administration increased systemic BRS and BV concentrations at 5 minutes compared to 0 minutes (t_0), with BRS and BV remaining elevated until 180 and 120 minutes, respectively (Figure 5.1A). Administration of BRS also significantly increased total bile pigment, BV, BRS and bilirubin conjugate excretion rate from 10 to 180 minutes (Figure 5.1B), compared to t_0 . Additional pharmacokinetic data are presented in Table 2.

BV (2.7 mg kg^{-1} of body weight) administration increased systemic BV from 5 until 120 minutes and significantly increased UCB concentrations from 5 until 90 minutes (Figure 5.1C). Administration of BV also significantly increased total bile pigment, BV and bilirubin conjugate excretion rate from 10 to 60 minutes, compared to t_0 . (Figure 5.1D).

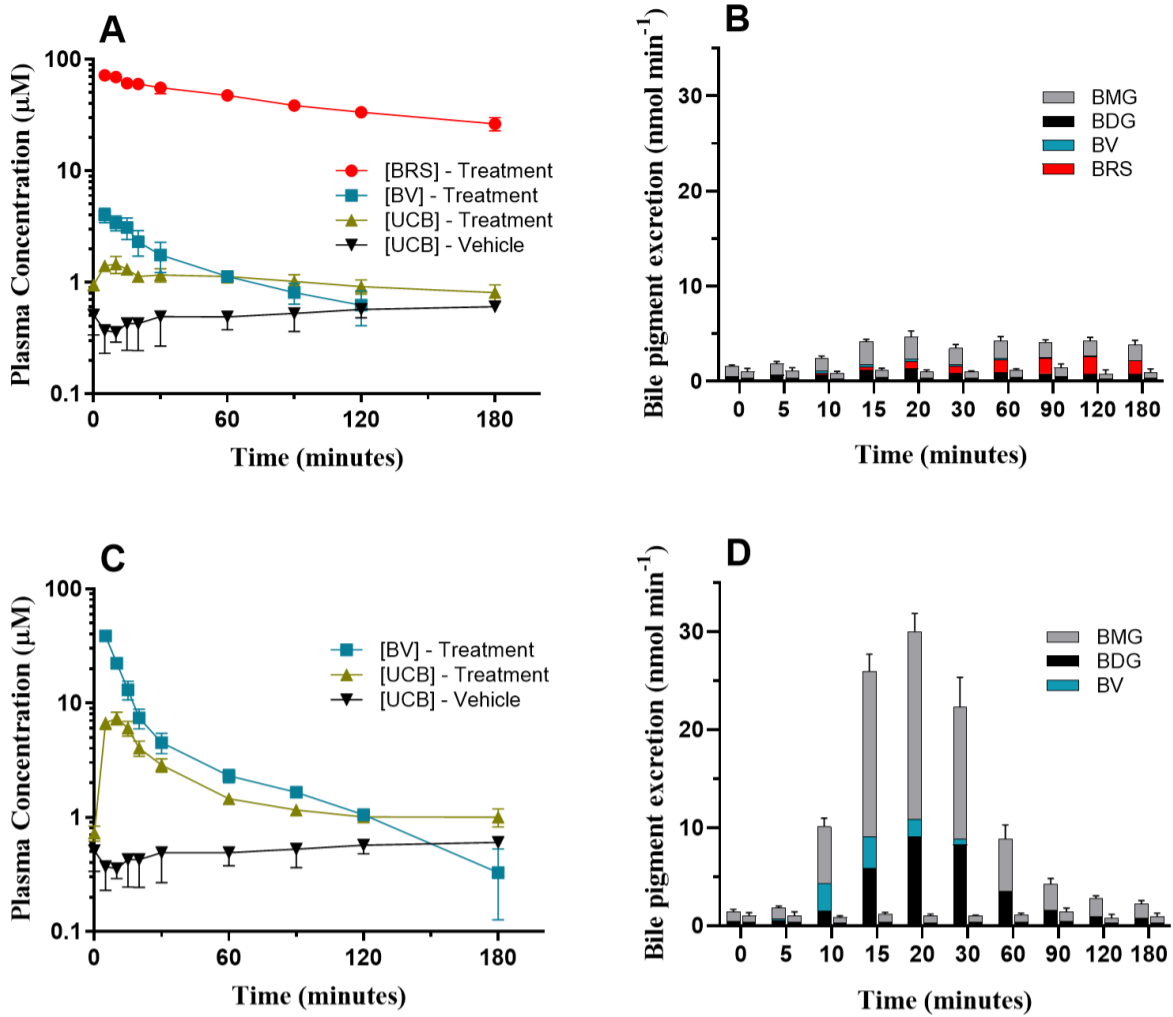


Figure 5.1: Effect of i.v. treatment with BRS (A, B; n=6) and BV (C, D; n=5) on the plasma concentration (left panels) of BRS, BV and UCB; and total bile pigment excretion rate (right panels; BDG, BMG, BV and BRS in stacked columns; left column is compound treatment and right column is compound treatment) over 180 minutes. Data points in A and C correspond with plasma concentrations at 0, 5, 10, 15, 20, 30, 60, 90, 120 and 180 minutes.

Table 2: Pharmacokinetic parameters in the systemic venous circulation after i.v., i.p. and i.d. administration of BRS and BV.

Compound	n	C _{peak} (μM)	C _{max} (μM)	V _d (L kg ⁻¹)	K _{distribution α} (nM minute ⁻¹)	t _{1/2 α} (minutes)	K _{elimination β} (nM minute ⁻¹)	t _{1/2 β} (minutes)	AUC ₁₈₀ (μM minutes)	Bioavailability (%)	Biliary excretion (%)
IV BRS	6	75.6 ± 7.27	86.4 ± 8.08	0.048 ± 0.005 *	19.3 ± 2.0 *	38.3 ± 4.8 *	5.0 ± 0.5 *	146.0 ± 14.6 *	7631 ± 746.6 *	-	35.4 ± 9.38
IV BV 2.7 mg/kg	5	57.7 ± 5.21	68.4 ± 5.20	0.065 ± 0.003	113.9 ± 10.9	6.3 ± 0.8	12.1 ± 1.6	61.3 ± 7.8	846 ± 90.7	-	58.7 ± 10.83
IP BRS	6	181.8 ± 9.6 *	-	-	-	-	-	-	24114 ± 2004 *	31.6	25.5 ± 3.80
IP BV 27 mg/kg	6	21.3 ± 2.5	-	-	-	-	-	-	2700 ± 349	31.9	28.6 ± 6.99
ID BRS	6	1.17 ± 0.18	-	-	-	-	-	-	110.1 ± 15.0 *	0.14	0.81 ± 0.37
ID BV 27 mg/kg	5	0.78 ± 0.17**	-	-	-	-	-	-	63.7 ± 12.2**	0.08**	0.22 ± 0.12

Data is presented as mean ± SEM.

* denotes p<0.05 when compared with BV treatment via the same route, using a t-test

** BV not detected, [BRS] reported due to the duodenal conversation of BV to BRS previously reported

Intraperitoneal administration

Intraperitoneal (i.p.) administration (27 mg kg^{-1} of body weight) of BRS increased the systemic concentration of BRS and BV, and significantly increased UCB concentration compared to t_0 , with the BRS peak occurring after 120 minutes ($\sim 172 \text{ } \mu\text{M}$; Figure 5.2A). The plasma BV concentration following BRS administration appeared after 15 minutes, surpassed $5 \text{ } \mu\text{M}$ after 30 minutes, peaked after 120 minutes ($\sim 7 \text{ } \mu\text{M}$) and remained elevated until 180 minutes (Figure 5.2A). Systemic UCB concentration for the BRS treatment group peaked after 90 minutes ($\sim 4.5 \text{ } \mu\text{M}$) and was significantly elevated from 30 until 180 minutes compared to t_0 . The rate of total bile pigment excretion (Figure 5.2B) was significantly elevated from 15 to 180 minutes when compared with the vehicle group, peaking at 150 minutes. BRS was also detected in the bile at high concentrations ($>100 \text{ } \mu\text{M}$ from 90-180 minutes inclusive; Figure 5.2B), in the BRS treatment group.

BV (27 mg kg^{-1} of body weight) administration increased the systemic concentration of BV and significantly increased the systemic concentration of UCB compared to t_0 , with the peak for both BV and UCB occurring after 30 minutes ($\sim 11 \text{ } \mu\text{M}$ and $\sim 5 \text{ } \mu\text{M}$, respectively; Figure 5.2C). After 30 minutes, BRS was quantifiable within the systemic concentration and peaked after 180 minutes ($\sim 4 \text{ } \mu\text{M}$). Systemic UCB concentration for the BV treatment group peaked after 30 minutes and remained elevated ($\sim 3 \text{ } \mu\text{M}$) until 180 minutes (Figure 5.2C). Total bile pigment excretion after BV administration was significantly elevated from 15 to 180 minutes (Figure 5.2D) when compared with the vehicle group, peaking at 60 minutes. Only BV and bilirubin conjugates were detected in bile.

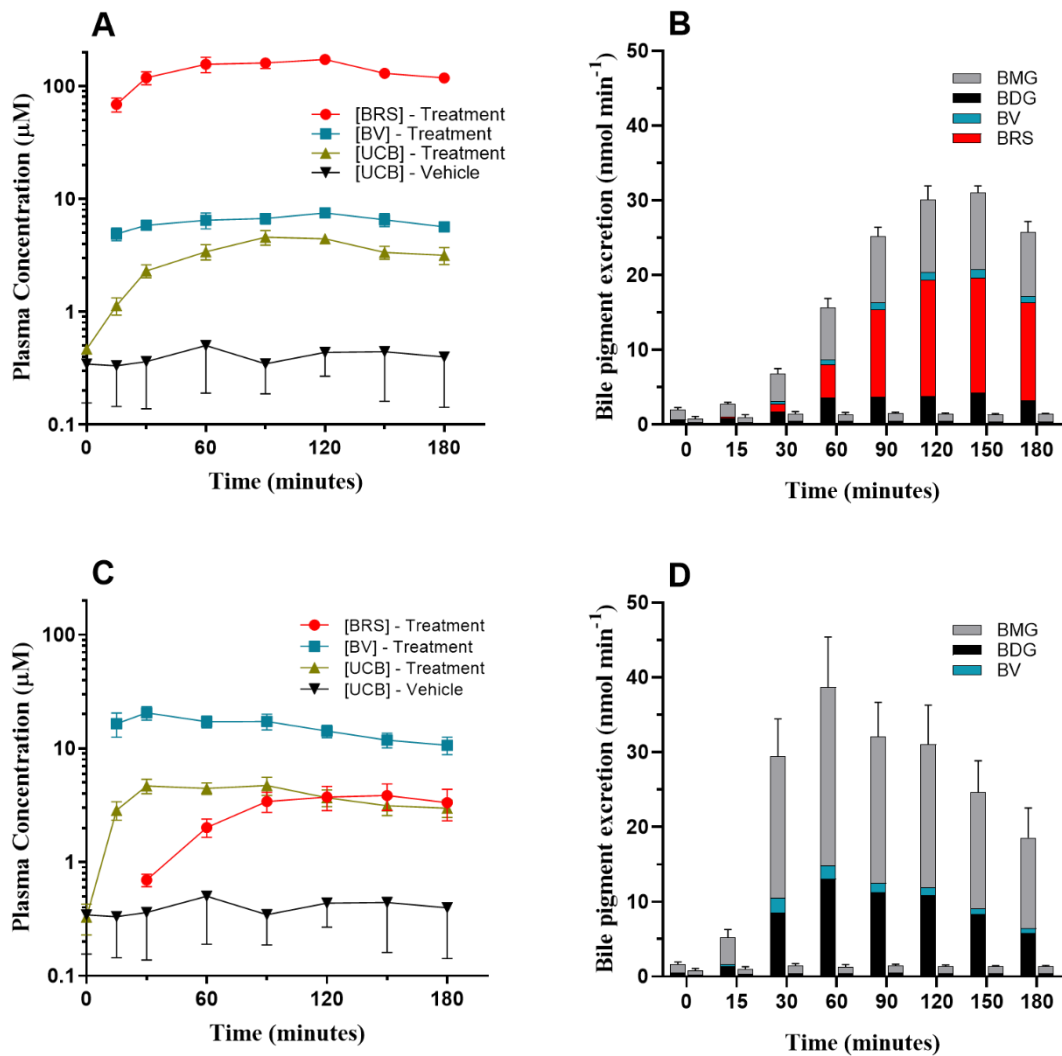


Figure 5.2: Effects of i.p. treatment with BRS (A, B) and BV (C, D) on the plasma concentration (left panels) of BRS, BV and UCB; and total bile pigment excretion rate (right panels; BDG, BMG, BV and BRS in stacked columns; left column is compound treatment and right column is compound treatment). Data points in A and C correspond with plasma concentrations at 0, 15, 30, 60, 90, 120, 150 and 180 minutes.

Intraduodenal administration

Intraduodenal (i.d.) administration (27 mg kg^{-1} of body weight) of BRS increased the systemic concentration of BRS compared to t_0 . BRS appeared after 30 minutes and peaked after 180 minutes ($\sim 1.1 \mu\text{M}$). There was no significant change in systemic UCB concentration or bile

pigment excretion when compared with t_0 and vehicle groups, respectively. Neither BV nor BRS was detected in bile.

BV (27 mg kg^{-1} of body weight) administration significantly increased the systemic concentration of BRS compared to t_0 , with BRS appearing at 60 minutes and peaking at 180 minutes ($\sim 0.7 \mu\text{M}$). There was no significant difference in systemic UCB concentration compared to t_0 or in bile pigment excretion compared with the vehicle group. Neither BV nor BRS was detected in bile.

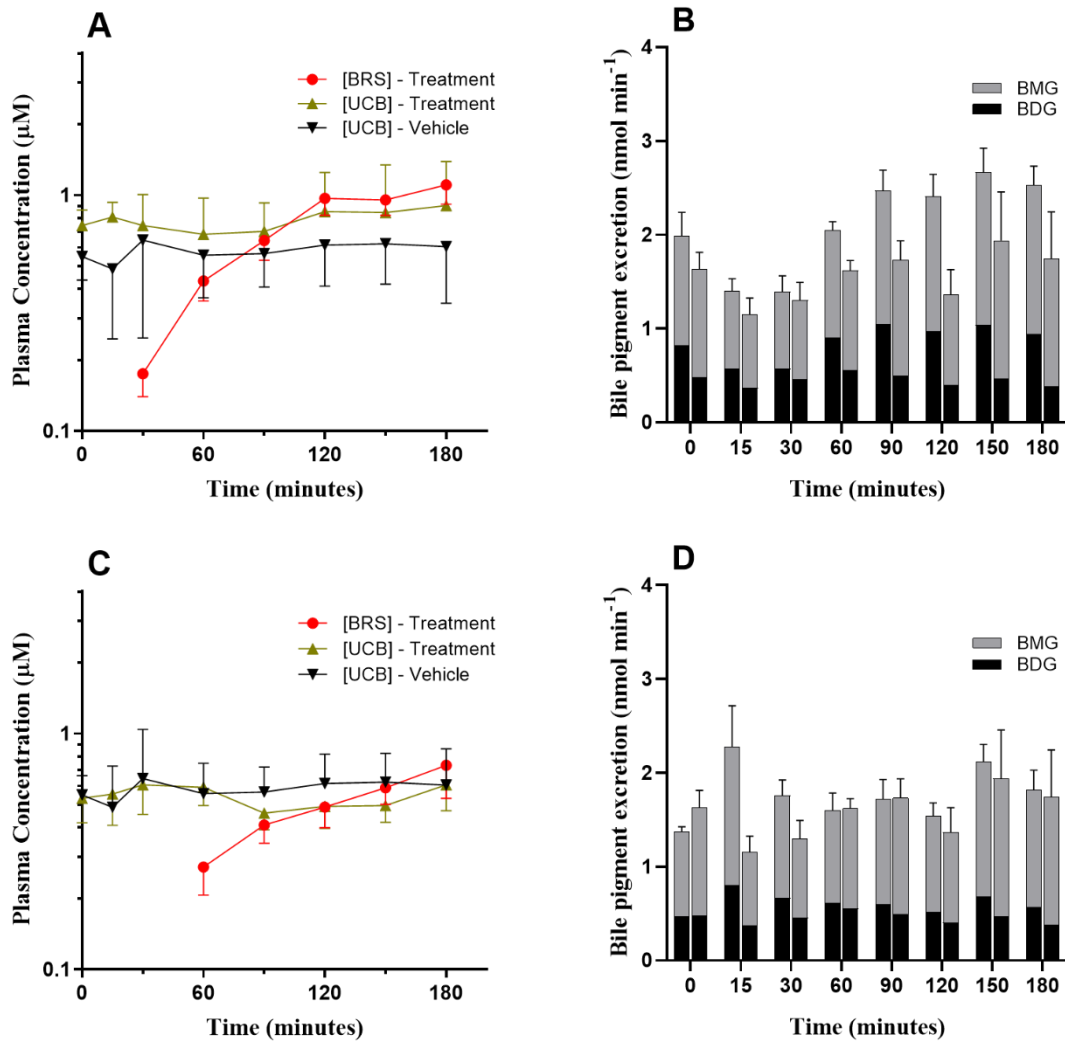


Figure 5.3: Effects of i.d. treatment with BRS (A, B) and BV (C, D) on the plasma concentration (left panels) of BRS, BV and UCB; and total bile pigment excretion rate (right panels; BDG and BMG stacked columns; left column is compound treatment and right column is compound treatment). Data points in A and C correspond with plasma concentrations at 0, 15, 30, 60, 90, 120, 150 and 180 minutes.

Comparative Analysis

i.v. administration

Pharmacokinetic parameters are presented in Table 2 and Figure 5.4 with the cumulative excreted doses corrected for bile pigment excretion of vehicle groups. The volume of distribution (V_d) was significantly smaller and distribution half-life was significantly greater after BRS administration compared to BV. Furthermore, the rate of elimination was significantly smaller while the elimination half-life and the AUC_{180} were significantly greater after BRS administration. The cumulative excreted dose after BV administration was significantly greater than BRS administration between 5 - 60 minutes inclusively, however no significant difference was detected at 180 minutes.

i.p. administration

Intraperitoneal bioavailability after BRS administration was similar to BV administration, and no significant difference was detected in the cumulative excreted dose at any timepoint between BRS and BV treatment groups. The AUC_{180} and peak concentration in plasma of BRS was significantly greater than BV (Table 2).

i.d. administration

The bioavailability of BV was assessed based on the resulting systemic BRS concentration because BV is converted to BRS in the duodenum prior to absorption. Bioavailability for BRS administration was non-significantly greater than that of BV administration. The AUC₁₈₀ of BRS was significantly greater than BV (Table 2), and no differences were detected in the cumulative excreted dose (Figure 5.4C).

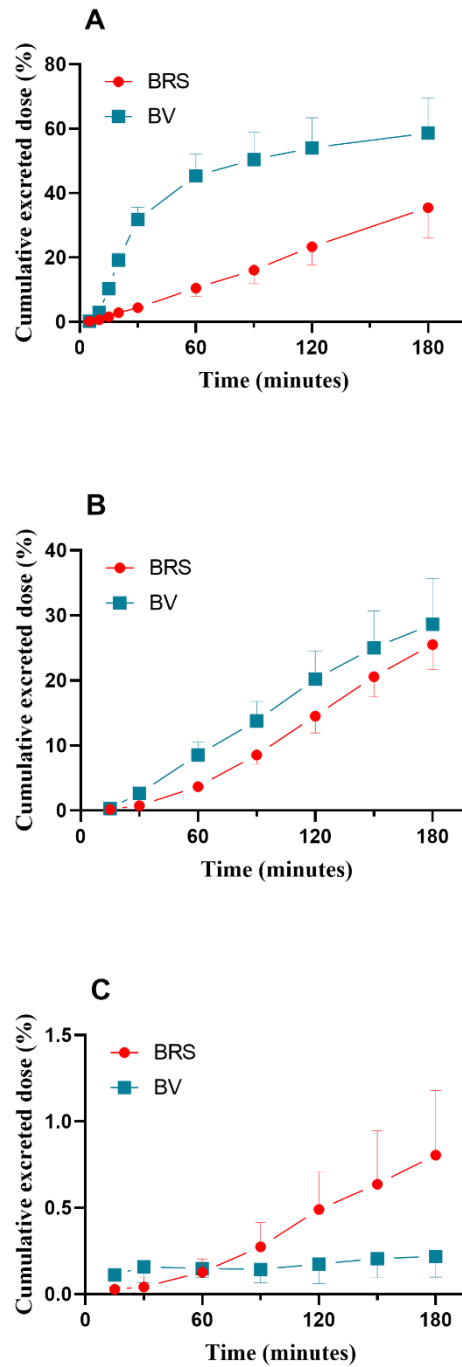


Figure 5.4: Cumulative biliary excretion of bile pigments after i.v. (A), i.p. (B) and i.d. (C) administration of BRS and BV. For neatness, SEM bars on the cumulative excreted dose data in each graph are shown in one direction.

Discussion and conclusions

This manuscript presents a comparative pharmacokinetic analysis of BV and a recently discovered active metabolite, bilirubin-10-sulfonate. Biliverdin administration induces potent anti-inflammatory effects, however, we recently demonstrated that i.p. and i.d. biliverdin administration results in appreciable bilirubin-10-sulfonate (~22%) conversion in vitro and ex vivo.⁽¹⁶⁰⁾ These findings raise questions as to the direct contribution of biliverdin to published anti-inflammatory findings. This study therefore aimed to reveal the extent of biliverdin transformation and its pharmacokinetic profile in vivo, in comparison to BRS, in order to better understand the potential efficacy of each compound. These data show that BRS had longer elimination and distribution half-lives than BV following i.v. administration, indicating less efficient BRS elimination. Both pigments were similarly bioavailable from the peritoneal cavity yet had limited intestinal bioavailability after 180 minutes. Interestingly, i.p. BRS administration induced a greater circulating concentration and reduced excretion rate, which resulted in a substantially elevated AUC₁₈₀ when compared to BV administration. Therefore, BRS is more likely to induce antioxidant effects, when compared to BV.⁽¹⁶⁰⁾ The current findings are enlightening, in that they also reveal new routes of biotransformation and metabolism of BV, which was traditionally thought only to undergo chemical reduction to unconjugated bilirubin. Therefore, this study will greatly impact the design and conclusions of future investigations that supplement biliverdin and/or bilirubin sulfonate in models of inflammatory/oxidant mediated disease.

i.v. administration

Rapid plasma clearance of BV has been previously documented in the rat⁽¹⁾, which is underpinned by its direct hepatic elimination and chemical reduction by biliverdin reductase

(BVR) to unconjugated bilirubin, which is then glucuronidated and excreted. Previously published⁽¹⁾ volume of distribution data in rats for i.v. administration of BV (0.069 L kg^{-1}) agrees with the data presented here (0.065 L kg^{-1}). Similar to previous studies, we show an increase followed by decrease in UCB concentration following i.v. BV administration, demonstrating this rapid conversion to UCB peaking at 10 minutes ($7.39 \text{ }\mu\text{M}$ vs $0.37 \text{ }\mu\text{M}$ compared to solvent control; Figure 5.1C).

No data regarding BRS pharmacokinetics exists, despite BRS pharmacokinetic studies in rats and bullfrogs alluded to within literature.⁽³⁶⁾ In contrast to BV, i.v. BRS reached a greater peak plasma concentration ($75.6 \text{ }\mu\text{M}$ BRS vs. $57.7 \text{ }\mu\text{M}$ BV; Table 2) and had significantly reduced rates of distribution and elimination, leading to substantially longer half-lives for both phases. The AUC_{180} data for BRS was therefore, ~ 9 fold greater than BV. These data clearly demonstrate that BRS is retained within the circulation for longer ($26.35 \text{ }\mu\text{M}$ BRS vs $0.33 \text{ }\mu\text{M}$ BV after 180 minutes) after i.v. administration and suggest that BRS may not be a substrate for UGT1A1 unlike unconjugated bilirubin.⁽¹⁶²⁾ These findings are intriguing, because BRS has two free propionate groups, similar to UCB, however, is highly water soluble likely due to C10 conjugation with sulfonate, which is ionised at physiological pH. It remains unknown whether BRS is carried by circulating albumin or whether it is a ligand for hepatic transport proteins including OATP⁽¹⁶³⁾ and MRP2⁽¹⁶⁴⁾, which might facilitate movement of BRS from plasma into the hepatocyte^(165, 166) and then into the bile canaliculus.

The biliary excretion profile after i.v. BRS and BV administration support the plasma disappearance data and show unique excretion profiles (Figure 5.1B, 5.1D). Approximately one third of bile pigment excreted was intact BRS and was quantitatively less than intact excreted BV after i.v. BV administration over the 180 minutes of experimentation. These data

support the notion that BV is excreted as BMG or BDG after its conversion to UCB by BVR⁽²²⁾, with a small amount of BV excreted intact in the bile, due to probable saturation of BVR.^(1, 162) While MRP2 is a primary transporter of organic anions from the hepatocyte to bile canaliculi, studies administering BV and C-10 substituted bilins to MRP2 deficient rats suggest that MRP2 is not essential for their excretion.⁽¹⁶²⁾ The authors instead suggest that albumin plays a part in biliary excretion, either directly or indirectly, and go on to describe the biliary excretion curve of C-10 substituted bilins as delayed, showing a very broad-peaked and trailing biliary excretion curve.⁽¹⁶²⁾ These data support the prolonged elimination half-life data and delayed peak of BRS excretion (Figure 5.1B) and strengthen the conclusion of impaired biliary excretory transport of BRS.

i.p. administration

Results obtained following i.p. administration suggest that; both BV and BRS diffuse through the peritoneum and into the circulation; they have a similar bioavailability (31.6% vs 31.9%; Table 2); however, both the AUC₁₈₀ and peak plasma concentration following BRS administration were much greater compared to BV administration. The most striking differences observed following i.p. administration (Table 2) were the ~8.5-fold increase in peak BRS plasma concentrations when compared to BV administration and the ~8.9-fold increase in BRS AUC₁₈₀. These data indicate that lower doses of i.p. BRS could be administered (perhaps one-eighth dose) to achieve similar circulating concentrations of BV, after BV administration. As previously reported, the majority of bile pigment excretion after BV administration is in the form of BMG:BDG (2:1 approx. ratio). In contrast, the major bile pigment excreted following BRS administration was BRS itself (in addition to increased BMG/BDG; 2:1 approx. ratio), further supporting a conclusion that hepatic conjugation is not

required for its excretion. These data, in the context of similar cumulative excreted dose over 180 minutes, demonstrate that enhanced absorption/impaired excretion of BRS are likely responsible for vascular retention of BRS. Such retention could be highly beneficial in promoting antioxidant efficacy as demonstrated in the FRAP assay⁽¹⁶⁰⁾ and reducing the necessary dose to achieve therapeutic concentrations as indicated earlier.

The appearance of BV in the plasma following BRS administration (Figure 5.2C) is an interesting observation. These findings are consistent with BRS decomposition to BV observed over time in plasma and following ESI ionisation during LCMS analysis.⁽¹⁶⁰⁾ The labile nature of BRS, a result of nucleophilic addition should be considered carefully, as this C10 addition is in thermodynamic equilibrium and is therefore, reversible.⁽¹⁶⁷⁻¹⁷⁰⁾ Furthermore, BRS was detected following i.p. BV administration, and this is likely caused by reaction with bisulfite ions present in peritoneal fluid.^(171, 172) This is a novel and unexpected finding, suggesting that BRS may confer some *in vivo* anti-inflammatory protection following i.p. BV administration and raises questions as to how much, if any, of the inflammatory protection reported in the literature^(7, 132, 134, 141, 143, 144) could instead be attributed to BRS.

These data demonstrate substantial intraperitoneal bioavailability and absorption of BRS and BV over 3 hours. Standard liver transaminases, released during hepatic injury, were tested following compound administration, revealing no significant elevation after 3 hours.

i.d. administration

Results obtained following i.d. administration confirm that BV is converted to BRS in the duodenum, as reported previously (~22% conversion)^(1, 160) and suggest that BRS and BV are absorbed poorly through the intestine with bioavailability marginally increased for BRS

compared to BV (0.14% vs 0.08%; Table 2). However, BRS administration resulted in a significantly greater AUC₁₈₀ compared to BV, which was a probable consequence of partial intraduodenal BV to BRS conversion, which was then absorbed. Limited duodenal absorption of both compounds is further supported by insignificant changes in biliary bile pigment excretion and cumulative excreted dose over 180 minutes.

These data are supported by reports indicating paracellular diffusion of bile pigments in the caco-2 cell permeability assay.^(173, 174) Interestingly, the authors demonstrated mildly improved permeability of BV and BRDT (a water soluble bilirubin analogue) compared with mannitol control.⁽¹⁷⁴⁾ We speculate that enteric paracellular absorption occurs over greater than the 180 minutes assessed here. Therefore, the administration of BRS and BV to conscious animals with intermittent blood sampling over 1-2 days may be required to accurately assess enteric bioavailability.

Limitations

The single compartment model applied here assumes homogenous compound distribution throughout tissues. In this case, true tissue distribution may be confounded by rapid conversion of BV to UCB via ubiquitous BVR, which may lead to overestimation of distribution volumes here. While no data exists regarding the affinity of BRS for BVR, the literature shows other bilins substituted at C10 are not substrates for BVR⁽¹⁷⁵⁾ and therefore the volume of distribution is less likely to be overestimated for BRS. Additionally, the same dose (mg kg⁻¹) of BV and BRS was administered, however the molar mass of BRS is greater than BV (~663 vs ~582 amu). Therefore, BRS concentrations are marginally underestimated from a stoichiometric perspective. Finally, given that the bile duct was permanently cannulated,

entero-hepatic circulation of BV and BRS was interrupted and therefore, circulating concentrations have likely been underestimated here.

Conclusion

This study describes the complete plasma absorption, clearance and biliary excretion profiles of BRS and BV following i.v., i.p. and i.d. administration, identifying i.p. administration as the suggested route for future study of their therapeutic efficacy. This manuscript describes the complex interplay of BV and BRS metabolism, which is critical to understanding BV's apparent anti-inflammatory effects, with i.p. and i.d. BV administration leading to BRS formation in rats. Therefore, assessment of the contribution of BRS in models of BV administration is warranted and may lead to the development of BRS as a therapeutic molecule. Following i.p. administration of both compounds, sustained elevations in plasma concentrations are shown; however, BRS and BV were poorly absorbed following i.d. administration. These conclusions provide a justification for i.p. BRS and BV administration studies in animal models of inflammation to determine their therapeutic potential.

Additional information

Author contribution statement

A.C.B. and R.S. conceived the design of this study. A.C.B., R.G.S and W.H performed animal experimentation and interpretation of data. R.G.S and W.H performed HPLC and LCMS method development and statistical analysis of data. J.V. assisted with statistical analysis and performed biochemical analysis of liver function. A.P. and K.H.W assisted with concept, design and final approval. A.C.B. and K.H.W. secured funding for the project. All authors contributed to revision of the MS and provided their final approval for manuscript submission.

Competing interests

The author(s) declare no competing interests.

Acknowledgement

The authors acknowledge the support received through an Australian Government Research Training Program Scholarship as well as the generosity of Patricia Barlow in providing a scholarship. The research was supported by the Griffith Enterprise Innovation Fund, which utilised funding provided by Griffith University and the Queensland Government.

Animal Use

All animal care and experimental procedures complied with the Guidelines of the Australian National Health and Medical Research Council and were approved by the Griffith University Animal Ethics Committee.

Human Tissue

Human blood was obtained under permission from the Griffith University Human Research Ethics Committee.

Chapter Six: Biliverdin and bilirubin sulfonate inhibit monosodium urate induced sterile inflammation in the rat

Foreword: Guided by the pharmacokinetics documented in Chapter Five, this study sought to investigate the effects of intraperitoneal BV and BRS administration in animals experiencing sterile inflammation induced by monosodium urate crystal administration into a subcutaneous air pouch. As the third and final research chapter, this study demonstrates for the first time, the anti-inflammatory effects of BRS and BV in an animal model of gouty arthritis and identifies BRS as a novel anti-inflammatory worthy of further study.

The abbreviations, formatting and referencing of this document have been altered slightly to more closely reflect the formatting of other chapters and published work in this thesis.

Statement of Contribution to a Co-Authored Paper Submitted for Publication

This chapter is in the form of a co-authored paper currently under consideration. The bibliographic details of the co-authored published paper are:

Shiels, R.G., Hewage, W., Pennell, E.N., Vidimce, J., Grant, G., Pearson, A.G., Wagner, K-H., Morgan, M., and Bulmer, A.C. Biliverdin and bilirubin sulfonate inhibit monosodium urate induced sterile inflammation in the rat. Submitted to *European Journal of Pharmaceutical Science*.

Appropriate acknowledgements of those who contributed to the research but did not qualify as authors are included in the paper.

My contribution to the published paper involved:

- Experimental design and planning
- Development and validation of the analytical methods
- Experimental execution and sample collection
- Data acquisition and statistical analysis
- Manuscript preparation, critical review and submission

(Sign) _____

(Date) 11th February 2020

First Author
Ryan Shiels

(Sign) _____ (Date) 11th February 2020

Corresponding Author and Supervisor
Associate Professor Andrew Bulmer

**Biliverdin and bilirubin sulfonate inhibit monosodium urate induced sterile inflammation
in the rat**

Ryan G. Shiels^{1,2}, Wenu Hewage^{1,2}, Evan N. Pennell^{1,2}, Josif Vidimce^{1,2}, Gary Grant¹, Andrew
G. Pearson^{1,2}, Karl-Heinz Wagner³, Michael Morgan⁴ and Andrew C. Bulmer^{1,2*}

¹ School of Medical Science, Griffith University, Gold Coast, Queensland, Australia

² Menzies Health Institute Queensland, Griffith University, Gold Coast, Queensland, Australia

³ Department of Nutritional Sciences, University of Vienna, Vienna, Austria

⁴ Department of Anatomy and Neuroscience, University of Melbourne, Melbourne, Australia

Background: Biliverdin, a by-product of haem catabolism, possesses potent endogenous antioxidant and anti-inflammatory properties. Bilirubin-C10-sulfonate (BRS), an active metabolite formed after enteral administration of BV in the rat, also possess antioxidant properties. Therefore, we investigated the anti-inflammatory and antioxidant activity of BV and BRS in an *in vivo* model of monosodium urate induced sterile inflammation.

Methods: Subcutaneous air pouches were created on the dorsal flanks of Wistar rats (10-12 weeks of age). Prior to stimulation of the 6-day old pouch with monosodium urate (25 mg), groups were pre-treated with intraperitoneal BRS (27 mg/kg) and BV (27 mg/kg). Total and differential leukocyte counts were determined in pouch fluid aspirate at 1, 6, 12, 24 and 48 h. Biliverdin (BV), BRS and unconjugated bilirubin (UCB) concentrations in the serum and pouch fluid were quantified using liquid chromatography-mass spectrometry. Pouch fluid cytokine concentrations (IL-1 β , IL-1 α , TNF, IL-17A, IL-12, GM-CSF, IL-33, IFN- γ , IL-18, IL-10, MCP-1, CXCL-1 and IL-6) were assessed after 6 hours. In addition, 24 h protein carbonyl and chloramine concentrations were assessed in pouch fluid using ELISA and spectrophotometry, respectively.

Results: BRS and BV significantly ($p < 0.05$) inhibited leukocyte (total, neutrophil and macrophage) infiltration into the pouch fluid from 6 to 48 h. For example, after 6 h neutrophil counts decreased following BRS ($0.32 \pm 0.11 \times 10^6$ cells mL⁻¹) and BV ($0.17 \pm 0.03 \times 10^6$ cells mL⁻¹) compared to MSU only ($3.51 \pm 1.07 \times 10^6$ cells mL⁻¹). Both BV and BRS significantly ($p < 0.05$) reduced pouch GM-CSF (BV: 5.8 ± 1.2 pg mL⁻¹, BRS: 6.9 ± 1.5 pg mL⁻¹ vs MSU only: 13.0 ± 1.9 pg mL⁻¹) and MCP-1 concentrations at 6 h (BV: 1804 ± 269 pg mL⁻¹, BRS: 7927 ± 2668 pg mL⁻¹ vs MSU only: 17290 ± 4503 pg mL⁻¹), whilst BV additionally inhibited IL-6 (4354 ± 977 pg mL⁻¹ vs MSU only: 25070 ± 5178 pg mL⁻¹) and IL-18 (17.6 ± 2.0 pg mL⁻¹ vs MSU only: 81.5 ± 19.9 pg mL⁻¹) concentrations at 6 h ($p < 0.05$). Despite these differences, no change in pouch

chloramine or protein carbonyl concentrations occurred at 24 h ($p > 0.05$). Serum BV concentrations rapidly diminished over 6 h, however, BRS was readily detected in the serum over 48 h, and in pouch fluid over 12 h.

Conclusions: This study is the first to elucidate anti-inflammatory activity of BRS and the efficacy of BV administration in a model of gouty inflammation. Reduced leukocyte infiltration and cytokine production in response to sterile inflammation further support the importance of these molecules in physiology and their therapeutic potential in sterile inflammation.

Introduction

Tetrapyrroles are involved in cellular metabolic processes including respiration and photosynthesis, and are evolutionarily conserved across all kingdoms of life.⁽¹⁷⁶⁾ From a precursor for phycobilin synthesis in cyanobacteria and algae⁽¹¹³⁾, to a part of the haem catabolic pathway/anti-inflammatory mechanism in mammals^(28, 42), these tetrapyrroles appear to be vital for the survival of all organisms that synthesise them.

Tetrapyrrolic bile pigments such as biliverdin (BV) and unconjugated bilirubin (UCB) are formed during haem catabolism following red blood cell breakdown, an event associated with acute tissue injury.⁽¹¹⁹⁾ The innate inflammatory responses to injury occurs in the early phases of tissue injury, however tissue injury is accompanied by the production of BV and UCB, which attenuates the subsequent inflammatory response and improves wound healing.⁽¹³⁴⁾ Additionally, Gilbert's Syndrome (GS) is a condition presenting with a mildly elevated circulating UCB concentration caused by a reduced uridine glucuronosyltransferase 1A1 (UGT1A1) deficiency due to a polymorphism (~%60 reduction in function), and is associated with protection against oxidative processes underpinned by a greater antioxidant capacity in plasma which contributes to the 10.1% lower incidence of cardiovascular disease within the GS population.^(2, 15, 116, 118, 119)

Administration of BV protects from inflammatory and oxidant-mediated damage *in vivo*.^(7, 132, 141, 144) Specifically, BV administration protects via reducing the expression or release of inflammatory cytokines IL-6, MCP-1 and TNF in models of ischemia-reperfusion injury.^(41, 133, 144) Additionally, BV protects from Forssmann reagent induced anaphylaxis⁽¹⁴⁷⁾, tissue transplantation⁽¹⁴¹⁾, and endotoxin-induced acute lung injury⁽¹³²⁾ with a recent study

demonstrating that BV and related bile pigments neutralise the harmful effects of superoxide.⁽⁴⁰⁾ Interestingly, intraduodenal (i.d.) and intraperitoneal (i.p.) administration of BV in rodents also leads to the formation of bilirubin-10-sulfonate (BRS)^(1, 160), a novel antioxidant with the potential to confer protection against oxidative and, potentially, inflammatory processes.⁽¹⁶⁰⁾ Testing the anti-inflammatory therapeutic potential of these bile pigments clearly requires further *in vivo* investigation in models of sterile inflammation with clinical relevance to human inflammatory conditions in order to determine their potential physiological importance and their suitability as novel therapeutics. Gouty arthritis is a common clinically relevant sterile inflammatory condition. In the United States alone, the financial burden of gouty arthritis in 2013 was ~\$1 billion, with acute gouty arthritis attacks accounting for 32% of this cost.⁽¹⁷⁷⁾ New treatments could potentially aid in the treatment of this condition, however, it remains unknown whether bile pigments can influence the course of this condition or its pathophysiology.

MSU crystals can activate the NLRP3 inflammasome via lysosomal leakage of cathepsins into the cytosol.⁽¹⁷⁸⁾ Furthermore, it is well documented that MSU crystals induce inflammatory cytokine and chemokine production^(84, 103) and initiate an acute inflammatory response mimicking the condition of gout in humans.^(84, 179) This response is likely induced by multiple mechanisms, including direct activation of leukocytes, membrane lysis and complement activation.⁽⁸⁰⁾ During the acute phase of the inflammatory response, inflammatory cytokines monocyte chemoattractant protein-1 (MCP-1), interferon-gamma (IFN- γ), interleukin-6 (IL-6), interleukin-1 β (IL-1 β), myeloperoxidase (MPO), macrophage inflammatory protein-1 α (MIP-1), tumour necrosis factor (TNF), chemokine ligand 1 and 2 (CXCL-1 and CCL-2 respectively), interleukin-8 (IL-8), and macrophage inflammatory protein-2 (MIP-2) have been reported to

increase in MSU crystal air pouch inflammation models.⁽¹⁰³⁾ Bile pigments attenuate MCP-1, IL-6 and MPO responses, therefore, it was hypothesised that BRS and BV administration to the MSU subcutaneous air pouch model of inflammation would significantly reduce both leukocyte infiltration, inflammatory cytokines and biomarkers of oxidative stress/modifications within the inflammatory milieu of the pouch.

Materials and Methods

Materials

Biliverdin hydrochloride and bilirubin sulfonate were obtained from Frontier Scientific (Utah, USA). All other reagents were obtained from Sigma-Aldrich (Australia), unless otherwise stated.

Sodium biliverdinate synthesis

50.07 mg of NaOH (1.252 mmol) was added to 400 mL of ethanol and sonicated for 10 min at 32°C. This solution was then added to a flask containing 250 mg of BV-HCl (0.404 mmol). This solution was again sonicated for 10 min at 32°C, then 20 mL aliquots of the 0.625 mg mL⁻¹ BV solution were transferred to 50 mL Falcon tubes, with each containing 12.5 mg of BV. These solutions were then evaporated to dryness (Speedyvac centrifuge vacuum concentrator; LabGear, Australia) at 400 × g, 32°C for 12 h at a pressure of ~2 millibar. The dry aliquots were sealed, transferred to a -80°C freezer and reconstituted in PBS immediately prior to use. All solutions were protected from light during preparation using aluminium foil and a darkened laboratory.

Monosodium Urate Crystal synthesis

Monosodium urate crystals were synthesised using previously published methods.⁽¹⁸⁰⁾ Uric acid (1.680 g; Abcam, United Kingdom) was added to 400 mL of double distilled H₂O and stirred at 15 RPM for 5 s. Then, 2.25 mL of 5 M NaOH was added and the solution was stirred at 15 RPM for 5 s. The solution was then rapidly heated to 60°C, allowed to cool with the heat source removed and left at room temperature for 24 h. Following this, the solution was

filtered under light vacuum (grade 5 Whatman paper, Thomas Scientific, USA) and the resulting crystalline solids were washed with 200 mL of 100% ethanol before being dried under vacuum. The crystals were observed via Scanning Electron Microscopy (SEM) at 15 kV under high vacuum with images taken at 10 random fields of view (15 kV × 1000). In each field, 10 crystals were counted, and their respective length and width quantified (Neoscope JCM-5000, Jeol, Japan) and were observed to have the characteristic needle-like appearance and dimensions observed in clinical gout (length: $11.4 \pm 5.52 \mu\text{m}$, $n=100$, width: $2.09 \pm 0.73 \mu\text{m}$, $n=100$)^(180, 181), (Figure 6.1). MSU crystals were gently pressed and distributed over electrical tape and loaded onto a sample stub, which was then coated with gold for 2 min using a NeoCoater (MP-19020NCTR, Jeol, Japan). Administered MSU crystals were tested via gel-forming limulus amoebocyte lysate kit and were endotoxin free ($<0.03 \text{ EU mg}^{-1}$; Genscript, USA).

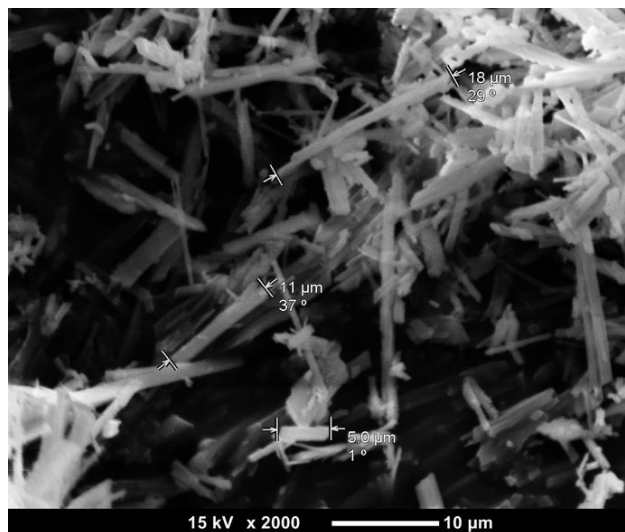


Figure 6.1: A representative scanning electron microscope image of monosodium urate crystals used to induce sterile inflammation within the air pouch model.

Sterile Inflammation Air Pouch Model

Adult male Wistar rats (10-12 weeks of age; 344–440 g) were housed at constant temperature, under a 12 h light-dark cycle and with free access to food and water. Prior to each procedure, animals were anaesthetised using 3% isoflurane (Pharmachem, Australia), at 1 L min⁻¹ in 100% oxygen and maintained under anaesthesia via nose cone. Initially, the animals' dorsal flanks were shaved, and subcutaneous air pouches were formed immediately below the scapulae via subcutaneous delivery of 20 mL of sterile filtered air (0.22 µm syringe filter and a 27G needle). On the fourth day, a further 10 mL of filtered air was delivered to the pouch to maintain patency and assist the formation of a pseudosynovial joint capsule.⁽⁸⁵⁾

On the sixth day, under light anaesthesia, 5 mL of a 5 mg mL⁻¹ sterile suspension of MSU crystals in 0.9% NaCl (Baxter, Australia) was injected into the air pouch of each rat via a 21G needle, except for the sham group (n=3), which received only 5 mL of saline. Thirty min prior to MSU delivery, rats received a 3.5 mL i.p. injection of BRS (27mg kg⁻¹, n=6), BV (27 mg kg⁻¹, n=5, dissolved 1:1 in PBS:0.9% NaCl), ibuprofen (positive control; 8.1 mg kg⁻¹, n=5; Glentham Life Sciences, United Kingdom) or PBS (MSU only and sham groups) through a 5 mL syringe and 0.45 µm syringe filter. The dose of BV and BRS were chosen following a recent pharmacokinetic study⁽¹⁾ and the dose of ibuprofen was chosen as it represents molar equivalence with BV and a low range effective dose.⁽¹⁸²⁾ All compounds were dissolved in PBS and injected with a 25G needle unless otherwise stated.

Samples of pouch exudate were taken under light anaesthesia periodically at 1, 6, 12, 24, and 48 h after MSU administration by injecting 5 mL of sterile saline into the pouch, gently massaging the pouch and withdrawing 4 mL of exudate which was collected into a 4 mL EDTA tube (5.3 mM EDTA; BD, USA) and stored on ice. Additionally, 200 µL of blood was collected via a tail vein bleed at each timepoint. Leukocyte counts were estimated via haemocytometer,

and the remaining fluid along with the blood sample were centrifuged for 8 min at $2000 \times g$ at room temperature (RT). The supernatant and serum were aliquoted, placed on dry ice and stored at -80°C , and cell pellets were used for differential staining using a Rapid Diff stain (Australian Biostain, Australia) according to the manufacturer's instructions.

Inflammatory markers

Cytokines (IL- 1β , IL- 1α , TNF- α , IL-17A, IL-12, GM-CSF, IL-33, IFN- γ , IL-18, IL-10, MCP-1, CXCL-1 and IL-6) were quantified in the 6 h pouch exudate using a bead-based immunoassay sandwich ELISA method (LEGENDplex, Biolegend, USA). Samples were processed and quantification of soluble analytes performed utilising a BD SORP LSR II Fortessa flow cytometer, as per the manufacturer's instructions for use (IFU). A minimum of 500 events per analyte was acquired in the classification channel fluorophore APC (Ex 640nm Em: 670/30) with Median Fluorescence Intensity (MFI) of the reported fluorophore (PE; Ex 561 Em 588/12) interpolated against relevant standard curves using the proprietary Biolegend Software (LEGENDplex v8.0).

Biomarkers of oxidative stress/modification

Protein carbonyl concentration in pouch fluid was assessed at 24 h via ELISA (Biocell, New Zealand) and chloramine concentration was assessed using previously published methods.⁽¹⁸³⁾ Protein concentration was assessed by Pierce BCA kit (ThermoFisher, Australia). Myeloperoxidase (MPO) was assessed at 6, 12 and 24 h via ELISA (resolvingIMAGES, Australia), however, the values were below the sensitivity of the assay and are not presented.

Bile pigment quantification

Serum samples were analysed for bile pigments via quantitative UHPLC-MS (LCMS-2020, Shimadzu, Japan). Separation of the targeted tetrapyrroles was achieved using a reverse phase C18 column (Vision HT C18HL, 2 mm × 100 mm, 1.5 µm, PhaseSep, Australia). The UHPLC column was preceded by a VisionHT C18HL guard column (2 mm × 5 mm, 1.5 µm, PhaseSep, Australia) and an UltraShield UHPLC precolumn filter (Restek, 0.2 µm, Shimadzu, Australia), respectively. The column oven and autosampler were set to 45°C and 4°C, respectively, and the flow rate was 0.35 mL min⁻¹.

Analysis of bile pigments in serum and pouch exudate

The initial mobile phase consisted of 34% mobile phase B (HPLC grade methanol, Scharlau, Spain) and 66% mobile phase A (10 mM ammonium acetate in 25% HPLC grade methanol and 75% Milli-Q H₂O), representing a 50.5% initial methanol concentration. The gradient program applied for the analytical portion of the analysis was as follows: 0.3 min - 50% B; 1.5 min - 74% B; 1.8 min - 92% B; 3.1 min - 92% B. The re-equilibration portion of the analysis ran from 3.1 min to 6.5 min at 34% B, with the flow rate increased to 0.42 mL min⁻¹ at 3.5 min, held until 4.0 min, reducing linearly to 0.35 mL min⁻¹ at 4.4 min and remaining so until 6.5 min. The total run time including re-equilibration was 6 min, with retention times of 2.00, 2.25 and 2.76 min for BRS, BV and UCB, respectively. A 2 µL injection volume was used for all analyses. ESI operating conditions were: desolvation line temperature 250°C, heat block temperature 200°C, nebulizing gas flow 1.5 L min⁻¹ (N₂), drying gas flow 15 L min⁻¹ with all detection voltages set via autotune using the manufacturer's tuning solution (Shimadzu, Japan). Data

were collected in negative ion mode via single ion monitoring (SIM) of the m/z corresponding with the deprotonated anion $[M-H]^-$ of each compound.

External and Internal Quantification Standards

Stock solutions of BRS, BV and UCB were dissolved individually at 8 mM in DMSO, then combined with additional DMSO to form a mixed stock solution containing 2 mM of each compound. This mixed stock solution was further diluted with DMSO in order to form 'working solutions' with concentrations from 390 nM to 200 μ M and were made fresh prior to each standard curve.

Internal standards (IS) included mesobilirubin-10-sulfonate, mesobiliverdin and mesobilirubin (mBRS, mBV and mUCB, respectively; Frontier Scientific, USA). A mixed IS solution was created by initially dissolving each IS at 8 mM in DMSO, which were then combined and further diluted with DMSO to form the final IS solution with mBRS/mBV/mUCB concentrations of 80/80/40 μ M, respectively. Aliquots of 500 μ L of the IS solutions were made, and frozen in liquid nitrogen prior to storage at -80°C . Prior to use, IS aliquots were defrosted in darkness at room temperature.

Calibration

Matrix matched calibration standards were prepared by adding 10 μ L of 'working solution' to 390 μ L of fresh rat serum to form spiked serum containing BRS/BV/UCB at concentrations from \sim 391 nM to 200 μ M plus one DMSO only blank. After 10 s of mixing via vortex and 10 min of incubation in the dark at room temperature, 40 μ L of spiked serum was added to 10 μ L of IS solution followed by mixing for 5 s via vortex. To this solution, 150 μ L of 1:4 DMSO:methanol was added and mixed via vortex again for 10 s before being centrifuged

(21500 × *g*; 10 min). Prior to injection, the supernatant was passed through a 0.22 μm syringe filter (PhaseSep, Australia) and 2 μL of the filtrate was injected for analysis.

Quality control

Quality control (QC) standards were prepared as per the calibration standards above at BRS/BV/UCB concentrations of 1.56/12.5/50 μM representing a low/medium/high concentration, and 40 μL of each were aliquoted into 1.5 mL microtubes. Prior to flash freezing in liquid N₂ and storage at -80°C, 10 μL of IS was spiked into each aliquot of rat serum spiked with mixed standard and vortexed for 10 s. Prior to each batch of sample analysis, one aliquot of each concentration level was defrosted while shielded from light, prepared as above and injected for analysis to confirm accuracy within acceptance criteria range of 85 - 115%. Following every 10th sample injection, one QC standard was reanalysed to ensure assay validity over time.

Sample analysis

Prior to serum analysis, 10 μL of IS solution was added to 40 μL of sample serum or pouch exudate, mixed via vortex for 10 s before adding 150 μL of 1:4 DMSO:methanol and mixing via vortex again for 10 s before being centrifuged (21500 × *g*; 10 min). The supernatant was then passed through a 0.22 μm syringe filter (PhaseSep, Australia) and 2 μL of the resulting filtrate was injected for analysis.

Concentrations of tetrapyrroles in serum were calculated via the internal standard method using AUC integration of single ion monitoring (SIM) mass chromatograms at the relevant *m/z* to compare each analyte to its meso internal standard. Linear calibration curves ($r^2 > 0.9995$) were generated in Labsolutions software (version 5.87 sp1, Shimadzu, Japan) and the limit of

quantification for bile pigments in serum and exudate approximated to be 250 nM for all analytes.

Statistical analysis

Statistical analysis was performed using GraphPad Prism version 8.1. Differences in leukocyte counts, cytokines and oxidative stress/damage markers were analysed via one-way ANOVA (Holm-Sidak *post hoc*) to test for differences between MSU only and treatment groups at each time point. Normality of data sets was assessed using the Shapiro-Wilk test. If data sets lacked normal distribution, equivalent non-parametric tests were conducted and outliers were removed using the ROUT test (Q = 1%). All error bars are displayed as SEM throughout.

Results

An acute, sterile inflammatory response was observed in the air pouch of rats following the administration of MSU crystals, which was assessed by measuring leukocyte infiltration, cytokine concentrations and markers of oxidative stress. The population of the infiltrating leukocytes primarily consisted of neutrophils and monocytes, which peaked at 12 and 48 h respectively (Figures 6.2 and 6.3).

Leukocyte infiltration

Leukocyte infiltration was determined by measuring leukocyte counts in the pouch exudate at each timepoint via haemocytometer (Figures 6.2 and 6.3). A marked and significant ($p < 0.05$) increase in leukocyte infiltration was observed for the MSU only group when compared with the sham group from 6 to 48 h inclusive (Figure 6.2). All treatment groups (BRS, BV and

ibuprofen) had significantly decreased total leukocyte and neutrophil counts compared with the MSU only group from 6 to 48 h inclusive (Figure 6.2).

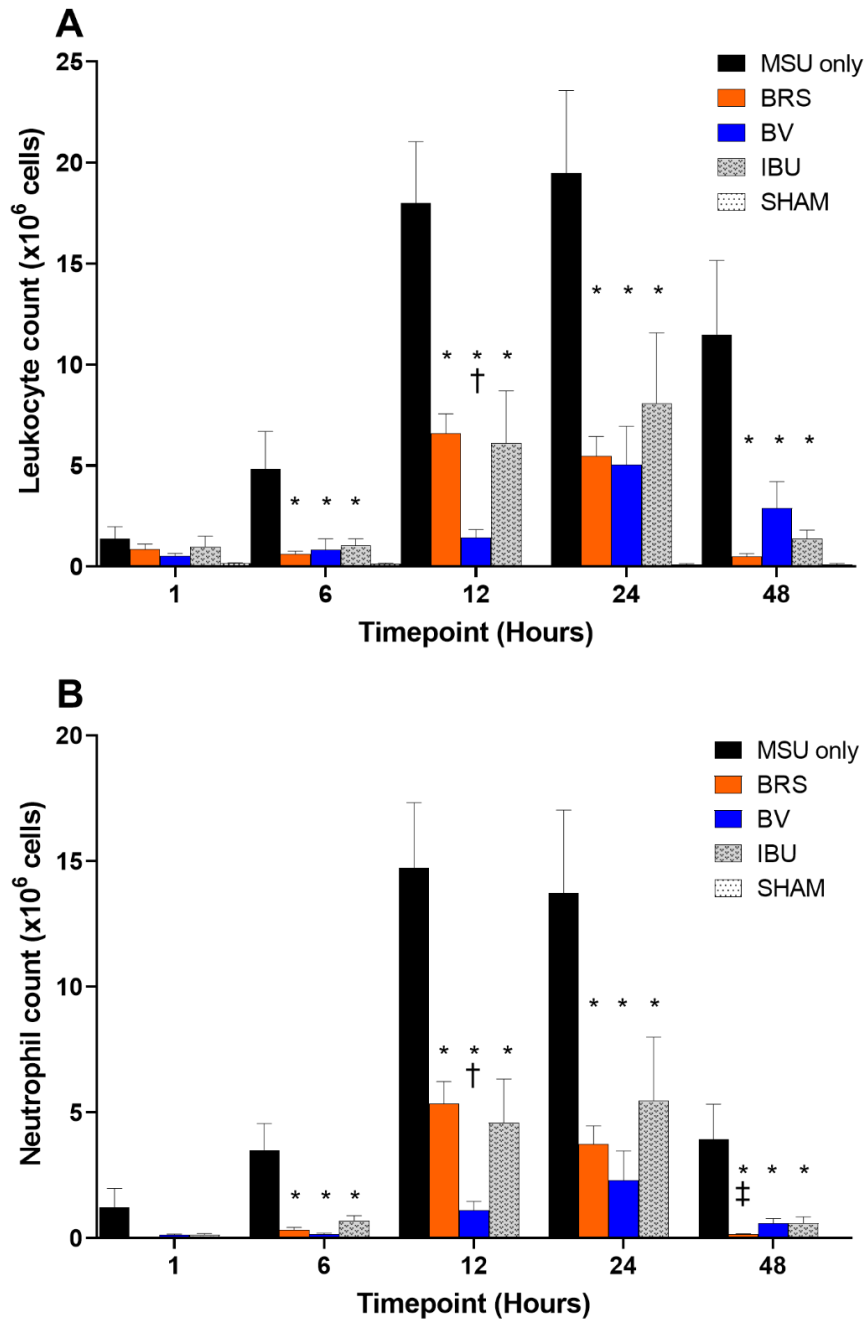


Figure 6.2: Effects of 27 mg kg⁻¹ i.p. pre-treatment of BRS (n=6, orange) and BV (n=5, blue) on leukocyte infiltration (A) and neutrophil infiltration (B) following MSU administration (25 mg in 5 mL sterile saline) to a 6 day old air pouch model of acute inflammation. Ibuprofen (8.11 mg kg⁻¹ i.p. molar equivalent to BRS) was administered as a positive control (IBU n=5, grey), and PBS (3.5 mL, i.p.) was administered as a negative control (MSU only n=5, black). The sham group (SHAM, white) was pre-treated with 3.5 mL PBS i.p. and

received 5 mL of saline into the pouch instead of MSU. * denotes significant difference ($p < 0.05$) compared to MSU only, † denotes significant difference ($p < 0.05$) compared to BRS at the same timepoint and ‡ denotes significant difference ($p < 0.05$) compared to BV for the same time point. From 6-48 h, the sham group was significantly lower than MSU only (not shown with symbol for neatness). Data are presented as mean \pm SEM.

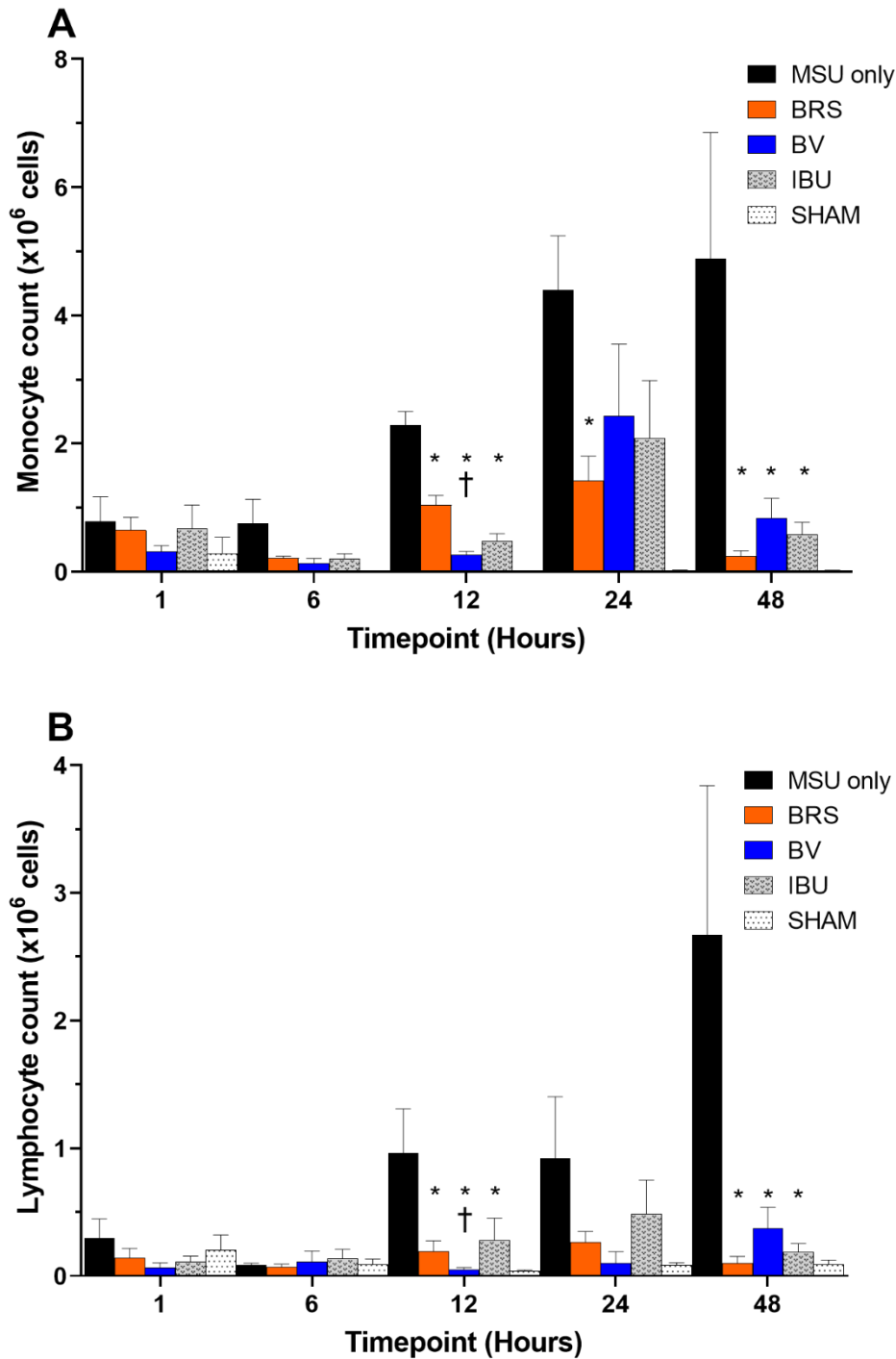


Figure 6.3: Effects of 27 mg kg^{-1} i.p. pre-treatment of BRS ($n=6$, orange) and BV ($n=5$, blue) on monocyte infiltration (A) and lymphocyte infiltration (B) following MSU administration

(25 mg in 5 mL sterile saline) to a 6 day old air pouch model of acute inflammation. Ibuprofen (8.11 mg kg⁻¹ i.p., molar equivalent to BRS) was administered as a positive control (IBU n=5, grey), and PBS (3.5 mL, i.p. n=3) was administered as a negative control (MSU only, n=5, black). * denotes significant difference (p < 0.05) compared with VEH, † denotes significant difference (p < 0.05) compared to BRS. From 12-48 h, the sham group was significantly lower than MSU only (not shown with symbol for neatness). Data are presented as mean ± SEM.

Inflammatory Cytokines

Concentrations of cytokines in pouch exudate at 6 h were determined using a multiplexed bead-based flow cytometric immunoassay. Only cytokines that were significantly (p < 0.05; unpaired t-test) elevated in MSU only groups versus sham and significantly decreased in treatment groups versus MSU only (p < 0.05; ANOVA) are reported here (Figure 6.4). All other cytokine responses can be found in Figure 6.9.

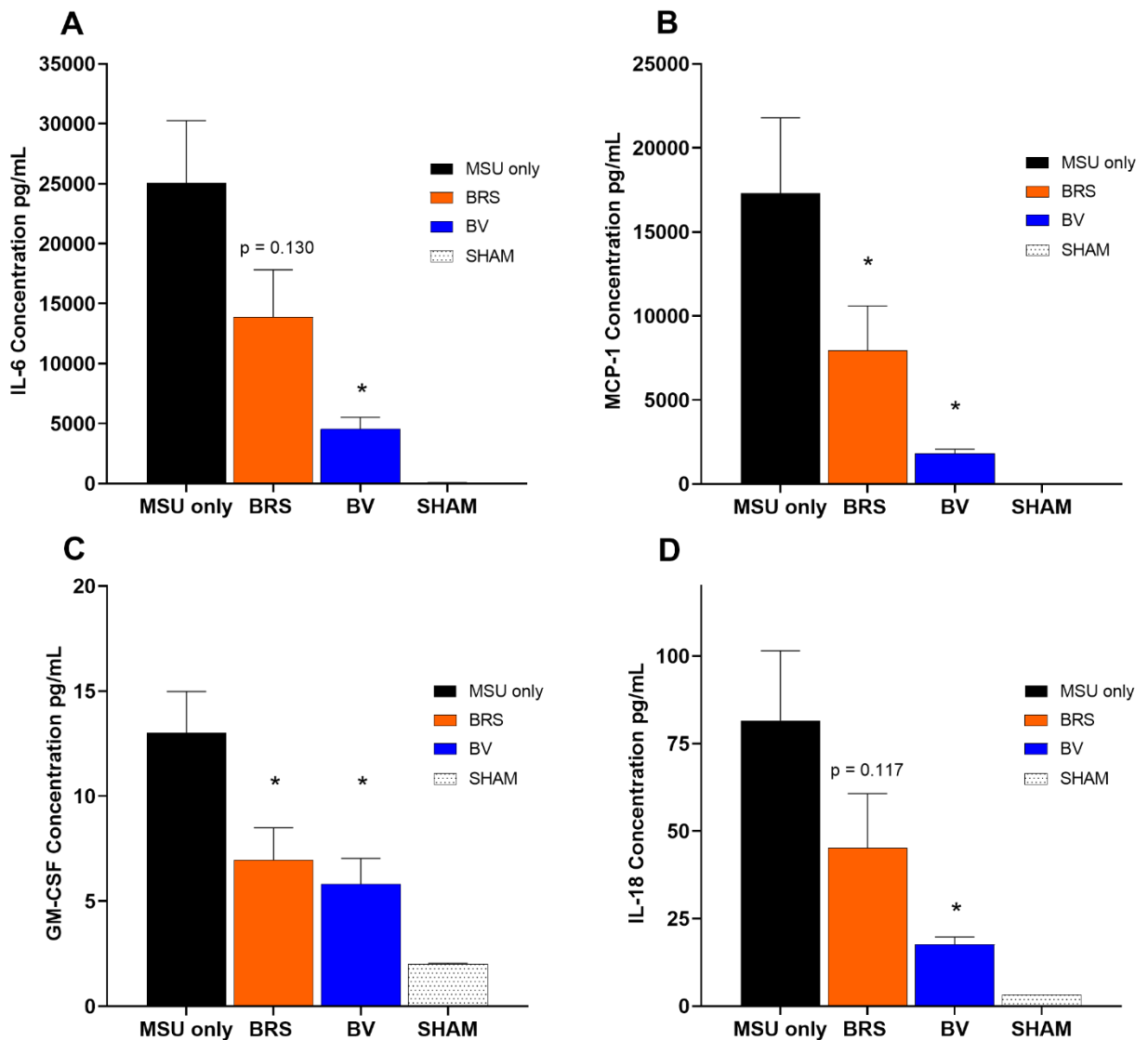


Figure 6.4: Effects of 27 mg kg⁻¹ i.p. pre-treatment of BRS (n=6, orange) and BV (n=5, blue) on concentrations of IL-6 (A), MCP-1 (B), GM-CSF (C) and IL-18 (D) in pouch exudate following MSU administration (25 mg in 5 mL sterile saline) to a 6 day old air pouch model of acute inflammation at the 6 h time point. * denotes p < 0.05 (ANOVA) compared with MSU only (black). Data are presented as mean ± SEM.

Markers of Oxidative Stress

Chloramine and protein carbonyl concentrations in BRS and BV treated animals were not significantly different when compared to the MSU only (Figure 6.5 and 6.6).

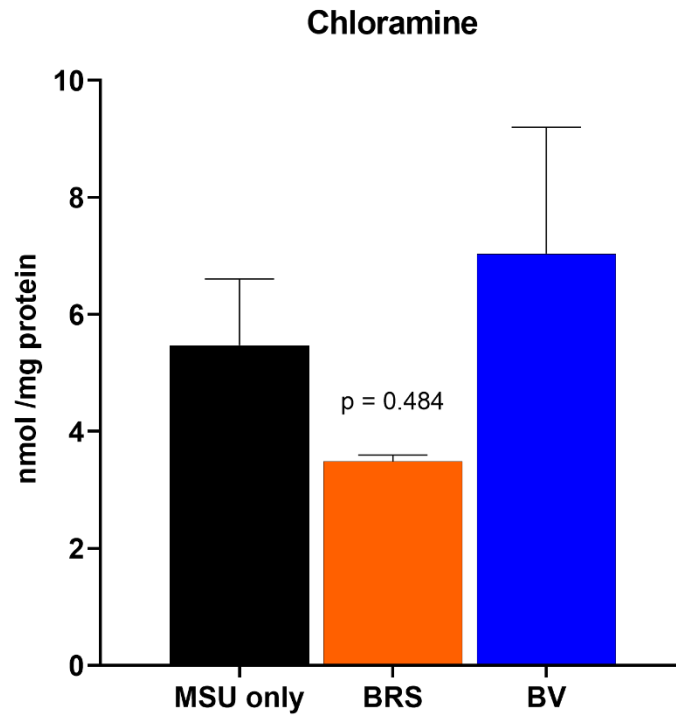


Figure 6.5: Effects of 27 mg kg⁻¹ i.p. pre-treatment with MSU only (n=5, black), BRS (n=6, orange) and BV (n=5, blue) on concentrations of chloramine expressed in nmol chloramine per mg of protein in pouch exudate following MSU administration (25 mg in 5 mL sterile saline) into the 6 day old air pouch at the 24 h time point. No significant differences were detected between groups. Data are presented as mean \pm SEM.

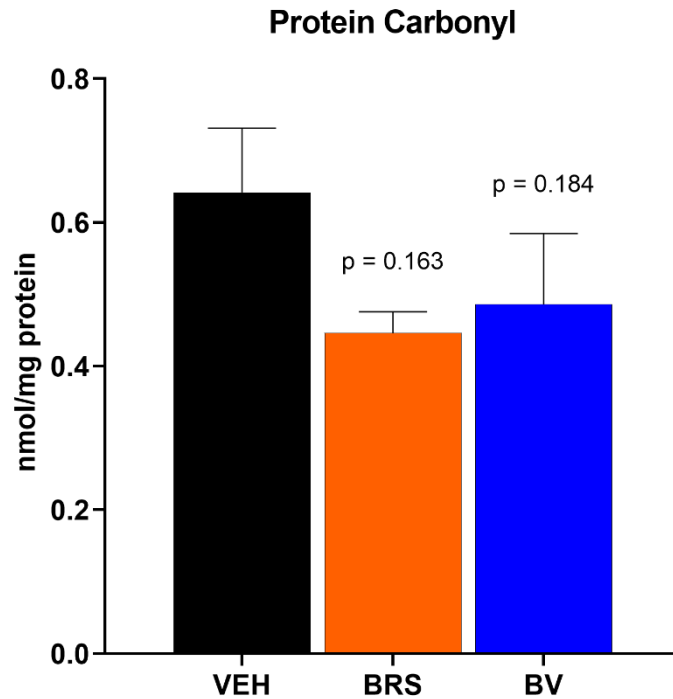


Figure 6.6: Effects of 27 mg kg⁻¹ i.p. pre-treatment with MSU only (n=5, black), BRS (n=6, orange) and BV (n=5, blue) on concentrations of protein carbonyl (nmol carbonyl per mg of protein) in pouch exudate following MSU administration (25 mg in 5 mL sterile saline) into the a 6 day old air pouch. Data are presented as mean ± SEM.

Bile Pigment Concentrations

Concentrations of BRS, BV and UCB were determined in venous blood over the course of 48 h and are shown in Figure 6.7.

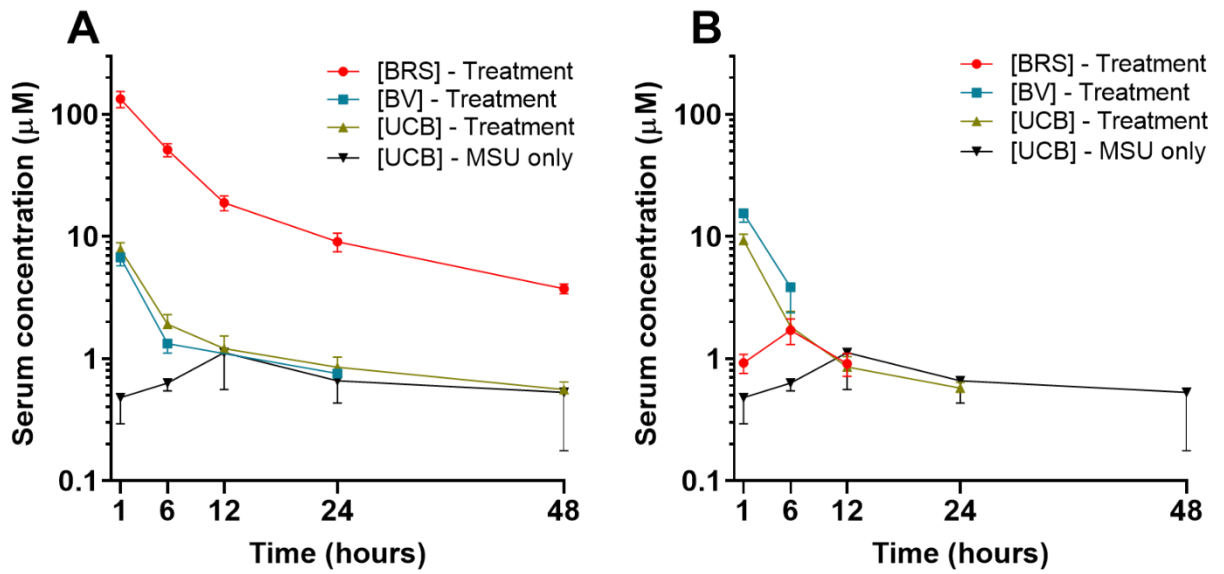


Figure 6.7: Effects of 27 mg kg⁻¹ i.p. pre-treatment of BRS (n=6, A, left) and BV (n=5, B, right) on serum concentrations of BRS, BV and UCB. Data is omitted where compound concentrations were not detectable. Data are presented as mean ± SEM.

Samples of pouch exudate were also analysed for bile pigment concentrations. No bile pigments were detected in the pouch exudate of MSU only or BV treated animals, however BRS was detected in pouch exudate of BRS treated animals between 1 and 24 h of MSU administration (Figure 6.8).

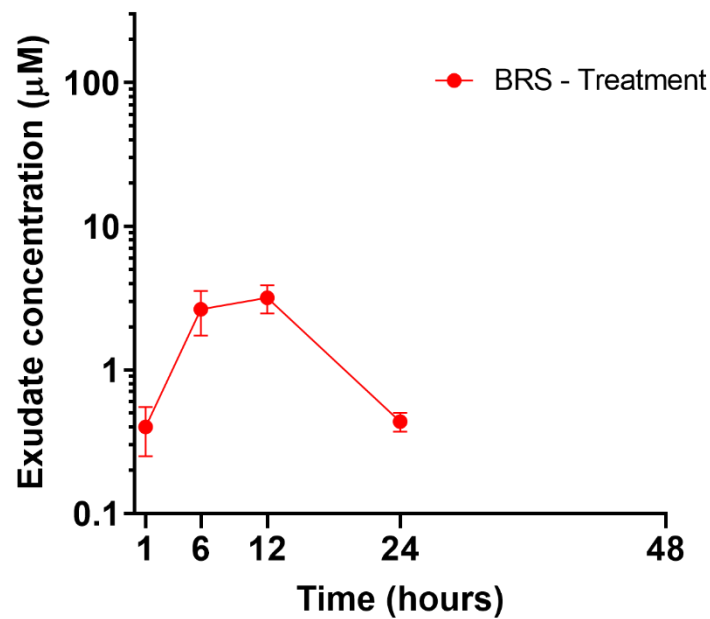


Figure 6.8: Effects of 27mg kg⁻¹ i.p. BRS pretreatment of (n=6) on exudate BRS concentrations. BV and MSU only treatment had no quantifiable bile pigment concentrations.

Discussion

The role of inflammation in chronic disease is well established, and bile pigments continue to show therapeutic potential across a range of models of non-sterile, sterile inflammation and oxidative damage.^(1, 2, 5, 42, 160, 184) This manuscript is the first to explore the anti-inflammatory potential of bile pigment administration against gouty inflammation, and the first to describe the anti-inflammatory activity of BRS. BV and BRS pre-treatment decreased leukocyte infiltration (Figure 6.2A), neutrophil and monocyte ingress (Figure 6.2B and 6.3A) from 6-48 h and cytokine concentrations in pouch exudate (IL-6, MCP-1, GM-CSF and IL-18; Figure 6.4A-D) at 6 h following treatment compared with the MSU only group. Additionally, these data show that BRS is retained in the circulation, peaking at approximately 120 µM and remaining above 5 µM after 48 h, demonstrating a favourable pharmacokinetic profile and potential to confer protection over a greater time period compared to BV.

Leukocyte Infiltration

In addition to the significant decrease in leukocyte and neutrophil infiltration observed in the BV and BRS treatment groups, monocyte and lymphocyte infiltration into the pouch from 12-48 h were also significantly decreased (Figure 6.3). These data suggest initial suppression of the inflammatory cascade during the early phase of the inflammatory response may have reduced the severity of subsequent leukocyte infiltration promoting prompt resolution. At 12 h, the neutrophil (Figure 6.2A) and monocyte (Figure 6.3B) counts were significantly reduced in the BV group compared to BRS, suggesting more potent inhibition of leukocyte infiltration by BV. Interestingly, at 48 h BV and BRS both significantly reduced leukocyte infiltration compared with MSU only (Figures 6.2 and 6.3) and were similar with the effect observed with ibuprofen treatment, suggesting the capacity to acutely resolve inflammation is shared by both compounds and has a similar effect to that of ibuprofen. Furthermore, BRS significantly reduced neutrophil infiltration compared with BV at 48 h (Figure 6.2B), indicating that BRS administration may have been more effective in resolving and preventing neutrophil infiltration, or promoted neutrophil apoptosis/phagocytosis after 48 h compared to BV. Neutrophil infiltration into tissues during an inflammatory response occurs following rolling, adhesion and transmigration of neutrophils on endothelial cells.⁽¹⁸⁵⁾ Significant down-regulation of these events occurs following BV administration in adult Balb/c mice (i.p. 9 mg kg⁻¹).⁽¹⁸⁵⁾ BV pre-treatment in swine (single bolus i.v. 50 µmol kg⁻¹) also significantly inhibits neutrophil infiltration following hepatic ischaemic reperfusion injury.⁽¹⁴¹⁾ Furthermore, *in vitro* studies conclude that binding of BV to biliverdin reductase-A (BVR-A) on the surface of neutrophils and macrophages interferes with TLR4, PI3 kinase and Akt signalling pathways, thus reducing leukocyte infiltration via inhibition of chemotaxis.^(22, 135, 186-188) Further studies

show that BVR deletion enhances macrophage chemotaxis, demonstrating an inhibitory role for BVR-A.⁽¹⁸⁷⁾ While there are no previous data regarding BRS, UCB is reported to inhibit leukocyte extravasation with no changes observed in ICAM-1 or VCAM-1 expression.⁽¹⁸⁹⁾ These data imply that UCB may have interfered with adhesion molecule signalling and contributed to the improved resolution seen here after 48 h. These data further corroborate BV's inhibitory effects on chemotaxis and demonstrate, for the first time, that BRS also exhibits similar effects which in part, may occur following the spontaneous decomposition of BRS to BV.⁽¹⁶⁰⁾

Inflammatory Cytokines

These data show that BV treatment significantly reduces IL-6, MCP-1, GM-CSF and IL-18 pro-inflammatory cytokine concentrations in pouch exudate 6 h post treatment (Figure 6.3) and BRS administration reduced MCP-1 and GM-CSF concentrations ($p < 0.05$; Figure 6.3).

Inflammatory cytokines that are clinically associated with gout-induced inflammation⁽¹⁰⁰⁾ were decreased following BV treatment. These data supported the hypothesis and agree with published literature reporting administration of BV generally reduces pro-inflammatory cytokine expression. For example, 50 mg kg⁻¹ i.p. BV treatment prior to and immediately after small bowel transplant in Lewis rats significantly decreases serum IL-6.⁽¹³¹⁾ Another study reports significant decreases in IL-6 and MCP-1 for i.p. BV (5 mg kg⁻¹) treatment in a caecal ligation model⁽¹⁹⁰⁾, with BV treatment delivered 8, 6, and 3 h before laparotomy, once immediately prior to laparotomy closure and 15 h postoperatively. This study repeatedly dosed BV, to ensure bioavailability of BV over a longer period, which was achieved in our study following single BRS treatment (Figure 6.7A). The decrease in MCP-1, a mediator of

monocyte and lymphocyte recruitment associated with inflammation/insulin resistance⁽¹⁹¹⁾, observed in both BV and BRS administered conditions here and in the caecal ligation study⁽¹⁹⁰⁾, support the decrease in monocyte and lymphocyte recruitment (Figure 6.3).

The significant decrease in IL-18 following BV treatment is a novel finding of this study. Canonically, IL-18 is an inducing factor for interferon gamma (IFN- γ)⁽¹⁹²⁾, suggesting that BV might have inhibit macrophage M1 polarisation as recently shown in BVR knockout macrophages.⁽¹⁸⁸⁾ The IL-18 receptor exerts similar effects to the IL-1 receptor and plays an important role in regulating the differentiation of cell types of the adaptive immune system.⁽¹⁹³⁾ Interestingly, serum IL-18 concentrations are significantly reduced in aged UGT1A1-deficient Gunn rats (i.e. rats with naturally elevated serum UCB) compared to the wild type.⁽¹⁹⁴⁾ Biliverdin is rapidly reduced to UCB *in vivo* (Figure 6.7B), therefore, it is possible that physiological reduction of BV mediated the IL-18 response in this study.

Finally, GM-CSF, a mediator of neutrophil recruitment⁽¹⁹⁵⁾, was significantly reduced in pouch exudate at 6 h (Figure 6.4C) for BV and BRS, which supports the decreased leukocyte infiltration findings here. Additionally, a recent *in vitro* study reports that proinflammatory cytokine production, including GM-CSF, is downregulated by BV and phycocyanobilin (PCB; an algal linear tetrapyrrole structurally similar to BV) pre-treatment of human peripheral blood mononuclear cells (PBMC) stimulated by a mixed lymphocyte reaction.⁽¹⁹⁶⁾

These data agree with recent reports that BV and enzymes involved in bile pigment metabolism (BVR/Haem Oxygenase-1) inhibit sterile inflammatory responses. For example, BV treatment protects rats from acetaminophen-induced toxicity⁽¹⁹⁷⁾, ameliorates cerebral ischemia reperfusion injury in rats⁽¹⁹⁸⁾ and supresses inflammatory cytokine release in

ischemia reperfusion injury and insulin resistance models.⁽¹⁹⁹⁾ These studies, while they measure different outcomes, add to a growing body of evidence demonstrating that these bile pigments play a significant role in attenuating inflammation. Improved understanding of these compounds' roles within mammalian physiology could lead to their future development as safe and effective anti-inflammatory therapeutics.

Bile Pigments in Serum

Biliverdin administration induces potent anti-inflammatory effects^(7, 132, 133, 144); however, we recently demonstrated that i.p. and i.d. biliverdin administration results in appreciable bilirubin-10-sulfonate (~22%) conversion *in vitro* and *ex vivo*.⁽¹⁶⁰⁾ Following i.p. BV and BRS administration, bile pigments were systemically and readily available during the acute phase of inflammation. In addition, this manuscript brings very important information regarding longer term systemic concentrations of BRS retained in the circulation. In conscious animals, circulating concentrations ranged between 120 and 5 μM over 48 h. While BV rapidly decreased over time (i.e., 24 h) with consequent formation of unconjugated bilirubin (presumably due to metabolism via BVR⁽¹⁾) and a small amount of BRS (Figure 6.7B). After BRS administration however, serum BRS concentrations were elevated for 48 h, with only small amounts of BV present over 24 h (Figure 6.7A). These data demonstrate that BRS slowly decomposes, releasing BV, which could mediate longer term anti-inflammatory effects via BVR signalling.

We also detected BRS in pouch exudate (Figure 6.8) over 24 h, indicating that it either leaked into the pouch with exudate formation, or diffused through tissues into this compartment. Surprisingly, markers of oxidative stress were not significantly impacted by BV or BRS (despite

consistent reductions in protein carbonyl for BRS and BV) (Figures 6.5 and 6.6). These data are, however, most likely related to the relatively low local concentrations of bile pigments in the pouch environment. Future studies could investigate the effect of injecting the compounds directly into the pouch (akin to the joint) to determine whether local concentrations can similarly inhibit inflammatory and oxidative processes. Additionally, MPO concentrations in pouch exudate were below the limit of detection for our assay; however, it is possible that BRS, which possesses a reduced C10 bridge, behaves similar to UCB, which inhibits neutrophil burst and neutralises superoxide radicals.⁽⁴⁰⁾ Furthermore, high urate concentrations in the pouch may also have competed for radical formation over the relatively low concentrations of BRS, impacting protection from pouch fluid oxidation. Therefore perhaps increased bile pigment concentrations in pouch fluid could inhibit MPO mediated chloramine and protein carbonyl formation⁽⁴³⁾, supporting the need for further studies to address this question.

Conclusion

Current human and clinical data indicates consistent benefits associated with mild elevation of UCB (as observed in Gilbert's Syndrome) as well as the potential of tetrapyrrole administration⁽¹⁸⁴⁾ to treat a myriad of inflammatory diseases including cardiovascular disease and type 2 diabetes mellitus.

This study describes the *in vivo* anti-inflammatory efficacy of BRS and BV in an MSU crystal induced model of sterile inflammation in the rat, as well as longer term serum pharmacokinetics in conscious animals for both compounds. The data presented demonstrates the importance of bile pigments as endogenous anti-inflammatory compounds

that are actively produced during sterile inflammation and indicates that BV/BRS administration are potential therapeutic avenues for the treatment of sterile inflammation/gout. BRS administration confers similar benefits to BV administration while remaining in systemic circulation for up to 48 h following treatment. We propose that the administration of BRS, a hydrophilic compound, is a simple method to increase BV and UCB *in vivo*, which could help in realising the anti-inflammatory therapeutic potential of bile pigments.

Additional information

Author contribution statement

A.C.B., M.M. and R.G.S. conceived the design of this study. R.G.S. and W.H. performed animal experimentation and interpretation of data. R.G.S. and W.H. performed HPLC and LCMS analysis, pouch exudate analysis and statistical analysis of data. J.V. assisted with statistical analysis and performed quantification of protein carbonyl. E.N.P. assisted with the quantification of cytokines via flow cytometry. A.G.P., G.G. and K.H.W. assisted with concept, technical advice and input. A.C.B. and K.H.W. secured funding for the project. All authors contributed to revision of the MS and provided their final approval for manuscript submission.

Competing interests

The author(s) declare no competing interests.

Acknowledgement

The authors acknowledge the support received through an Australian Government Research Training Program Scholarship as well as the generosity of Patricia Barlow in providing a Research Higher Degree scholarship. The research was supported by the Griffith Enterprise

Innovation Fund, which utilised funding provided by Griffith University and the Queensland Government.

Animal Use

All animal care and experimental procedures complied with the Guidelines of the Australian National Health and Medical Research Council and were approved by the Griffith University Animal Ethics Committee (MSC/03/18/AEC).

Supplementary Information

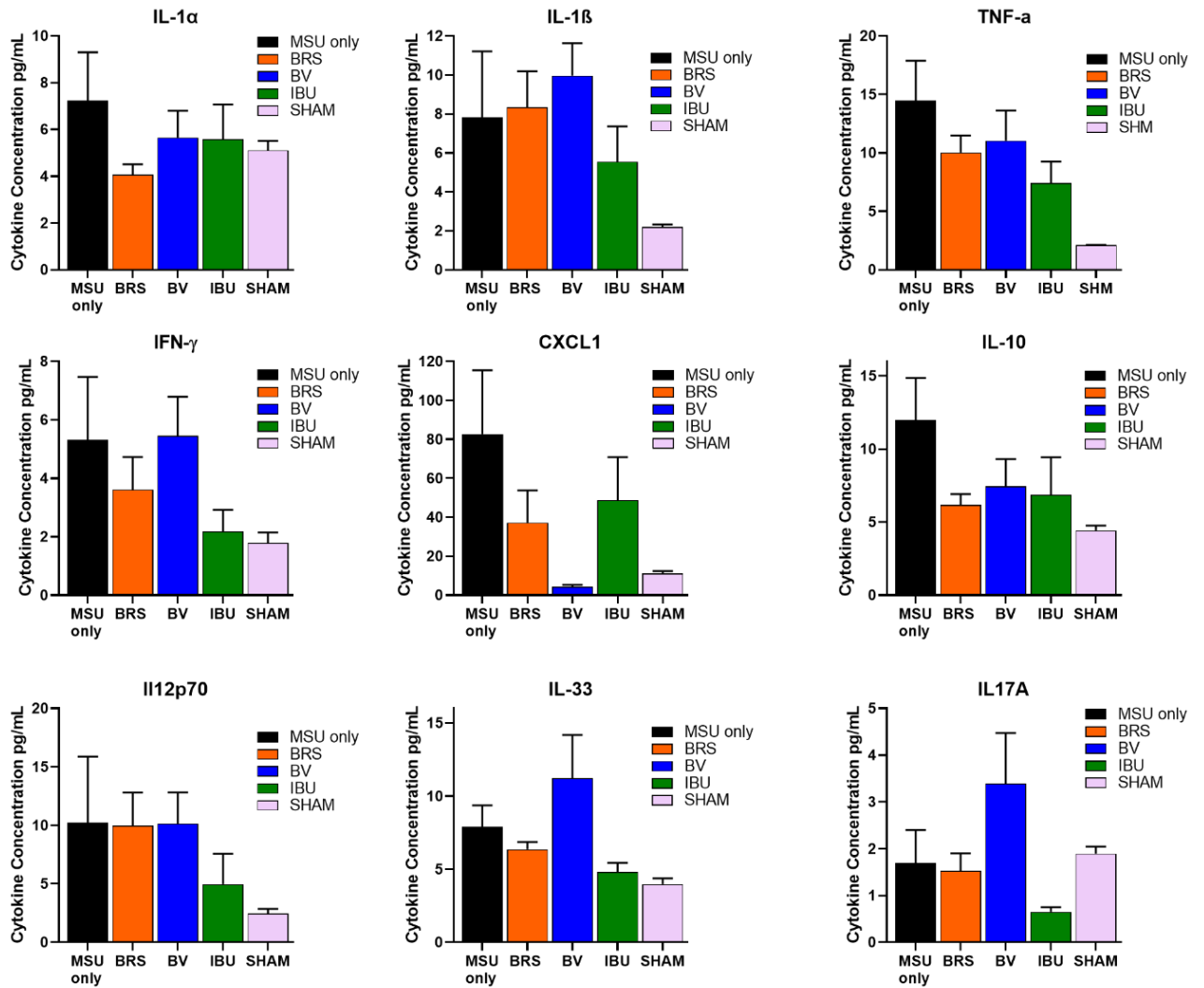


Figure 6.9: Concentrations of cytokines in pouch exudate at 6 h were determined using a multiplexed bead-based flow cytometric immunoassay.

Chapter Seven: Thesis Summary and Conclusion

This thesis includes three original investigations, presented as a series of chapters which examine the discovery, pharmacokinetics and *in vivo* anti-inflammatory effects of bilirubin-10-sulfonate and compared to biliverdin. This final chapter will discuss the implications of the combined experimental chapters and outline future research directions based upon the reported findings.

7.1 Introduction

This thesis investigated bilirubin-10-sulfonate (BRS), a novel metabolite of biliverdin (BV), and details the discovery and characterisation of BRS as well as its pharmacokinetics and anti-inflammatory/antioxidant properties in an animal model of gouty arthritis. The findings of this thesis identify BRS as a molecule of therapeutic potential, based upon favourable pharmacokinetic profile and anti-inflammatory efficacy in a model of sterile inflammation.

7.2 Project Summary

The first study (Chapter 4) documents the discovery of BRS following intraduodenal administration in the rat. Our current understanding of bile pigment metabolism is limited to the canonical haem catabolic pathway, ending with the conversion of BV to UCB and conjugation of UCB prior to biliary excretion where bacterial reduction/oxidation converts the excreted pigments into stercobilins and urobilins, which provide colour to urine and faeces. Chapter 4 was important because it presents the first evidence of a new metabolic pathway for bile pigment metabolism in the gut. This chapter showed that biliverdin was metabolised to BRS and that bacteria were responsible. This implies that any BV excreted in bile would likely be metabolised to BRS and raises important questions surrounding previous research

conclusions involving BV administration *in vivo*. Specifically, previous studies that administered BV in mammals and attributed any effects to it, may have done so erroneously, due to BRS formation. Additionally, very little is known regarding the pharmacology, including pharmacokinetics, of BRS, with McDonagh discovering it in bullfrogs and performing limited hepatic metabolism studies showing intravenous administration of BRS is excreted intact in the bile of the bullfrog, but *not* the rat.⁽³⁶⁾

It was hypothesised that enteric bacteria were responsible for the conversion of BV to an unknown tetrapyrrolic compound via addition at the C10 bridge. Following the identification of BRS following BV treatment of bacteria, as well as formation of BRS in aseptic controls with BV added to nutrient broth containing sodium thioglycolate, tandem mass spectrometric analysis concluded that the unknown compound was bilirubin-10-sulfonate (BRS), and was a product of bisulfite (HSO_3^-) addition to BV at the C10 carbon bridge. This was confirmed by the analysis of synthetic BRS, where sodium bisulfite was added to BV and analysed by NMR to confirm identify. This study also showed the antioxidant capacity of BRS in plasma to be comparable with that of BV, thereby identifying BRS as a compound with therapeutic (antioxidant) potential.

Having discovered this compound and the possibility of a new enteric metabolic pathway for biliverdin, we hypothesised that BRS (from BV) would be absorbed from the gut into the blood stream and re-excreted in bile. Based upon BRS possessing structural similarities with unconjugated bilirubin, we speculated that its half-life would be greater, and distribution and elimination rates would be significantly greater than BV. In order to answer this question, BRS and BV were administered intravenously, intraperitoneally and intraduodenally to anaesthetised rats, with blood and bile concentrations assessed over 3 hours (Chapter 5). The

results supported the hypothesis in that BV and BRS were absorbed from the peritoneum and intestine, with intraperitoneal administration causing a much larger increase of circulating bile pigments in serum compared with intraduodenal administration. These data are supported by previous preliminary data following intraperitoneal and intraduodenal biliverdin administration.⁽¹⁾ The data also showed that BRS was excreted intact in the bile, with increases in conjugated bilirubin suggesting some conversion of BRS to BV prior to biliary excretion occurred. This stands in stark contrast to historically published data that reported BRS was *not* excreted in the bile of rats following intravenous administration of BRS.⁽³⁶⁾ The pharmacokinetic data showed that BRS has a significantly smaller volume of distribution and rates of elimination and distribution, a greater intravenous half-life, and an increased AUC₁₈₀ compared with BV administration. Additionally, detection of trace BRS after intraperitoneal administration also challenges the possibility of bacteria being the sole source of bisulfite for BV reduction. Other cellular sources may exist that contribute *in vivo* to this transformation and this should be considered carefully, when investigating the efficacy of intraperitoneal BV administration in models of inflammation. Furthermore, the poor intestinal bioavailability of BRS and BV as well as an acceptable and similar intraperitoneal bioavailability (~30%) suggested that intraduodenal administration is not a viable route of administration. Further studies are required to confirm this and explore means to improve intraduodenal bioavailability.⁽²⁰⁰⁾ This study was important because was the first to document the pharmacokinetic profile of BRS versus BV and it guided the next study in terms of selecting an appropriate dose and route of BRS administration in order to test both compounds for their anti-inflammatory properties.

Based upon the varying pharmacokinetics of both BRS and BV along with the increased vascular retention of BRS, we tested their anti-inflammatory efficacy in an animal model of sterile inflammation. This third study (Chapter 6), investigated the effects of intraperitoneal BV and BRS administration in animals experiencing sterile inflammation induced by monosodium urate crystal administration into a subcutaneous air pouch. This study was important because bile pigments (including BRS) have not been tested in any models of joint based inflammation to date. It was hypothesised that BV and BRS treated animals would have decreased leukocyte infiltration, cytokine concentrations and oxidative stress markers in the pouch over a period of 48 hours. The results partially supported the hypothesis, showing significant decreases in leukocyte infiltration (BV and BRS) and cytokine concentrations (MCP-1 and GM-CSF for BV and BRS with BV also having decreased IL-6 and IL-18), however no significant decreases in markers of oxidative stress were noted. Bile pigments in serum were also measured, and BRS was still detectable up to 48 hours after administration in conscious animals, while BV was not detected after 12 hours, building on data in Chapter 5 and suggesting that BRS has a favourable pharmacokinetic profile over the longer term in conscious animals.

Due to its favourable pharmacokinetic profile and ability to inhibit inflammatory processes such as leukocyte infiltration and release of inflammatory cytokines, this thesis concludes that BRS may be a viable treatment for inflammatory joint disease such as gout.

7.3 Future Directions

Cumulatively, this thesis has broken new ground in that it has discovered 1) a new pathway of BV metabolism in mammals 2) documented the pharmacokinetics of this compound in rats and 3) tested the therapeutic efficacy of BRS and BV in sterile model of inflammation. These

data make an important contribution to realising the potential utility of bile pigments that could be used therapeutically in future.

As this thesis did not perform *in vitro* mechanistic research on these compounds, this type of study will need to be performed in order to determine the mechanisms of action in which BRS exerts its effect, its mechanism of formation and pathways which that lead to its production *in vivo*. Given BRS ostensibly exists in a thermodynamic equilibrium with BV in solution, and has a much greater half-life than BV, it is possible that BRS administration also activated biliverdin reductase, which has well appreciated cell signalling and anti-inflammatory effects.⁽²⁰¹⁾ Therefore, the activation of PI3Kinase and Akt signalling pathways in the presence of BRS is warranted in macrophages. Furthermore, adding BRS to BVR knockout cells could show whether BRS exerts anti-inflammatory effects, independent of BVR.⁽¹⁸⁷⁾ Where possible in both *in vivo* and *in vitro* studies, flow cytometry should also be used to measure any changes that a regular availability of BV (via BRS degradation) may induce on the differentiation of monocytes and neutrophils. Furthermore, Chapter 3 provided a preliminary investigation of BRS antioxidant capacity. However, Chapter 5 showed no significant reduction in chloramine and protein carbonyl formation in pouch exudate. Therefore, based upon bilirubin's known capacity to inhibit chloramine and protein carbonylation (and lipid peroxidation)⁽⁴³⁾, further studies investigating BRS antioxidant properties and ability to inhibit protein and lipid oxidation are warranted. It is possible that the monosodium urate model was unable to detect protection from inflammatory oxidation, due to very low MPO concentrations and large urate (antioxidant) concentrations within the pouch. Therefore, BRS could be tested in other inflammatory models characterised by strong MPO and hypochlorous

acid induced injury (e.g. in a hypochlorous acid induced model of systemic sclerosis^(202, 203)), which BRS is likely to protect against.

Regardless of the theorised mechanism of action and possible concerns regarding BRS degradation, the efficacy of BRS could be broadly applicable to many disease processes. Considering that BRS possesses antioxidant and anti-inflammatory activity and that it is excreted intact in the bile (and found in the circulation) in high concentrations, future research could also explore its efficacy of BRS in models of gastrointestinal inflammatory disease.⁽²⁰⁴⁾ Furthermore, future research should also include dose-response studies, subcutaneous/rectal administration pharmacokinetics, efficacy testing after gout is induced, as well as a focus on whether bile pigment administration leads to better clinical outcomes. (i.e. pain assessment).

Finally, following the investigation of BRS mechanisms of action and its relevance in gastrointestinal inflammatory disease, the safety and efficacy of BRS will have to be demonstrated in larger mammals, such as swine, before being made available for testing in humans. Once determined to be safe in humans, BRS will need to demonstrate efficacy in phase 2 and 3 clinical studies in patients with inflammatory disease prior to approval for use in humans.

In conclusion, it is hoped that this thesis has clearly documented the discovery of a novel bile pigment, performed a comprehensive pharmacokinetic evaluation of this compound and provided a 'proof of concept' for the use of BRS as a treatment of sterile inflammation. It is hoped that this data will lay the foundation for future studies which aim to develop new treatments for patients with conditions that are currently poorly managed and therefore impact patient quality of life. As such, this thesis hopes to demonstrate how investment in

early biomedical science can be translated into research that in future has the potential to benefit human health and wellbeing.

References

1. Bulmer, A.C., et al. (2011). Bile pigment pharmacokinetics and absorption in the rat: therapeutic potential for enteral administration. *Br J Pharmacol.* **164**(7): p. 1857-70.
2. Bulmer, A.C., Blanchfield, J.T., Toth, I.F., & Coombes, J.S. (2008). Improved resistance to serum oxidation in Gilbert's Syndrome; a mechanism for cardioprotection. *Atherosclerosis.* **199**(2): p. 390-396.
3. Vitek, L. and H.A. Schwertner (2007). The heme catabolic pathway and its protective effects on oxidative stress-mediated diseases. *Adv Clin Chem.* **43**(1): p. 1-57.
4. Bernhard, K., Ritzen, G. & Steiner, K.U. (1954). The biological importance of bile pigments. Bilirubin and biliverdin as antioxidants for vitamin A and essential fatty acids. *Helvetica Chimica Acta.* **37**(1): p. 306-313.
5. Bulmer, A.C., H.J. Verkade, and K.H. Wagner (2013). Bilirubin and beyond: a review of lipid status in Gilbert's syndrome and its relevance to cardiovascular disease protection. *Prog Lipid Res.* **52**(2): p. 193-205.
6. Vitek, L. and J.D. Ostrow (2009). Bilirubin chemistry and metabolism; harmful and protective aspects. *Curr Pharm Des.* **15**(25): p. 2869-83.
7. Nakagami, T., Toyomura, K., Kinoshita, T. & Morisawa, S. (1993). A beneficial role of bile pigments as an endogenous tissue protector: Anti-complement effects of biliverdin and conjugated bilirubin. *Biochimica et Biophysica Acta – General Subjects.* **1158**(2): p. 189-193.
8. Stocker, R., Yamamoto, Y., McDonagh, A.F., Glazer, A.N. & Ames, B.N. (1987). Bilirubin is an antioxidant of possible physiological importance. *Science.* **235**(4792): p. 1043-1046.

9. Lundvig, D.M., Immenschuh, S. & Wagener, F.A. (2012). Hemeoxygenase, inflammation, and fibrosis: the good, the bad, and the ugly? *Frontiers of Pharmacology*. **3**(81).
10. Rountree, R. (2010). Roundoc Rx: Inflammation and Functional Medicine Interventions: Part 1 - Inflammation and Chronic Disease. *Alternative and Complementary Therapies*. **16**(2): p. 72-76.
11. Coffey, M., et al. (1989). Rheumatoid factors in cystic fibrosis: associations with disease manifestations and recurrent bacterial infections. *Clin Exp Immunol*. **77**(1): p. 52-7.
12. Siegel, M.P., et al. (2011). Reduced coupling of oxidative phosphorylation in vivo precedes electron transport chain defects due to mild oxidative stress in mice. *PLoS One*. **6**(11): p. e26963.
13. Thomas, C. and A.B. Lumb (2012). Physiology of haemoglobin. *Continuing Education in Anaesthesia Critical Care & Pain*. **12**(5): p. 251-256.
14. Franco, R.S. (2012). Measurement of red cell lifespan and aging. *Transfusion medicine and hemotherapy : offizielles Organ der Deutschen Gesellschaft fur Transfusionsmedizin und Immunhamatologie*. **39**(5): p. 302-307.
15. Wagner, K.H., et al. (2018). Diagnostic criteria and contributors to Gilbert's syndrome. *Crit Rev Clin Lab Sci*. **55**(2): p. 129-139.
16. D'Alessandro, A., et al. (2019). Protect, repair, destroy or sacrifice: a role of oxidative stress biology in inter-donor variability of blood storage? *Blood Transfus*. **17**(4): p. 281-288.
17. Bandyopadhyay, U.K., S. (2005). Free heme toxicity and its detoxification systems in humans. *Toxicology Letters*. **157**(1): p. 175-188.

18. Van Avondt, K., E. Nur, and S. Zeerleder (2019). Mechanisms of haemolysis-induced kidney injury. *Nature Reviews Nephrology*. **15**(11): p. 671-692.
19. Jeffers, A., Xiuli, X., Huang, K.T., Man, C., Hogg, N., Rakesh, P., Patel & Kim-Shapiro, D.B. (2005). Hemoglobin mediated nitrite activation of soluble guanylyl cyclase. *Comparative Biochemistry and Physiology Part A: Molecular & Integrative Physiology*. **142**(2): p. 130-135.
20. Araujo, J.A., M. Zhang, and F. Yin (2012). Heme oxygenase-1, oxidation, inflammation, and atherosclerosis. *Front Pharmacol*. **3**(119): p. 119.
21. Schaer, D.J., et al. (2014). Haptoglobin, hemopexin, and related defense pathways—basic science, clinical perspectives, and drug development. *Frontiers in Physiology*. **5**(415).
22. Wegiel, B. and L.E. Otterbein (2012). Go green: the anti-inflammatory effects of biliverdin reductase. *Front Pharmacol*. **3**(1): p. 47.
23. Iga, T., D.L. Eaton, and C.D. Klaassen (1979). Uptake of unconjugated bilirubin by isolated rat hepatocytes. *Am J Physiol*. **236**(1): p. C9-14.
24. Perlman, J.M. and J.J. Volpe, *Bilirubin*, in *Volpe's Neurology of the Newborn*, J.J. Volpe, et al., Editors. 2018, Elsevier. p. 730-762.e4.
25. Katalin, J., Zsuzsa, V., Regina, T. & Laszlo, V. (2008). Modulation of bilirubin-glucuronide transport via MRP2/MRP3 using sandwich culture of primary human and rat hepatocytes. *Drug Metabolism Reviews*. **40**(1): p. 163.
26. Wang, X., Chowdhury, J.R. & Chowdhury, N.R. (2006). Bilirubin metabolism: Applied physiology. *Current Paediatrics*. **16**(1): p. 70-74.
27. Tirribelli, C.O., J.D. (2005). Intestinal flora and bilirubin. *Journal of Hepatology*. **42**(2): p. 170-172.

28. Vitek, L., et al. (2006). Identification of bilirubin reduction products formed by *Clostridium perfringens* isolated from human neonatal fecal flora. *J Chromatogr B Analyt Technol Biomed Life Sci.* **833**(2): p. 149-57.
29. Vitek, L. and M.C. Carey (2012). New pathophysiological concepts underlying pathogenesis of pigment gallstones. *Clin Res Hepatol Gastroenterol.* **36**(2): p. 122-9.
30. Fang, L.S. (1985). Study on a special binding phenomenon of biliverdin in the blood of the eel, *Anguilla japonica*. *Comp Biochem Physiol B.* **81**(3): p. 723-6.
31. Fang, L.S. and J.L. Bada (1990). The blue-green blood plasma of marine fish. *Comp Biochem Physiol B.* **97**(1): p. 37-45.
32. Fang, L.S.B., J.L. (1983). A Comparative-Study of the Occurrence, Extent of Conjugation, and Excretion of the Bile Pigment Biliverdin in Marine Fish. *Marine Biology Letters.* **4**(1): p. 341-348.
33. Dennery, P.A. (2012). Evaluating the beneficial and detrimental effects of bile pigments in early and later life. *Front Pharmacol.* **3**: p. 115.
34. Stanford, S.J., et al. (2005). Transition from placental to air breathing stimulates haem-oxygenase-1 expression without functional consequence for pulmonary vascular adaptation in pigs and mice. *Br J Pharmacol.* **144**(4): p. 467-76.
35. Morton, S.U. and D. Brodsky (2016). Fetal Physiology and the Transition to Extrauterine Life. *Clin Perinatol.* **43**(3): p. 395-407.
36. Tiribelli, C. and J.D. Ostrow (1996). New concepts in bilirubin and jaundice: report of the Third International Bilirubin Workshop, April 6-8, 1995, Trieste, Italy. *Hepatology.* **24**(5): p. 1296-311.

37. Rocha, P.L. and L.G. Branco (1998). Seasonal changes in the cardiovascular, respiratory and metabolic responses to temperature and hypoxia in the bullfrog *Rana catesbeiana*. *J Exp Biol.* **201**(Pt 5): p. 761-8.
38. Jones, L., et al. (2010). Antioxidant Defense System in Tadpoles of the American Bullfrog (*Lithobates catesbeianus*) Exposed to Paraquat. *Journal of Herpetology.* **44**(2): p. 222-228.
39. Sedlak, T.W. and S.H. Snyder (2004). Bilirubin benefits: cellular protection by a biliverdin reductase antioxidant cycle. *Pediatrics.* **113**(6): p. 1776-82.
40. Vasavda, C., et al. (2019). Bilirubin Links Heme Metabolism to Neuroprotection by Scavenging Superoxide. *Cell Chem Biol.* **26**(10): p. 1450-1460 e7.
41. Bakrania, B., et al. (2016). Pre- or post-ischemic bilirubin ditaurate treatment reduces oxidative tissue damage and improves cardiac function. *Int J Cardiol.* **202**: p. 27-33.
42. Bulmer, A.C., Blanchfield, J.T., Riedc, K. & Wagner, K.H. (2008). The anti-mutagenic properties of bile pigment. *Reviews in Mutation Research.* **658**(1): p. 28-41.
43. Boon, A.C., et al. (2015). Bilirubin scavenges chloramines and inhibits myeloperoxidase-induced protein/lipid oxidation in physiologically relevant hyperbilirubinemic serum. *Free Radic Biol Med.* **86**(1873-4596 (Electronic)): p. 259-68.
44. Pizzino, G., et al. (2017). Oxidative Stress: Harms and Benefits for Human Health. *Oxid Med Cell Longev.* **2017**: p. 8416763.
45. Wu, J.Q., T.R. Kosten, and X.Y. Zhang (2013). Free radicals, antioxidant defense systems, and schizophrenia. *Prog Neuropsychopharmacol Biol Psychiatry.* **46**(1878-4216 (Electronic)): p. 200-6.

46. Ogawa, K., et al. (2008). The association of elevated reactive oxygen species levels from neutrophils with low-grade inflammation in the elderly. *Immun Ageing*. **5**: p. 13.
47. Cheng, D., et al. (2019). Inhibition of MPO (Myeloperoxidase) Attenuates Endothelial Dysfunction in Mouse Models of Vascular Inflammation and Atherosclerosis. *Arterioscler Thromb Vasc Biol*. **39**(7): p. 1448-1457.
48. Suzuki, K., et al. (1996). Capacity of circulating neutrophils to produce reactive oxygen species after exhaustive exercise. *J Appl Physiol (1985)*. **81**(3): p. 1213-22.
49. Global, regional, and national age-sex-specific mortality for 282 causes of death in 195 countries and territories, 1980-2017: a systematic analysis for the Global Burden of Disease Study 2017. (1474-547X (Electronic)).
50. Newton, K. and V.M. Dixit (2012). Signaling in innate immunity and inflammation. *Cold Spring Harb Perspect Biol*. **4**(3): p. a006049.
51. Denk, S., M. Perl, and M. Huber-Lang (2012). Damage- and pathogen-associated molecular patterns and alarmins: keys to sepsis? *Eur Surg Res*. **48**(4): p. 171-9.
52. Mortaz, E., et al. (2018). Update on Neutrophil Function in Severe Inflammation. *Front Immunol*. **9**: p. 2171.
53. Gong, T., et al. (2020). DAMP-sensing receptors in sterile inflammation and inflammatory diseases. *Nat Rev Immunol*. **20**(2): p. 95-112.
54. Degtarev, A., et al. (2005). Chemical inhibitor of nonapoptotic cell death with therapeutic potential for ischemic brain injury. *Nat Chem Biol*. **1**(2): p. 112-9.
55. Dhuriya, Y.K. and D. Sharma (2018). Necroptosis: a regulated inflammatory mode of cell death. *J Neuroinflammation*. **15**(1): p. 199.

56. Mulay, S.R., et al. (2016). Cytotoxicity of crystals involves RIPK3-MLKL-mediated necroptosis. *Nat Commun.* **7**: p. 10274.
57. Frank, D. and J.E. Vince (2019). Pyroptosis versus necroptosis: similarities, differences, and crosstalk. *Cell Death Differ.* **26**(1): p. 99-114.
58. Brault, M. and A. Oberst (2017). Controlled detonation: evolution of necroptosis in pathogen defense. *Immunol Cell Biol.* **95**(2): p. 131-136.
59. Furze, R.C. and S.M. Rankin (2008). Neutrophil mobilization and clearance in the bone marrow. *Immunology.* **125**(3): p. 281-8.
60. Manz, M.G. and S. Boettcher (2014). Emergency granulopoiesis. *Nat Rev Immunol.* **14**(5): p. 302-14.
61. Kruger, P., et al. (2015). Neutrophils: Between host defence, immune modulation, and tissue injury. *PLoS Pathog.* **11**(3): p. e1004651.
62. Prame Kumar, K., A.J. Nicholls, and C.H.Y. Wong (2018). Partners in crime: neutrophils and monocytes/macrophages in inflammation and disease. *Cell Tissue Res.* **371**(3): p. 551-565.
63. Soehnlein, O., et al. (2008). Neutrophil secretion products pave the way for inflammatory monocytes. *Blood.* **112**(4): p. 1461-71.
64. Lee, T.D., et al. (2003). CAP37, a neutrophil-derived inflammatory mediator, augments leukocyte adhesion to endothelial monolayers. *Microvasc Res.* **66**(1): p. 38-48.
65. Sica, A. and A. Mantovani (2012). Macrophage plasticity and polarization: in vivo veritas. *J Clin Invest.* **122**(3): p. 787-95.

66. Jeong, J.H., et al. (2017). CD14(+) Cells with the Phenotype of Infiltrated Monocytes Consist of Distinct Populations Characterized by Anti-inflammatory as well as Pro-inflammatory Activity in Gouty Arthritis. *Front Immunol.* **8**(1260): p. 1260.
67. Xiao, L., Y. Liu, and N. Wang (2014). New paradigms in inflammatory signaling in vascular endothelial cells. *Am J Physiol Heart Circ Physiol.* **306**(3): p. H317-25.
68. Wojkowska, D.W., P. Szpakowski, and A. Glabinski (2017). Interleukin 17A Promotes Lymphocytes Adhesion and Induces CCL2 and CXCL1 Release from Brain Endothelial Cells. *Int J Mol Sci.* **18**(5): p. 1000.
69. Mehrad, B., R.M. Keane Mp Fau - Strieter, and R.M. Strieter Chemokines as mediators of angiogenesis. (0340-6245 (Print)).
70. Yang, X., Y. Chang, and W. Wei (2016). Endothelial Dysfunction and Inflammation: Immunity in Rheumatoid Arthritis. *Mediators Inflamm.* **2016**: p. 6813016.
71. Campbell, J.J., et al. (1998). Chemokines and the arrest of lymphocytes rolling under flow conditions. *Science.* **279**(5349): p. 381-4.
72. Sprague, A.H. and R.A. Khalil (2009). Inflammatory cytokines in vascular dysfunction and vascular disease. *Biochem Pharmacol.* **78**(6): p. 539-52.
73. Gimbrone, M.A., Jr. and G. García-Cardeña (2016). Endothelial Cell Dysfunction and the Pathobiology of Atherosclerosis. *Circulation research.* **118**(4): p. 620-636.
74. Zhang, J.M. and J. An (2007). Cytokines, inflammation, and pain. *Int Anesthesiol Clin.* **45**(2): p. 27-37.
75. Dinarello, C.A. (2011). Interleukin-1 in the pathogenesis and treatment of inflammatory diseases. *Blood.* **117**(14): p. 3720-32.
76. Lukens, J.R., J.M. Gross, and T.D. Kanneganti (2012). IL-1 family cytokines trigger sterile inflammatory disease. *Front Immunol.* **3**: p. 315.

77. Malik, A. and T.D. Kanneganti (2017). Inflammasome activation and assembly at a glance. *J Cell Sci.* **130**(23): p. 3955-3963.
78. Ding J Fau - Wang, K., et al. Pore-forming activity and structural autoinhibition of the gasdermin family. (1476-4687 (Electronic)).
79. Erdei, J., et al. (2018). Induction of NLRP3 Inflammasome Activation by Heme in Human Endothelial Cells. *Oxid Med Cell Longev.* **2018**(1942-0994 (Electronic)): p. 4310816.
80. Busso, N. and A. So (2010). Mechanisms of inflammation in gout. *Arthritis Res Ther.* **12**(2): p. 206.
81. Yilmaz, O. and K.L. Lee (2015). The inflammasome and danger molecule signaling: at the crossroads of inflammation and pathogen persistence in the oral cavity. *Periodontol 2000.* **69**(1): p. 83-95.
82. Richette, P. and T. Bardin Gout. (1474-547X (Electronic)).
83. Sin, Y.M., et al. (1986). Mast cells in newly formed lining tissue during acute inflammation: a six day air pouch model in the mouse. *Ann Rheum Dis.* **45**(10): p. 873-7.
84. Brooks, P.M., D. Burton, and M.J. Forrest (1987). Crystal-induced inflammation in the rat subcutaneous air-pouch. *Br J Pharmacol.* **90**(2): p. 413-9.
85. Martin, S.W., et al. (1994). The six-day-old rat air pouch model of inflammation: characterization of the inflammatory response to carrageenan. *J Pharmacol Toxicol Methods.* **32**(3): p. 139-47.
86. Ferrari, A.J., et al. (1996). Nonsteroidal Anti-Inflammatory Drugs and Prostaglandins: Their Interactions and Effects on the Particulate-Induced Inflammatory Process

- Implicated in Joint Implant-Loosening and on Monosodium Urate Crystal-Induced Inflammation. *Am J Ther.* **3**(3): p. 189-194.
87. Liote, F., et al. (1996). Inhibition and prevention of monosodium urate monohydrate crystal-induced acute inflammation in vivo by transforming growth factor beta1. *Arthritis Rheum.* **39**(7): p. 1192-8.
88. Kotiw, M., et al. (2010). Detection of anti-TNFalpha activity in canine hyperimmune serum using a TNFalpha inhibition assay. *Vet Clin Pathol.* **39**(1): p. 46-52.
89. Hsu, D.Z., et al. (2013). Therapeutic effects of sesame oil on monosodium urate crystal-induced acute inflammatory response in rats. *Springerplus.* **2**(1): p. 659.
90. Moilanen, L.J., et al. (2015). Urate crystal induced inflammation and joint pain are reduced in transient receptor potential ankyrin 1 deficient mice--potential role for transient receptor potential ankyrin 1 in gout. *PLoS One.* **10**(2): p. e0117770.
91. Scanu, A., et al. (2015). High-density lipoproteins inhibit urate crystal-induced inflammation in mice. *Ann Rheum Dis.* **74**(3): p. 587-94.
92. Oliviero, F. and A. Scanu (2017). How Factors Involved in the Resolution of Crystal-Induced Inflammation Target IL-1beta. *Front Pharmacol.* **8**: p. 164.
93. Yao, X., et al. (2012). Inhibition of monosodium urate crystal-induced inflammation by scopoletin and underlying mechanisms. *Int Immunopharmacol.* **14**(4): p. 454-62.
94. Edwards, J.C., A.D. Sedgwick, and D.A. Willoughby (1981). The formation of a structure with the features of synovial lining by subcutaneous injection of air: an in vivo tissue culture system. *J Pathol.* **134**(2): p. 147-56.
95. McWherter, C., et al. (2018). Arhalofenate acid inhibits monosodium urate crystal-induced inflammatory responses through activation of AMP-activated protein kinase (AMPK) signaling. *Arthritis Res Ther.* **20**(1): p. 204.

96. Dhanasekar, C., S. Kalaiselvan, and M. Rasool (2015). Morin, a Bioflavonoid Suppresses Monosodium Urate Crystal-Induced Inflammatory Immune Response in RAW 264.7 Macrophages through the Inhibition of Inflammatory Mediators, Intracellular ROS Levels and NF-kappaB Activation. *PLoS One*. **10**(12): p. e0145093.
97. Dalbeth, N. and D.O. Haskard (2005). Mechanisms of inflammation in gout. *Rheumatology (Oxford)*. **44**(9): p. 1090-6.
98. Chen, L., et al. (2013). Dolichos falcata Klein attenuated the inflammation induced by monosodium urate crystals in vivo and in vitro. *J Ethnopharmacol*. **150**(2): p. 545-52.
99. Reber, L.L., et al. (2014). Contribution of mast cell-derived interleukin-1beta to uric acid crystal-induced acute arthritis in mice. *Arthritis Rheumatol*. **66**(10): p. 2881-91.
100. Cavalcanti, N.G., et al. (2016). Cytokine Profile in Gout: Inflammation Driven by IL-6 and IL-18? *Immunol Invest*. **45**(5): p. 383-95.
101. Sabina, E.P., H. Indu, and M. Rasool (2012). Efficacy of boswellic acid on lysosomal acid hydrolases, lipid peroxidation and anti-oxidant status in gouty arthritic mice. *Asian Pac J Trop Biomed*. **2**(2): p. 128-33.
102. Meotti, F.C., et al. (2011). Urate as a physiological substrate for myeloperoxidase: implications for hyperuricemia and inflammation. *J Biol Chem*. **286**(15): p. 12901-11.
103. Jaramillo, M., P.H. Naccache, and M. Olivier (2004). Monosodium urate crystals synergize with IFN-gamma to generate macrophage nitric oxide: involvement of extracellular signal-regulated kinase 1/2 and NF-kappa B. *J Immunol*. **172**(9): p. 5734-42.
104. Uratsuji, H., et al. (2012). P2Y6 receptor signaling pathway mediates inflammatory responses induced by monosodium urate crystals. *J Immunol*. **188**(1): p. 436-44.

105. Goncalves, D.M. and D. Girard (2011). Titanium dioxide (TiO₂) nanoparticles induce neutrophil influx and local production of several pro-inflammatory mediators in vivo. *Int Immunopharmacol.* **11**(8): p. 1109-15.
106. Wallace SI Fau - Robinson, H., et al. Preliminary criteria for the classification of the acute arthritis of primary gout. (0004-3591 (Print)).
107. Dalbeth, N., et al. (2019). Gout. *Nat Rev Dis Primers.* **5**(1): p. 69.
108. Schauer, C., et al. (2014). Aggregated neutrophil extracellular traps limit inflammation by degrading cytokines and chemokines. *Nat Med.* **20**(5): p. 511-7.
109. Reber, L.L., et al. Neutrophils are not required for resolution of acute gouty arthritis in mice. (1546-170X (Electronic)).
110. Reinwald, C., et al. Reply to "Neutrophils are not required for resolution of acute gouty arthritis in mice". (1546-170X (Electronic)).
111. Steiger, S. and J.L. Harper (2014). Mechanisms of spontaneous resolution of acute gouty inflammation. *Curr Rheumatol Rep.* **16**(1): p. 392.
112. Marcolongo, R., et al. The "switch-off" mechanism of spontaneous resolution of acute gout attack. (0315-162X (Print)).
113. McDonagh, A.F. *Bile pigments: Bilatrienes and 5,15-biladienes*. The Porphyrins, ed. D. D. Vol. VI. 1979, New York: Academic.
114. Moser, S., et al. (2009). Fluorescent chlorophyll catabolites in bananas light up blue halos of cell death. *Proc Natl Acad Sci U S A.* **106**(37): p. 15538-43.
115. Stocker, R. (2004). Antioxidant activities of bile pigments. *Antioxid Redox Signal.* **6**(5): p. 841-9.

116. Vitek, L.N., L. (2003). Inverse relationship between serum bilirubin and atherosclerosis in men: a meta-analysis of published studies. *Experimental Biology & Medicine*. **228**(5): p. 568-571.
117. Molzer, C., et al. (2012). In vitro antioxidant capacity and antigenotoxic properties of protoporphyrin and structurally related tetrapyrroles. *Free Radic Res*. **46**(11): p. 1369-77.
118. Stocker, R. and J.F. Keaney, Jr. (2004). Role of oxidative modifications in atherosclerosis. *Physiol Rev*. **84**(4): p. 1381-478.
119. Bulmer, A.C., et al. (2018). Bilirubin acts as a multipotent guardian of cardiovascular integrity: more than just a radical idea. (1522-1539 (Electronic)).
120. McDonagh, A.F. (2010). The biliverdin-bilirubin antioxidant cycle of cellular protection: Missing a wheel? *Free Radic Biol Med*. **49**(5): p. 814-20.
121. Maghzal, G.J., et al. (2009). Limited role for the bilirubin-biliverdin redox amplification cycle in the cellular antioxidant protection by biliverdin reductase. *J Biol Chem*. **284**(43): p. 29251-9.
122. Sedlak, T.W. and S.H. Snyder (2009). Cycling the wagons for biliverdin reductase. *J Biol Chem*. **284**(46): p. le11; author reply le12.
123. Stocker, R. and G. Maghzal (2009). Reply to Sedlak and Snyder: The Little Bighorn of the Biliverdin Reductase Amplification Cycle. *Journal of Biological Chemistry*. **284**(46): p. le12-le12.
124. Ma, J.S., Yan, F., Wang, C.Q. & Chen, J.H. (1990). Addition of sodium bisulfite to biliverdin. *Chinese Chemical Letters*. **1**(1): p. 171-173.
125. Abu-Bakar, A., et al. (2012). Metabolism of bilirubin by human cytochrome P450 2A6. *Toxicol Appl Pharmacol*. **261**(1): p. 50-8.

126. McDonagh, A.F. and L.A. Palma (1982). Heme catabolism in fish. Bile pigments in gallbladder bile of the electric torpedo, *Torpedo californicus*. *Comp Biochem Physiol B*. **73**(3): p. 501-7.
127. Houston, A.I. (2010). Evolutionary models of metabolism, behaviour and personality. *Philos Trans R Soc Lond B Biol Sci*. **365**(1560): p. 3969-75.
128. Ahanger, A.A., et al. (2016). Pro-healing effects of bilirubin in open excision wound model in rats. *Int Wound J*. **13**(3): p. 398-402.
129. Ram, M., et al. (2016). Bilirubin modulated cytokines, growth factors and angiogenesis to improve cutaneous wound healing process in diabetic rats. *Int Immunopharmacol*. **30**: p. 137-149.
130. Zhu, H., et al. (2010). Bilirubin protects grafts against nonspecific inflammation-induced injury in syngeneic intraportal islet transplantation. *Exp Mol Med*. **42**(11): p. 739-48.
131. Nakao, A., et al. (2004). Biliverdin protects the functional integrity of a transplanted syngeneic small bowel. *Gastroenterology*. **127**(2): p. 595-606.
132. Sarady-Andrews, J.K., et al. (2005). Biliverdin administration protects against endotoxin-induced acute lung injury in rats. *Am J Physiol Lung Cell Mol Physiol*. **289**(6): p. L1131-7.
133. Fondevila, C., et al. (2004). Biliverdin therapy protects rat livers from ischemia and reperfusion injury. *Hepatology*. **40**(6): p. 1333-41.
134. Bellner, L., et al. (2011). Biliverdin Rescues the HO-2 Null Mouse Phenotype of Unresolved Chronic Inflammation Following Corneal Epithelial Injury. *Invest Ophthalmol Vis Sci*. **52**(6): p. 3246-53.

135. Wegiel, B., et al. (2011). Biliverdin inhibits Toll-like receptor-4 (TLR4) expression through nitric oxide-dependent nuclear translocation of biliverdin reductase. *Proc Natl Acad Sci U S A*. **108**(46): p. 18849-54.
136. Gorchein, A., Lim, C.K. & Cassey, P. (2009). Extraction and analysis of colourful eggshell pigments using HPLC and HPLC/electrospray ionization tandem mass spectrometry. *Biomedical Chromatography*. **23**(6): p. 602-606.
137. Bigo, C., et al. (2014). PPARalpha: A Master Regulator of Bilirubin Homeostasis. *PPAR Res*. **2014**: p. 747014.
138. Iwamori, S., et al. (2015). A novel and sensitive assay for heme oxygenase activity. *Am J Physiol Renal Physiol*. **309**(7): p. F667-71.
139. Zelenka, J., et al. (2008). Highly sensitive method for quantitative determination of bilirubin in biological fluids and tissues. *J Chromatogr B Analyt Technol Biomed Life Sci*. **867**(1): p. 37-42.
140. Htun, N.M., et al. (2017). Near-infrared autofluorescence induced by intraplaque hemorrhage and heme degradation as marker for high-risk atherosclerotic plaques. *Nat Commun*. **8**(1): p. 75.
141. Andria, B., et al. (2013). Biliverdin protects against liver ischemia reperfusion injury in swine. *PLoS One*. **8**(7): p. e69972.
142. Barclay, C., Cheplev, L.L., Beshara, C.S., Maclean, P.D., Hatfield, G.L., Rand, A.A., Thompson, A. & Wright, J.S. (2006). Polypyrrroles as Antioxidants: Kinetic Studies on Reactions of Bilirubin and Biliverdin Dimethyl Esters and Synthetic Model Compounds with Peroxyl Radicals in Solution. *Journal of Organic Chemistry*. **71**(1): p. 22-30.

143. Kosaka, J., et al. (2013). Effects of biliverdin administration on acute lung injury induced by hemorrhagic shock and resuscitation in rats. *PLoS One*. **8**(5): p. e63606.
144. Nakao, A., et al. (2005). Biliverdin administration prevents the formation of intimal hyperplasia induced by vascular injury. *Circulation*. **112**(4): p. 587-91.
145. Tian, W.F., et al. (2017). Biliverdin Protects the Isolated Rat Lungs from Ischemia-reperfusion Injury via Antioxidative, Anti-inflammatory and Anti-apoptotic Effects. *Chin Med J (Engl)*. **130**(7): p. 859-865.
146. Wang, J., et al. (2010). Exogenous biliverdin improves the function of lung grafts from brain dead donors in rats. *Transplant Proc*. **42**(5): p. 1602-9.
147. Nakagami, T., et al. (1993). A beneficial role of bile pigments as an endogenous tissue protector: Anti-complement effects of biliverdin and conjugated bilirubin. *Biochimica et Biophysica Acta (BBA) - General Subjects*. **1158**(2): p. 189-193.
148. Benzie, I.F. and J.J. Strain (1996). The ferric reducing ability of plasma (FRAP) as a measure of "antioxidant power": the FRAP assay. *Anal Biochem*. **239**(1): p. 70-6.
149. Yang, J., et al. (2011). Metabolism of gambogic acid in rats: a rare intestinal metabolic pathway responsible for its final disposition. *Drug Metab Dispos*. **39**(4): p. 617-26.
150. Franski, R. and T. Kozik (2017). Unexpected interaction between deprotonated biliverdin and alcohols as studied by ESI-MS. *J Mass Spectrom*. **52**(2): p. 65-68.
151. Koenig, A.M., et al. (2018). Serum profile changes in postpartum women with a history of childhood maltreatment: a combined metabolite and lipid fingerprinting study. *Sci Rep*. **8**(1): p. 3468.

152. Franklin, E.M., et al. (2009). The use of synthetic linear tetrapyrroles to probe the verdin sites of human biliverdin-IXalpha reductase and human biliverdin-IXbeta reductase. *FEBS J.* **276**(16): p. 4405-13.
153. Konickova, R., et al. (2012). Reduction of bilirubin ditaurate by the intestinal bacterium *Clostridium perfringens*. *Acta Biochim Pol.* **59**(2): p. 289-92.
154. Winter, S.E., et al. (2010). Gut inflammation provides a respiratory electron acceptor for *Salmonella*. *Nature.* **467**(7314): p. 426-9.
155. Novotny, C. and F. Kapralek (1979). Participation of quinone and cytochrome b in tetrathionate reductase respiratory chain of *Citrobacter freundii*. *Biochem J.* **178**(1): p. 237-40.
156. Barrett, E.L. and M.A. Clark (1987). Tetrathionate reduction and production of hydrogen sulfide from thiosulfate. *Microbiol Rev.* **51**(2): p. 192-205.
157. Mowat, C.G., et al. (2004). Octaheme tetrathionate reductase is a respiratory enzyme with novel heme ligation. *Nat Struct Mol Biol.* **11**(10): p. 1023-1024.
158. Kuwabara, W.M., et al. (2015). NADPH oxidase-dependent production of reactive oxygen species induces endoplasmic reticulum stress in neutrophil-like HL60 cells. *PLoS One.* **10**(2): p. e0116410.
159. Wang, X., et al. (2011). NADPH oxidase activation is required in reactive oxygen species generation and cell transformation induced by hexavalent chromium. *Toxicol Sci.* **123**(2): p. 399-410.
160. Shiels, R.G., et al. (2019). Unprecedented Microbial Conversion of Biliverdin into Bilirubin-10-sulfonate. *Sci Rep.* **9**(1): p. 2988.

161. Zhang, Y., et al. (2010). PKSolver: An add-in program for pharmacokinetic and pharmacodynamic data analysis in Microsoft Excel. *Comput Methods Programs Biomed.* **99**(3): p. 306-14.
162. McDonagh, A.F., et al. (2002). Hepatobiliary excretion of biliverdin isomers and C10-substituted biliverdins in Mrp2-deficient (TR(-)) rats. *Biochem Biophys Res Commun.* **293**(3): p. 1077-83.
163. Wolkoff, A.W. (2014). Organic anion uptake by hepatocytes. *Compr Physiol.* **4**(4): p. 1715-35.
164. Chen, Q., et al. (1999). Synthesis of a 10-Oxo-Bilirubin: Effects of the Oxo Group on Conformation, Transhepatic Transport, and Glucuronidation. *Journal of the American Chemical Society.* **121**(40): p. 9253-9264.
165. van de Steeg, E., et al. (2012). Complete OATP1B1 and OATP1B3 deficiency causes human Rotor syndrome by interrupting conjugated bilirubin reuptake into the liver. *J Clin Invest.* **122**(2): p. 519-28.
166. Cvorovic, J. and S. Passamonti (2017). Membrane Transporters for Bilirubin and Its Conjugates: A Systematic Review. *Front Pharmacol.* **8**: p. 887.
167. Ma, Q., et al. (2012). A rising tide of blue-absorbing biliprotein photoreceptors: characterization of seven such bilin-binding GAF domains in *Nostoc* sp. PCC7120. *FEBS J.* **279**(21): p. 4095-108.
168. Küfer, W. and H. Scheer, *Rubins and Rubinoid Addition Products from Phycocyanin*, in *Zeitschrift für Naturforschung C.* 1982. p. 179.
169. Kufer, W. and H. Scheer (1979). Studies on plant bile pigments, VII. Preparation and characterization of phycobiliproteins with chromophores chemically modified by reduction. *Hoppe Seylers Z Physiol Chem.* **360**(7): p. 935-56.

170. Falk, H., F. Lehner, and M. Rothbeck (1985). Zur regioselektiven nucleophilen Addition an 2,3-Dihydrobilatriene-abc. *Monatshefte für Chemie Chemical Monthly*. **116**(11): p. 1359-1361.
171. Ji, A.J., S.R. Savon, and D.W. Jacobsen (1995). Determination of total serum sulfite by HPLC with fluorescence detection. *Clin Chem*. **41**(6 Pt 1): p. 897-903.
172. DeHeer, H.L., B.W. Parry, and C.B. Grindem, *Peritoneal Fluid*, in *Diagnostic Cytology and Hematology of the Horse*, R.L. Cowell and R.D. Tyler, Editors. 2002, Mosby: Saint Louis. p. 127-162.
173. Raimondi, F., et al. Unconjugated bilirubin modulates the intestinal epithelial barrier function in a human-derived in vitro model. (0031-3998 (Print)).
174. Bulmer, A.C., et al. (2008). In vitro permeability and metabolic stability of bile pigments and the effects of hydrophilic and lipophilic modification of biliverdin. *Bioorg Med Chem*. **16**(7): p. 3616-25.
175. Cunningham, O., et al. (2000). Studies on the specificity of the tetrapyrrole substrate for human biliverdin-IXalpha reductase and biliverdin-IXbeta reductase. Structure-activity relationships define models for both active sites. *J Biol Chem*. **275**(25): p. 19009-17.
176. Busch, A.W. and B.L. Montgomery (2015). Interdependence of tetrapyrrole metabolism, the generation of oxidative stress and the mitigative oxidative stress response. *Redox Biol*. **4**: p. 260-71.
177. Li, C., et al. (2013). Ambulatory Resource Utilization and Cost for Gout in United States. *The American Journal of Pharmacy Benefits*. **5**(2): p. e46 - e54.
178. Orłowski, G.M., et al. (2015). Multiple Cathepsins Promote Pro-IL-1beta Synthesis and NLRP3-Mediated IL-1beta Activation. *J Immunol*. **195**(4): p. 1685-97.

179. Chapman, P.T., et al. (1997). Endothelial activation in monosodium urate monohydrate crystal-induced inflammation: in vitro and in vivo studies on the roles of tumor necrosis factor alpha and interleukin-1. *Arthritis Rheum.* **40**(5): p. 955-65.
180. McCarty, D.J., Jr. (1965). The inflammatory reaction to microcrystalline sodium urate. *Arthritis Rheum.* **8**(5): p. 726-35.
181. Fam, A.G., et al. (1992). A comparison of five preparations of synthetic monosodium urate monohydrate crystals. *J Rheumatol.* **19**(5): p. 780-7.
182. Kaur, S., P.L. Bijjem Kr Fau - Sharma, and P.L. Sharma Anti-inflammatory and antihyperalgesic effects of the combination of ibuprofen and hemin in adjuvant-induced arthritis in the Wistar rat. (1568-5608 (Electronic)).
183. Dypbukt, J.M., et al. (2005). A sensitive and selective assay for chloramine production by myeloperoxidase. *Free Radic Biol Med.* **39**(11): p. 1468-77.
184. Vitek, L., C. Bellarosa, and C. Tiribelli (2019). Induction of Mild Hyperbilirubinemia: Hype or Real Therapeutic Opportunity? *Clin Pharmacol Ther.* **106**(3): p. 568-575.
185. Freitas, A., et al. (2006). Heme oxygenase/carbon monoxide-biliverdin pathway down regulates neutrophil rolling, adhesion and migration in acute inflammation. *Br J Pharmacol.* **149**(4): p. 345-54.
186. Ishikawa, K., et al. (1997). Induction of heme oxygenase-1 inhibits the monocyte transmigration induced by mildly oxidized LDL. *J Clin Invest.* **100**(5): p. 1209-16.
187. Bisht, K., et al. (2019). Deletion of Biliverdin Reductase A in Myeloid Cells Promotes Chemokine Expression and Chemotaxis in Part via a Complement C5a--C5aR1 Pathway. *J Immunol.* **202**(10): p. 2982-2990.
188. Bisht, K., et al. (2014). Biliverdin modulates the expression of C5aR in response to endotoxin in part via mTOR signaling. *Biochem Biophys Res Commun.* **449**(1): p. 94-9.

189. Vogel, M.E., et al. (2017). Bilirubin Prevents Atherosclerotic Lesion Formation in Low-Density Lipoprotein Receptor-Deficient Mice by Inhibiting Endothelial VCAM-1 and ICAM-1 Signaling. *J Am Heart Assoc.* **6**(4): p. e004820.
190. Overhaus, M., et al. (2006). Biliverdin protects against polymicrobial sepsis by modulating inflammatory mediators. *Am J Physiol Gastrointest Liver Physiol.* **290**(4): p. G695-703.
191. Cranford, T.L., et al. (2016). Role of MCP-1 on inflammatory processes and metabolic dysfunction following high-fat feedings in the FVB/N strain. *Int J Obes (Lond).* **40**(5): p. 844-51.
192. Yasuda, K., K. Nakanishi, and H. Tsutsui (2019). Interleukin-18 in Health and Disease. *Int J Mol Sci.* **20**(3): p. 649.
193. Zaki, M.H., et al. (2010). IL-18 production downstream of the Nlrp3 inflammasome confers protection against colorectal tumor formation. *J Immunol.* **185**(8): p. 4912-20.
194. Zelenka, J., et al. (2016). Hyperbilirubinemia Protects against Aging-Associated Inflammation and Metabolic Deterioration. *Oxid Med Cell Longev.* **2016**: p. 6190609.
195. Mehta, H.M., M. Malandra, and S.J. Corey (2015). G-CSF and GM-CSF in Neutropenia. *J Immunol.* **195**(4): p. 1341-9.
196. Basdeo, S.A., et al. (2016). Suppression of human alloreactive T cells by linear tetrapyrroles; relevance for transplantation. *Transl Res.* **178**(1878-1810 (Electronic)): p. 81-94 e2.
197. Chiu, H., J.A. Brittingham, and D.L. Laskin (2002). Differential induction of heme oxygenase-1 in macrophages and hepatocytes during acetaminophen-induced

- hepatotoxicity in the rat: effects of hemin and biliverdin. *Toxicol Appl Pharmacol.* **181**(2): p. 106-15.
198. Li, J.J., et al. (2017). Biliverdin administration ameliorates cerebral ischemia reperfusion injury in rats and is associated with proinflammatory factor downregulation. *Exp Ther Med.* **14**(1): p. 671-679.
199. Takei, R., et al. (2019). Bilirubin reduces visceral obesity and insulin resistance by suppression of inflammatory cytokines. *PLoS One.* **14**(10): p. e0223302.
200. Morgan, M., et al. (2008). Pharmacokinetics of a C5a receptor antagonist in the rat after different sites of enteral administration. *Eur J Pharm Sci.* **33**(4-5): p. 390-8.
201. Wegiel, B., et al. (2009). Cell surface biliverdin reductase mediates biliverdin-induced anti-inflammatory effects via phosphatidylinositol 3-kinase and Akt. *J Biol Chem.* **284**(32): p. 21369-78.
202. Meng, M., et al. (2019). The Fibrosis and Immunological Features of Hypochlorous Acid Induced Mouse Model of Systemic Sclerosis. *Front Immunol.* **10**(1861): p. 1861.
203. Servettaz, A., et al. (2009). Selective oxidation of DNA topoisomerase 1 induces systemic sclerosis in the mouse. *J Immunol.* **182**(9): p. 5855-64.
204. Gundamaraju, R., et al. (2019). Bilirubin Attenuates ER Stress-Mediated Inflammation, Escalates Apoptosis and Reduces Proliferation in the LS174T Colonic Epithelial Cell Line. *Int J Med Sci.* **16**(1): p. 135-144.